"INFLUENCE OF COMPOSITION AND THERMOMECHANICAL PROCESSING ON MICROSTRUCTURE EVOLUTION IN AISI 430 FERRITIC STAINLESS STEELS (FSS)"

By

Nyongesa Machio

Thesis prepared in fulfilment of the requirements for the degree of Master of Science in Applied Science (Materials Engineering).

Department of Materials Engineering
University of Cape Town

September 1998.

Abstract

This thesis examines the influence of austenite potential and hot roll finish temperature on the evolution of microstructure in the ferritic stainless steel grade AISI 430. In particular, it focuses on the influence of these variables on the hot band annealing behaviour of this steel. The material employed was obtained from laboratory and commercial heats.

Two hot roll finish temperatures, viz. 600°C and 800°C for the commercial heats and two alloy compositions of austenite potential 11 and 61% for the laboratory heats were studied. Electron channelling contrast (ECC) obtained in scanning electron microscopy was used to follow the evolution of microstructure. Limited microtexture measurements were made using electron backscattered techniques.

It was found that a low finish temperature produced a hot rolled microstructure that showed limited softening and a fully recrystallised microstructure after annealing while a high hot roll finish temperature produced a completely softened as-hot-rolled microstructure and only partial recrystallisation after annealing.

A high austenite potential encouraged the ferrite phase to undergo extensive continuous recrystallisation during hot band annealing. However, the affinity for the precipitation of carbo-nitrides tended to play a role in slowing down the process. On the other hand, the ferrite phase deformed in the presence of a low austenite content mostly underwent extended recovery during hot band annealing. The softening here was affected by a low driving force. The end microstructures after annealing were however similar in both cases in as much as they consisted of elongated structures.

The martensite phase was found to behave similarly regardless of the austenite content, where both recovery to produce subgrains and occasional recrystallisation occurred.

During final recrystallisation after cold rolling, the high austenite potential coupled with a short hot band anneal time resulted in incomplete recrystallisation. This caused sharper alpha fibre texture components in the final sheet. A long hot band anneal time however resulted in sharper gamma-fibre texture components. In the case of low austenite potential, a long hot band anneal produced a random texture in the final texture.

Ridging was observed in all cases but a high austenite content was found to lessen its severity. Also, it (ridging) was reduced by the random texture produced by long hot band annealing in the case where the austenite potential was low.

Acknowledgements

I would like to thank the following people whose assistance and/or advice helped complete this thesis:

Assoc. Prof. R D Knutsen, my supervisor for his guidance with the project.

Departmental technical staff of Reggie Hendricks, Nick Dreze, Glen Newins, Mira Topic and Dave Dean for their assistance in the workshop.

Departmental Dark Room Staff of Bernard Greeves (now retired), James Petersen and Adriaan Loedolff for the printing of micrographs.

University of Cape Town's Electron Microscope Unit staff of Prof. Trevor Sewell, Miranda, Mohammed and William for helping with scanning electron microscopy.

Alan Duckham and Dr. Nicola Wittridge, for their help with the EBSD microtexture measurement technique. The latter also for her informative discussions.

Columbus Stainless Steel, Middleburg South Africa for providing the materials for the project and also for their financial assistance.

Deutscher Akademischer Austauschdienst (DAAD) of Bonn, Germany, for maintaining the scholarship throughout my Masters programme and for giving me a chance to travel overseas.

Dr Candy Lang, the Postgraduate student advisor, for helping me settle when I first arrived in South Africa.

Lastly, to my colleagues in the department for giving me a home away from home.

This thesis is dedicated to the two women in my life: My mother, Agnes, for her love and care through the years and my wife Eve-Chris for being patient while I was away.

TABLE OF CONTENTS

Chapter One

Introduction

Ferritic stainless steels have become an increasingly important group of materials since World War II. They have presented an ever-increasing challenge to the long-established austenitic stainless steels in applications where the most stringent requirements are not encountered. In particular, their virtual immunity from stress corrosion cracking has led them to become a household name in the chemical industry.

The most commonly used grade of these steels is the AISI 430. With a few alloying modifications, it has been used for automobile trim and similar purposes in which resistance to staining is the chief requirement e.g. kitchen sinks and domestic catering equipment. The main driving force behind the increased use of these materials is their cheapness. Compared to their austenitic counterparts, they are essentially free from the expensive nickel.

The increased use of these materials has, however, been hampered by a few mechanical property shortcomings. Use as structural members, for example, is very limited because of their low toughness. The latter poor property is a consequence of the grain size and the embrittling effect of chromium dissolved in the body-centred cubic iron. These materials are almost entirely ferritic up to the melting point and during manufacture, develop very coarse grains as a result of their non-transformable nature. Their increased tendency to soften by recovery, producing subgrains, also helps perpetuate the formation of the coarse grains.

These materials also have a low formability. In particular, during finishing processes like deep drawing, they have been known to develop rope marks on the sheet surfaces. The roping has been attributed to a crystallographic textural effect, with the unfavourable texture being developed during the hot rolling.

Industrial remedial measures against these problems have concentrated on the encouragement of recrystallisation during the hot band annealing stage of manufacture. This project, undertaken in co-operation with Columbus Stainless Steel, Middleburg, South Africa, aims at doing just that.

The objectives of the project are to study the influence of the following parameters on the evolution of microstructure:

- **Composition:**

The ferrite phase in a conventional AISI 430 ferritic stainless steel is known to recover during both hot rolling and the subsequent hot band annealing. Suggestions have been made by several researchers to the effect that the presence of austenite during the hot rolling of these steels could influence a deviation in the known response of the ferrite phase to the subsequent hot band annealing. The basis of this proposition comes from the fact that the ferrite phase with its 48 slip systems is softer than the austenite phase, which has 12 slip systems. During hot rolling, the hard austenite causes a partitioning of strain to the softer ferrite. As a result, the ferrite phase undergoes extensive deformation that leads to a higher amount of stored deformation energy. Also, the chances of introducing deformation inhomogeneities in the ferrite matrix become increasingly advanced, and the simultaneous existence of the inhomogeneities and the stored deformation energy could result in favourable conditions for recrystallisation of the ferrite phase.

For this study, a MEDUSA Model (v. 3) (1) computer program was used to vary alloying elements in a basic 17%Cr ferritic stainless steel to produce heats for which the austenite potential varied between 11 and 61%. These heats were subjected to near identical hot rolling schedules in a laboratory before their response to hot band annealing treatments was evaluated.

- **Hot roll finish temperature**:

The hot roll finish temperature has been reported to have an effect on both the microstructure and the texture of a hot band after annealing. Gullen and Jones [2], and D Vanderschueren et al [3], studying low carbon steels established that a low hot roll finish temperature results in sharper textures. In a study conducted on laboratory rolled ferritic stainless steels by Wittridge and Knutsen [4], it was established that a low hot roll finish temperature led to complete recrystallisation after hot band annealing.

This study was aimed at validating the observations in Ref. 4 as regards commercial application and two commercial heats with hot roll finish temperatures of 600°C and 800°C respectively, were employed.

Chapter Two

Literature Review

2.1: Description of Ferritic Stainless Steels (FSS):

This is a term used to loosely refer to a group of steels with chromium (Cr) contents ranging from 11 to 25 % [5]. The designation "ferritic" is due to their structure in the annealed condition [6]. However, at high temperatures, a duplex austenite-ferrite (γ and α) structure is possible. The basic Fe-Cr equilibrium phase diagram indicates the change in microstructure that occurs with increasing Cr content, fig. 2.1 below.

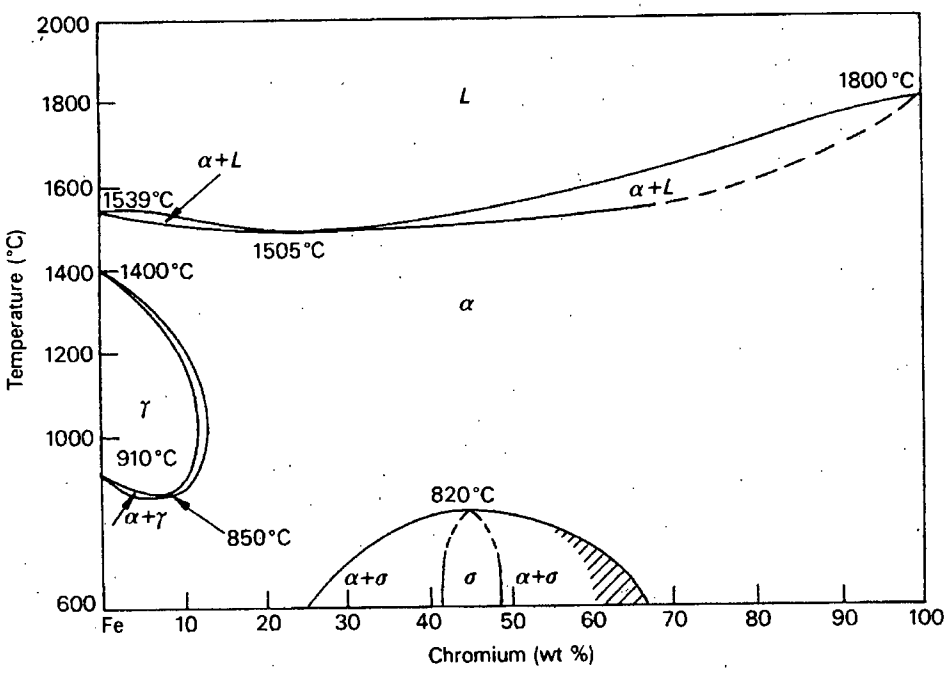

Fig. 2.1: Fe-Cr equilibrium phase diagram. [Ref. 7, pp. 212]

The phase diagram can be manipulated by alloying. For example, the addition of interstitial elements carbon and nitrogen, which are strong austenite formers, extends the gamma loop of the equilibrium diagram. Fig. 2.2 below shows the effect carbon has on the phase diagram.

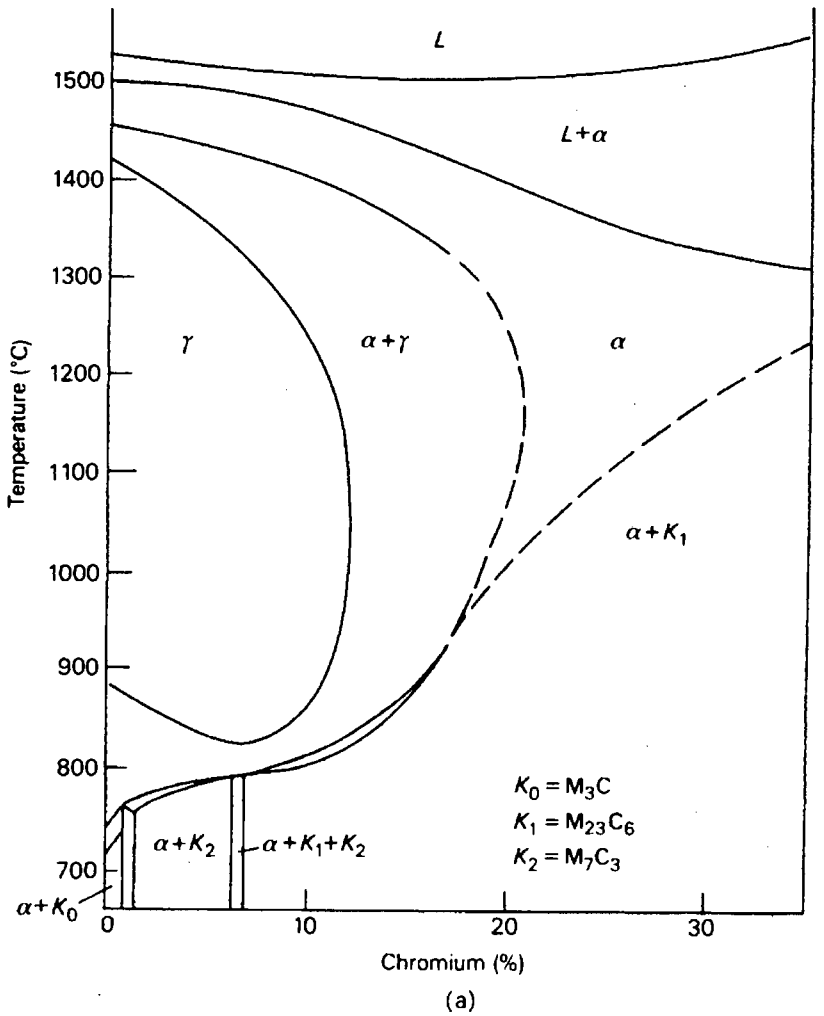

Fig. 2.2: Effect of carbon (0.05C) on the gamma-phase in the Fe-Cr phase diagram. [Ref. 7, pp. 213].

The most commonly used class of ferritic stainless steels is the AISI 430, which contains 17%Cr. Its applications range from the chemical industry, where it has been known to withstand chloride environments, to deep drawing applications e.g. household appliances. The latter use is as a result of their relatively good mechanical properties. The impetus for its increased use is partly derived from its low cost compared to the traditional austenitic stainless steels that contain nickel as an alloying element. Its extensive use is however hampered by industrial problems that are occasioned by its microstructure, chief among them being the ridging phenomenon that occurs when the sheets are either drawn or pulled in tension.

2.2: Processing of Flat Products:

Flat products from these steels are processed via the well-known thermomechanical processing route. It involves the continuous casting of molten metal into slabs. The slabs are hot rolled into strips that are commonly called hot bands. The strips are then batch annealed in box-furnaces, followed by pickling before cold rolling and final recrystallisation annealing. Fig. 2.3 below shows a schematic representation of the process.

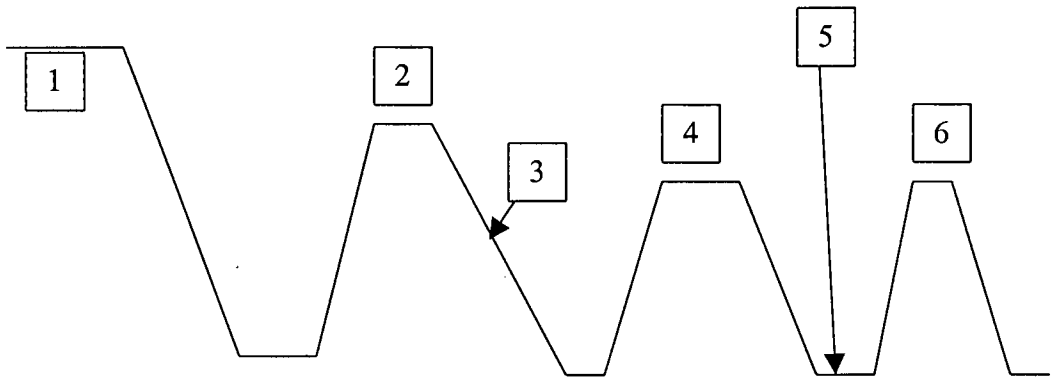

Fig. 2.3: Schematic diagram for thermomechanical processing of ferritic stainless steels (FSS).

Stage 1 is continuous casting, 2 slab reheating, 3 hot rolling, 4 hot band anneal, 5 cold rolling and 6 the final recrystallisation anneal. The thermomechanical processing is such that a few parameters can be varied in order to inculcate desired properties in the finished sheet. The parameters varied include slab reheat temperature, hot roll start and finish temperatures and hot roll reductions, duration of hot band annealing, percentage cold roll reductions and time and temperature of the final recrystallisation anneal.

The individual thermomechanical processes affect the microstructure of the final sheet. The following sections highlight, in a general sense, some of the changes that occur.

2.3: The Deformation Microstructure:

This microstructure is a result of the actual mechanical pressing encountered in both the hot and cold rolling processes.

Deformation in ferritic stainless steels occurs by slip and involves the motion of dislocations. This is a thermally activated process that involves the overcoming of the Peierls-Nabarro stress on the dislocations. The homogeneity of the deformed microstructure depends on the number of operating slip systems, which are dependent on the deformation temperature. At low temperatures when few slip systems are operating because of the high Peierls-Nabarro stress, the deformation is localised and the resulting microstructure is very inhomogeneous. As the deformation temperature increases, the deformation becomes more homogeneous as a result of the increased number of operating systems.

The relatively easy motion of dislocations at the high deformation temperature also allows them to annihilate each other and to re-arrange into well-organised low angle grain boundaries.

On the grain level however, the deformation could still be inhomogeneous even at high temperatures because different slip systems are operative in different grains. Also, neighbouring grains exert a constraint on each other, which influences shape change during deformation. This, coupled with the need to maintain contiguity during deformation, results in deformation processes that are different in various parts of the same grain. Since deformation is such that new grain orientations are developed, the factors above ensure that a polycrystalline material responds to deformation by developing orientations that are different from grain to grain and different from region to region within an individual grain [8].

The microstructural inhomogeneities that form during deformation are well documented and are classified below [8]:

a): Deformation Bands:

These are volumes of constant orientation(s) that are significantly different to the orientation(s) present elsewhere in a grain. Deformation bands almost always form with a double orientation change [8] and the region that comes between the orientations is called a transition band.

b): Microbands:

These inhomogeneities are confined to single grains and appear as long thin plate-like features of finite thickness whose walls consist of dislocation assemblies in which dislocation are tangle. They are known for a relatively high interior dislocation content.

c): Shear Bands:

Shear bands form as narrow regions of intense shear and occur independently of the grain structure and also of normal crystallographic considerations. In rolled materials, they occur at ~35° to the rolling plane and parallel to the transverse direction. In slipping materials, shear bands form in colonies, in each of which only one set of parallel bands develops. The colonies are usually several grains thick and the bands in alternate colonies are in opposite sense so that a herringbone pattern develops. Any grain boundaries in the colony are crossed without deviation. The formation of shear bands is favoured by large grain size and the presence of interstitial (carbon and/or nitrogen) atoms. [9].

d): Grain Boundaries:

The grain boundaries that exist before deformation give rise to inhomogeneity of slip and since different slip systems operate near them, they give rise to local misorientations.

The formation of these inhomogeneities gains importance during subsequent annealing processes, during which the deformed metal undergoes some form of softening.

2.4: Annealing Phenomena:

The following processes can occur, either separately or concurrently during both the hot band annealing and the final recrystallisation treatment.

2.4.1: Recovery:

Recovery is said to occur when the dislocations generated by the plastic deformation occasioned by an applied stress arrange themselves into low energy cell structures whose interiors are relatively free of dislocations. Tangled dislocations make up the cell walls and the orientation difference between neighbouring cells is small, generally less than 2°.

Annealing the cell structures allows further movement of the tangled dislocations at the walls into a more regular network. The walls then become low angle grain boundaries and this heralds the formation of subgrains. Fig. 2.4 below shows the transition from cells to subgrains where "messy" regions A and B have become regular dislocation networks after annealing.

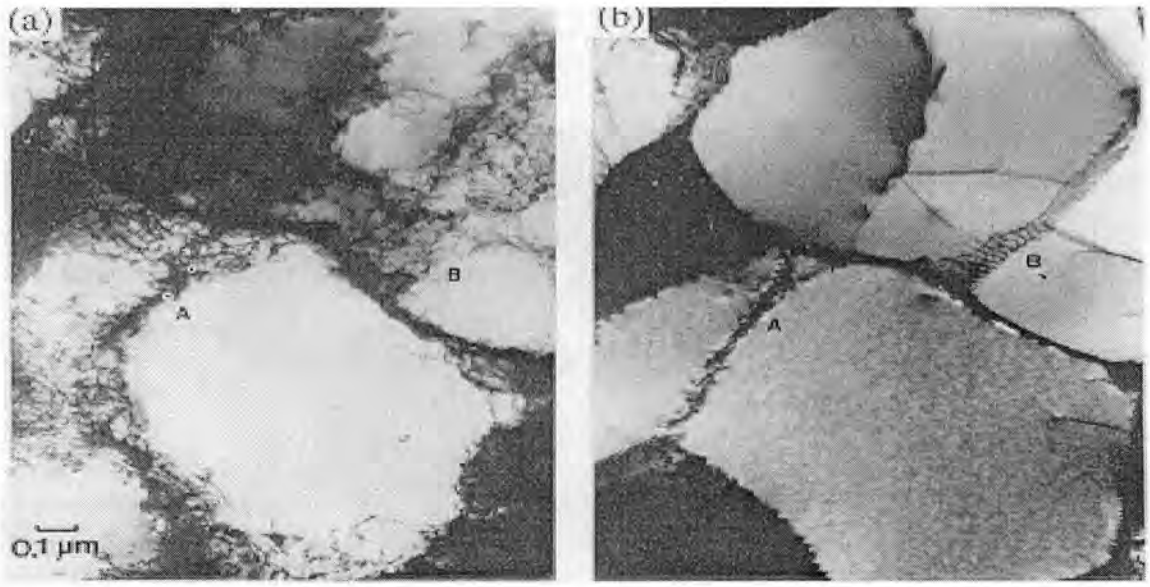

Fig. 2.4: Transition from cells to network of subgrains (Ref. 8).

Subgrain networks are fully defined by the orientation of each subgrain, orientation gradient and the wavelength of fluctuations of the misorientations of the individual subgrains.

2.4.1.1: Subgrain Energy:

The stored energy due to subgrains is given by [8]:

$$E_d = 3\,\gamma_s / D = \alpha\,\gamma_s / R \quad \text{.....(1)}$$

where E_d is the energy per unit volume, D is the subgrain diameter, R is the radius of the subgrain, γ_s is the specific energy for the low angle grain boundaries which comprise the subgrain walls, 3/D is the area of low angle grain boundary per unit volume, and α is a constant (~ 1.5).

The importance of Equation 1 is that the formation of subgrains could be viewed as a metastable state, since they store an appreciable amount of deformation energy.

2.4.1.2. Mobility of Subgrains

Subgrains change shape via the migration of their boundaries. The migration occurs during either an applied stress or subgrain growth.

a): Motion under an applied stress:

Motion of subgrain boundaries under a stress have been found to account for dynamic softening by continuous dynamic recrystallisation in both microduplex [10] and ferritic stainless steels [11]. The growth of subgrains via boundary migration during the early stages of deformation of microduplex stainless steel causes an increase of the misorientations of subgrains of the ferrite phase, converting them into high angle grains that undergo grain boundary sliding to produce the superplastic effect.

Belyakov et al [11], in explaining the occurrence of dynamic recrystallisation in ferritic stainless steel, postulate that the merging of migrating low angle boundaries with subgrain boundaries of higher misorientation increase the latter's misorientation to the regime of high angle grains i.e. $\theta > 15°$, where θ is the misorientation.

b): Subgrain Growth:

This is a post deformation recovery process that is driven by the tendency to reduce the total area of low angle boundaries in a material. The driving force, F, is defined as the rate of change of the stored energy E_d with respect to the subgrain radius, R:

$$F = \frac{dEd}{dR} \quad \text{.....(2)}$$

The change in the subgrain size with time during isothermal annealing has revealed kinetics of the form:

$$D^n - D_0^n = c\,t \quad \text{.....(3)}$$

where n is a constant, c is a temperature dependent rate constant and D_0 is the subgrain size at t = 0 [8]. Another version of this equation was found by Xiaoxu, et al [12] working on microduplex stainless steel, as a third power growth law:

$$D^n \sim t \quad \text{.....(4).}$$

Subgrain growth is an important aspect of thermomechanical processing because it determines the eventual softening mode of the deformed material. Whole scale subgrain growth leads to softening by extended recovery. The resulting grains are elongated and of a similar size scale as the initially deformed grains. In a situation where only a few subgrains preferentially grow at the expense of the other subgrains, the growing subgrains can form recrystallisation nuclei that grow to produce smaller, equi-axed grains. The softening process in this case becomes recrystallisation, or more appropriately, discontinuous recrystallisation.

The mechanism that best accounts for subgrain growth is that based on the migration of triple point Y junctions, fig. 2.5. When a triple point A is subjected to forces F1, F2, and F3 from 3 boundaries, the differences in F cause the boundaries to become curved (dotted lines) and to tend to migrate in the direction of the arrows so as to minimise their length. The triple point is thus forced to migrate and only stabilises when it reaches a position A` in which the boundaries are straight (dashed lines) and the angles are at equilibrium values (120°).

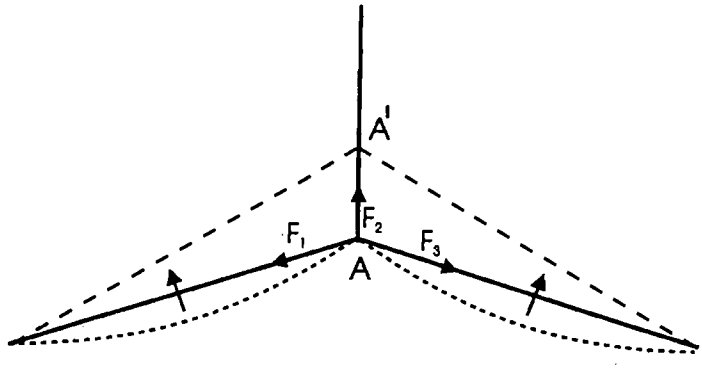

Fig. 2.5: Migration of low angle boundaries. (Ref. 8).

2.4.1.3: Effect of Subgrain Growth on Misorientation:

Whether subgrain growth affects misorientation depends on the existence of an orientation gradient in the subgrain network.

a). Growth in an Orientation Gradient:

The orientation gradient, β, is defined as the rate of change of orientation, θ, with respect to the subgrain radius, R:

$$\beta = \frac{d}{dR}\theta \quad \text{.....(5).}$$

As the subgrain grows, the misorientation increases. This increase results in the orientation of the growing subgrain changing from a low to a high angle regime heralding the formation of a recrystallisation nucleus or a high angle grain. Growth in an orientation gradient is thought to occur at deformation heterogeneities and has accounted for particle stimulated nucleation which occurs from a subgrain in the vicinity of a particle.

b). Growth in the absence of an orientation gradient:

The effect of growth of subgrains in the absence of an orientation gradient on the misorientation is not clear. Xiaoxu et al [12] found a significant growth of the subgrains without any obvious change of individual misorientations and only a slight increase in the average misorientation. The wavelength of the fluctuations of the misorientations determined whether the orientation increased or decreased during growth. When the size of a subgrain was less than half the wavelength, growth led to a linear increase in the misorientation and vice versa. On the other hand, Humphreys [13] found that the average misorientation decreased as subgrains grew.

The growth of subgrains in such a situation cannot alter the misorientation in the subgrain network appreciably. The low angle grain boundaries would be maintained and the resulting mode of softening would be extended recovery.

2.4.1.4: Effect of Particles on Subgrain Growth:

The presence of particles affects the kinetics of subgrain growth because the particles exert a pinning drag, first discovered by Zener, on the migrating subboundaries. The drag is related to the size of the particles through the following equation [8]:

$$P_z = (3 F_v \gamma) / 2 r \qquad (6)$$

where P_z is the pinning pressure, F_v the volume fraction of the particles, γ is the boundary energy and r is the radius of the particles.

A growing subgrain will have its effective driving force reduced as some is used to overcome the pinning pressure. The implication of this is that situations can arise in which the subgrain network is stabilised by the particles, forcing the deformed material to remain recovered after annealing. A coarsening of the particles however reduces the pinning pressure and a stabilised subgrain network would disintegrate.

2.4.2: Extended Recovery and Continuous Recrystallisation:

After the formation of subgrains, growth can occur on continued annealing. If the subgrain misorientations are small and the orientation change in a grain does not change very significantly during the subgrain growth, the subgrains would acquire progressively larger sizes. This is extended recovery. Eventually however, subgrain coalescence can occur to leave clear subgrain-free grains and a microstructure that consists of high angle boundaries. Such a situation is reminiscent of a recrystallised microstructure and the process of its formation is called continuous recrystallisation to

differentiate it from discontinuous recrystallisation that requires both nucleation and growth.

These processes have been found to occur during the annealing of alloys that have an accompanying precipitation of second phase particles. The coarsening of the particles allows the continued growth of subgrains because coarsening reduces their pinning effect.

2.4.3: Recrystallisation:

Discontinuous recrystallisation is defined as the formation of new strain free grains in certain parts of a deformed specimen and the subsequent growth of these to consume the deformed or recovered microstructure. It is a softening process in which the recovery of properties is complete. The process divides up the microstructure into recrystallised or non-recrystallised regions. It is made up of two consecutive regimes, nucleation and growth. Nucleation corresponds to the first appearance of the new grains in the microstructure and growth corresponds to the phase in which the new grains replace the deformed and/or recovered microstructure. These regimes affect both the homogeneity and kinetics of the recrystallisation process. They are random processes and the occurrence of, for example, nucleation in one part of the microstructure could be accompanied by the occurrence of growth in a different part of the same microstructure, and vice versa.

2.4.3.1: Nucleation

Nucleation is quantified by the number of nuclei per unit volume (N), of deformed structure. It determines both the size and orientation of the resulting grains. It is not a homogeneous process because it preferentially occurs at deformation heterogeneities. The strains encountered during thermomechanical processing favour a mechanism in which nucleation originates from a pre-formed nucleus to account for nucleation.

This model states that recrystallisation originates from dislocation cells or subgrains which are present after deformation. These subgrains are either highly strained or relatively free of strain and occur in regions that have an orientation gradient. They undergo rapid growth by subgrain boundary migration that converts their low angle boundaries to the high angle regime.

2.4.3.2: Growth

The growth of the nuclei occurs via the migration of high angle grain boundaries. It is quantified as a growth velocity, v, or a growth rate, G':

$$v = G' = MP \quad \text{.....(7)}$$

where M is the mobility of the high angle grain boundary (HAGB), and P is the net pressure on the boundary.

The driving pressure, P_d, for growth is provided by the dislocation density (ρ):

$$P_d = \alpha\rho Gb^2 ; \qquad \alpha = 0.5 \quad \text{.....(8)}$$

where G is the shear modulus and b is the Burgers vector

The driving pressure is influenced by a number of factors, which are outlined below:

a): Boundary Curvature, P_c:

A boundary curvature resulting from a growing nucleus produces an opposing force P_c. For a spherical new grain of radius R possessing a grain boundary of specific energy γ_b, P_c is expressed by the Gibbs-Thomson equation below:

$$P_c = 2\gamma_b/R \qquad (9)$$

The action of P_c is such as to reduce the grain boundary area. The critical size R_c of the nucleus occurs when $P_c = P_d$ and below it (R_c) there would be no net driving force for recrystallisation. In essence therefore, a minimum amount of deformation is required to initiate and sustain recrystallisation.

b): Deformation temperature and strain rate:

When the deformation temperature and/or the strain rate are such that dislocation climb occurs, dislocation annihilation and re-arrangement occurs in the familiar recovery process and this lowers the density of the stored dislocations.

The importance of this temperature and strain rate dependence of the dislocation density is that during hot rolling the amount of stored deformation energy would be far less than that stored after cold rolling.

c): Precipitating particles:

The effect of precipitating particles depends on their size and spacing. Closely spaced particles exert a significant pinning effect on migrating high angle grain boundaries known as Zener drag, P_z:

$$P_z = 3 F_v \gamma / 2 r \qquad (10)$$

where F_v is the volume fraction of the particles, r is the particle radius and γ is the boundary energy.

If all these forces were to act in the early stages of recrystallisation, the net driving pressure, P, would then be expressed as:

$$P = P_d - P_c - P_z \qquad (11)$$

The magnitude and distribution of P will affect the growth rate of the new grains and the homogeneity of the resulting microstructure.

2.4.3.3: Size and Shape of new grains:

The size of the new grains is a balance between the nucleation and growth processes. Smaller grains result when the number of nuclei is large as a result of a high nucleation rate. Since nucleation is not homogeneous, the distribution of grain sizes also tends to be inhomogeneous, being smaller at prior deformation inhomogeneities.

The shape of the grains is primarily determined by the dimension of growth. Isotropic growth results in equi-axed grains. Anisotropic growth on the other hand, as results for example when particles are distributed anisotropically, leads to the formation of elongated grains.

2.4.3.4: Quantifying the Kinetics of Recrystallisation:

The extent of recrystallisation is described by the volume fraction of material recrystallised, X_v. Since it resembles a phase transformation, a plot of X_v versus time for isothermal experiments has the characteristic sigmoidal form, fig. 2.6 below [8]:

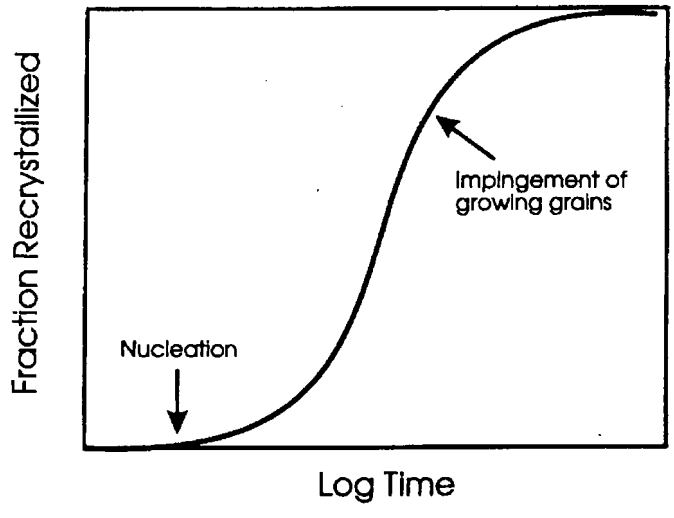

Fig. 2.6: Characteristic curve for the kinetics of phase transformation.

It has an incubation period before recrystallisation is detected which is followed by an increasing rate of recrystallisation, a linear region and finally a decreasing rate of recrystallisation when the growing grains impinge against each other.

The first attempt at quantifying the kinetics of recrystallisation produced the now well known Johnson-Mehl-Avrami-Kolmogorov (JMAK) model whose defining equation is:

$$X_v = 1 - \exp.(-B\, t^n) \qquad (12)$$

where $B = (f\, N'\, G')/\, 4$, f is a shape factor, N' is the rate of nucleation, G' is the growth rate, t is the time and n is the Avrami exponent.

The Avrami exponent depends on the nucleation rate, N' and the dimension of growth. This model assumes that nucleation is random and hence is very idealised. In practice, the kinetics it stipulates are never achieved because of the distribution of inhomogeneities in the deformed microstructure. The non-random distribution of these inhomogeneities leads to the non-random distribution of both the nucleation sites and stored deformation energy and results in a growth rate that decreases with time.

2.5: Tempering of Martensite:

Ferritic stainless steels, as the name suggests, are meant to be entirely ferritic at all temperatures. However, the (α and γ) two phase region exists in the Fe-Cr phase diagram when the amount of interstitials (carbon and nitrogen) exceeds 0.03% [14]. On rapid cooling, the austenite transforms to martensite.

The type of martensite formed depends on the amount of carbon present in the steel [15]. Lath martensite forms in low- and medium carbon-steels and has a body centred cubic (bcc) structure which transforms to a body centred tetragonal (bct) structure

when the amount of carbon exceeds 0.2%. The martensite units form in the shape of laths, grouped into sheaves or packets. The substructure in the laths consists of a high density of dislocations arranged in cells.

Plate martensite forms in high carbon. The structure is bct but bcc can also form. The martensite units form as individual lenticular plates whose substructure consists of very fine twins. The dislocation energy in plate martensite is lower than in lath martensite.

The annealing of low and medium carbon martensite is a dual process that involves the concurrent precipitation of carbides and recovery and recrystallisation, [15, 16, 17, 18]. The carbides, which initially precipitate as needles along lath boundaries and later in ferrite grains spheroidise with longer annealing times to reduce surface energy. Recovery occurs when the boundaries of the dislocation cells contained between lath boundaries and the random dislocations contained between them annihilate. This results in a low dislocation density acicular ferrite grain structure that resembles the lath-like units in the original martensite.

A recrystallisation nucleus is formed when a recovered subgrain grows to acquire a critical radius that grows in the shape of a roughly spherical grain that absorb the tempered martensite matrix. Recrystallisation has however been noted to be very sluggish in the presence of high densities of carbides as would happen when the carbon content is high [16]. The carbides impede the growth of the recrystallised nuclei making the observation of recrystallisation very difficult, if not impossible. In such a case, the martensite remains recovered after annealing.

2.6: Hot Band Annealing of Ferritic Steels:

Hot band annealing during thermomechanical processing of stainless steels has been found to be beneficial since it ensures complete softening for the following cold rolling process [19, 20]. The annealing dictates the precipitation, size and distribution of carbides and produces the parent texture for the subsequent processes.

For ferritic stainless steels, this annealing is carried out as a batch process below the A_{c1} temperature for times that produce microstructural changes that balance the properties of the sheet being processed. The complete softening is achieved through either recovery or recrystallisation. The latter is always sought for and whether or not it is achieved depends on the hot deformation parameters and the composition of the ferritic steel.

The annealing of the ferrite phase immediately after hot deformation has had a number of studies dedicated to it. As early as the 1960s, a few studies had been carried out to establish the occurrence and kinetics of any softening processes, e.g. the work due to Gorczyca as quoted by Wusatowski [21]. The softening processes were found to have broad similarities to the phenomena occurring during the annealing of cold worked metals. The most important conclusion from these studies was the realisation that the kinetics of the softening process depended on the hot working parameters. R Wusatowski [21], working on both 18Cr – 8Ni austenitic and ferritic stainless steels, established that the kinetics of recrystallisation during the annealing after hot working exhibited the Avrami kinetics. The constants in the equation were found to vary with the anneal time, deformation temperature and the percentage reduction during the deformation. Apparently, the hot working conditions were important in determining the driving force for the recrystallisation. Indeed, R Legeut et al (as quoted in ref. 22) had demonstrated that prior deformation at temperatures higher or lower than some constant annealing temperature produced respectively slower or faster recrystallisation than that resulting from deformation at the annealing temperature. This fact was further reinforced by Glover and Sellars [22] by their work on vacuum melted and zone-refined α-iron deformed in torsion. They established that static recrystallisation in dynamically recovered structures was faster than that in dynamically recrystallised structures produced at the same working stress and temperature. They attributed this to a constant but uniformly distributed driving force in the former case compared to the latter.

Glover and Sellars [22] also established that the rate of recrystallisation increased with increasing deformation strain and strain rate. A similar observation was made by B A Hugaas, et al [23] during a study of the static and dynamic recrystallisation of a hot worked ferritic Fe – 3%Si alloy. The increased strain was thought to cause an increased internal strain and hence, stored deformation energy and also increased misorientation between subgrain boundaries.

The use of increased hot roll reduction to cause recrystallisation during the hot band annealing of ferritic stainless steels has since gained acceptance and a few papers attest to this. Shindo and Furukawa [24] employed it during their study of the colony structure and its texture. They used two samples but gave one fewer hot roll passes for the same total hot roll reduction. Hardness measurements after annealing showed that it was softer than the sample that had been hot rolled with many passes. Also, its microstructure contained recrystallised grains even in the half thickness region.

T Takeshita et al [25] simulated the hot working of a 17%Cr ferritic stainless steel using plane compression. Working in both the high temperature α-ferrite single and the (α and γ) two-phase regions, they observed that the recrystallisation of the ferrite phase increased with raising strain. Their work also highlighted the importance of a stable, hard to deform, second phase in the ferrite matrix during deformation. The particles studied here were second phase gamma and decomposition product carbides. The hard-to-deform second phase was deemed beneficial because it substantially accelerated recrystallisation. They based their explanation of this observation on Cahn's version of the Avrami equation:

$$X=1-\exp(-2.S.G.t) \qquad (13)$$

where X is the volume recrystallised, S the nucleation sites, G the grain growth rate and t the anneal time. The harder second phase was thought to increase the nucleation sites, S, because the dislocation density introduced by deformation near them, and hence the driving force, was higher. Also, in this case, the particles increased the grain growth rate, G, by purifying the ferrite matrix by lowering the C and N content in

solution. These interstitials tend to drag migrating boundaries. The importance of the time dimension in this equation was elucidated by Raabe and Ylitalo [26] in their work on the effect of hot rolling procedure on the texture of 17%Cr ferritic stainless steel. The recovery that was observed after annealing in a set of the samples for which hot rolling began in the two phase ($\alpha + \gamma$) region was attributed to the lack of hold time between rolling passes. This prohibited nucleation by limiting the incubation time.

Work done by Y D Lee et al [27] on low carbon ferritic stainless steel also established that increased rolling reduction resulted, after annealing, in increased volume fraction of recrystallised grains. They also analysed the effect of hot roll finish temperature on recrystallisation and established that low hot roll finish temperature accelerated recrystallisation during annealing. The low hot roll finish temperature resulted in the formation of deformation bands which provided nucleation sites for recrystallisation during the subsequent annealing

The encouragement of recrystallisation in ferritic stainless steels has therefore involved altering the hot deformation parameters like hot roll reduction, hot roll finish temperature and controlled rolling of the ferrite matrix in the presence of hard second phase particles. The effects could be tremendous and the recrystallisation could be obtained in a very short annealing time. For example, F. Robbe-Valloire, et al. [20] obtained recrystallisation after a 1-minute continuous anneal.

2.7: Texture in Ferritic Stainless Steel:

Apart from modifying the macroscopic dimensions of a body, deformation also changes the orientation of the crystals of the material. The orientation changes are not random because the deformation occurs on the most favourably oriented slip system. As a result, the deformed material acquires a preferred orientation, hereafter referred to as texture. The texture becomes an important parameter because it controls the formability of the final sheet.

The different physical processes encountered during thermomechanical processing impart different textures on the material and, because of their sequential nature, the texture can continuously undergo a sequential modification.

The most important textures in ferritic stainless steels (FSS) have been labelled α, γ, and η and occur as fibres, table 2.1 [28].

Fibre	Definition	Components
α-fibre	< 1 1 0> // RD	{0 0 1}<1 1 0>, {1 1 2}<1 1 0}, {1 1 1}<1 1 0>
γ-fibre	{1 1 1} // ND	{1 1 1}<1 1 0}, {1 1 1}<1 1 2>
η-fibre	< 0 0 1> // RD	{0 0 1}<1 0 0>, {0 1 1}<1 0 0> (Goss).

Table 2.1: Important textures in FSS.

The α and γ fibres contain the most important rolling/deformation textures while η fibre contains the most important shear texture [29]. They are formed to varied intensities during both the hot and cold rolling processes, [28, 30, 31, 32, 33].

The γ fibre also contains the most important recrystallisation textures. These textures are dependent on a number of factors, most importantly the rolling reductions, mode of softening i.e. whether it is recovery or recrystallisation, and the presence and/or occurrence of particle precipitation during the annealing, [28, 31, 32, 35, and 36].

2.8: Phase transformation during thermomechanical processing:

The occurrence of phase transformation results in the formation of transformation textures that have their origin in the orientation relationships between the parent and product phases of the transformation. The austenite-ferrite-martensite transformation has been found by experiment to follow the well-known Kurdjumov-Sachs relationship [31, 37]:

$(111)_{\text{austenite }(\gamma)} // (110)_{\text{ferrite }(\alpha)}$;

$[1\ -1\ 0]_{\text{austenite }(\gamma)} // [1\ -1\ 1]_{\text{ferrite }(\alpha)}$.

Phase transformation is a process that can be used to control the evolution of texture. To be effective the scheduling is controlled such that the hot rolling is carried out in a temperature range in which only a single phase is stable. The phase transformation that occurs on cooling produces a texture in which no component is prominent. This has been shown to occur in low carbon steels [28, 36] hot rolled in the austenitic temperature range. The subsequent cooling to the low temperature ferrite results in a near random texture. Also, a diffuse texture was reported for 11%Cr ferritic stainless steels as compared to their 17% counterparts subjected to a similar thermomechanical processing route [31], the reason being that the former underwent an appreciable amount of phase transformation compared to the latter whose ferrite phase is stable. This explanation shows the limitation of this method to 17%Cr ferritic stainless steels. However, compositional manipulation that allows the existence of both the ferrite and austenite phases during hot rolling could have the ferrite transforming from the austenite having a different texture from that of the non-transforming ferrite, an event that could result in a more random texture than that for a conventional ferritic stainless steel. Alloy additions that encourage higher austenite contents would amplify the situation.

The transformation textures in ferritic stainless steels, obtained before by Raabe and Ylitalo [26], are summarised below:

$\{112\}\langle 111\rangle_{\text{austenite (as deformed state)}} \rightarrow \{112\}\langle 110\rangle_{\text{martensite}}$

$\{110\}\langle 112\rangle_{\text{austenite (as deformed state)}} \rightarrow \{111\}\langle 112\rangle_{\text{martensite}}$

`2.9: Recrystallisation Anneals during thermomechanical processing:

Recrystallisation anneal processes are important not only for grain size refinement but also for controlling texture. The occurrence of recrystallisation leads to the formation of a recrystallisation texture that can be different from the preceding texture. The texture change, if it occurs, takes the form of rotation relationships that occur between particular parent and recrystallisation textures. For example, the α-fibre {112}<110> has a 35°<110>//TD [30] angle axis rotation relationship with the γ-fibre component {111}<112>. During recrystallisation the α-fibre component can be replaced by the γ-fibre component. The role of primary recrystallisation in changing textures has been found in body centred cubic metals and alloys before, [24, 26, and 30]. Here, the cold roll component {112}<110> nearly completely disappears, accompanied by growth of the recrystallisation component {111}<112>. A similar scenario was found by Raabe and Ylitalo [26] after hot band annealing 2 samples of the same heat of ferritic stainless steel that had been given different hot rolling schedules. The intensity of textures in one sample that was partially recrystallised was half the intensity in the other sample that was recovered. Also, the texture in the partially recrystallised sample was devoid of the α-{001}<110>, which was the strongest component in the recovered sample.

2.10: Surface Defects During Forming

Final sheet products of thermomechanical processing are almost always processed further by either stretching or deep drawing operations. These processes, apart from producing the final shape of the product, can also be accompanied by the formation of surface defects.

Surface roughening is a general phenomenon that affects all materials, while roping is a unique case for just a few classes of materials e.g. ferritic stainless steels. Apart from producing an undesirable surface appearance, the occurrence of these phenomena limits the amount to which the forming operations can be done.

a): Surface Roughening

Extensive literature on this phenomenon has established that the grain size is the most important parameter governing the extent to which it occurs. This is because it is caused by the grain rotation that occurs in response to an applied strain/stress. The mechanism [38, 39] is such that when the specimen is strained, surface voids nucleate and grow. At the same time, slip lines emerge and increase. Continued crystalline slipping accompanied by the contraction of the material in the thickness direction causes the surface grains to rotate in the direction of the major principal strain. Since neighbouring grains have different crystallographic orientations, strain incompatibilities exist between a grain and its neighbours. At the surface, this incompatibility causes grains to move in a direction normal to the surface, leading to roughening. The peaks and valleys in the surface profile could be a result of the shape changes due to the shear [39] that accompanies stretching.

The extent of surface roughening depends linearly on the grain size. This has been shown in experiments by Yamaguchi and Mellor, as referenced by Guangnam [38], et al and Fukuda, M et al as referenced by Becker [39]. Wilson, et al [40] found a similar relationship during biaxial stretching.

Surface roughening is only a surface effect and does not go through the thickness of a specimen. It is specific to an individual surface [41]. It is reduced by reducing the grain size. The importance of discontinuous recrystallisation, which results in small grains after annealing, is therefore obvious.

b): Ridging

Ridging, also roping, has been a well-known phenomenon for more than five decades. It forms during stretching and drawing operations as corrugations or ridges, which extend over the whole sheet, parallel to the rolling direction (RD) regardless of the direction of the stressing [42]. It is distinguished from surface defects by the fact that the transverse section of such elongated sheets displays undulations with peaks on one

side of the strip coinciding with valleys (troughs) on the other side of the strip [43, 44]. Fig. 2.8 below [45] shows the undulations that characterise a waved sheet plane, with the displacements of the opposite sheet sides occurring in the same direction. Superimposed on the wave are small ripples on a much finer scale. The waves of the profiles are not necessarily periodic. The distance between the ridges is in the millimetre range while their amplitude is in the micrometer range.

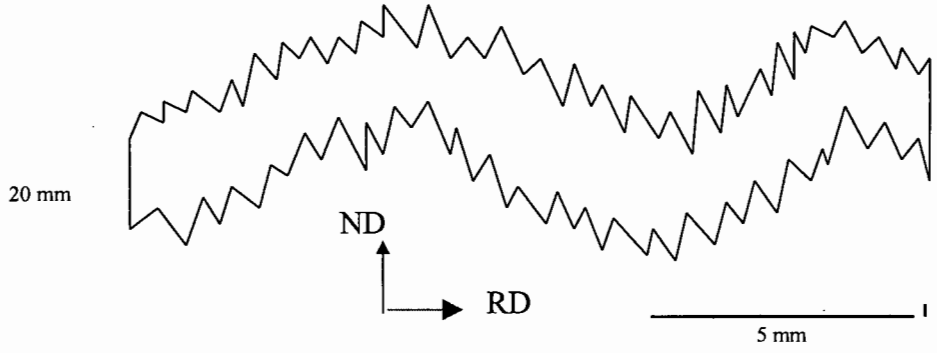

Fig. 2.8: The ridging phenomenon [45].

According to Chao [42], ridging should be expected for all directions of stressing. Experiments by Wright [44] however established that the amplitude of the characteristic transverse cross-section undulations was dependent on the orientation of the axis of the tensile strain with respect to rolling direction (RD). The amplitude was greatest for tensile elongation in the RD and decreased as the tensile axis diverged from the RD to a point where no undulations were apparent for the case of tensile elongation parallel to the transverse direction (TD). The difference in opinion seems to stem from the different proposals of the mechanisms of the ridging phenomenon.

The literature concerning the mechanisms of ridging is very extensive but it suffices to say that the cause has been attributed to the differential yielding of the sheet under tension, as a result of microstructural and/or textural inhomogeneities. Proponents of a ridging mechanism based on microstructural inhomogeneities have employed the basic Hall-Petch equation to show that these microstructural inhomogeneities will result in different stress-strain responses during tensile loading. Sheppard and Richards [41] account for ridging in a sheet obtained from hot rolled stock by citing the occurrence in bands, of austenite and ferrite. They found that scheduling processes

that led to the destruction of the bands and a homogeneous distribution of carbides resulted in a better surface quality. They argue that texture is only a contributing factor to the inheritance of the banded structure developed during hot rolling based on the fact that different textures respond to recrystallisation treatments differently because of the difference in the amount of stored deformation energy. Cube on face textures e.g. α- {1 0 0}<0 1 1> are difficult to recrystallise and help perpetuate grain size banding during thermomechanical processing.

Chao [42], Wright [44], Takechi et al [46] and Harase, et al [47] proposed mechanisms that revolved around the texture of the sheet. They employed plasticity calculations to support their arguments. A very recent mechanism based on similar arguments is that due to Wittridge [45]. At first glance, it appears to be an improvement on the mechanism due to Harase, et al [47]. The new mechanism postulates that ridging results when there is an asymmetric distribution of texture components or plastic flow properties about the mid-plane of the sheet. This arrangement initiates the development of differential transverse strains about the mid-plane when the sheet is loaded in tension. The variation in transverse strain results in turn in a series of localised bending events which, on a macroscopic level, produces longitudinal corrugations and overall ridged surface morphology. It does not require that a single texture component be clustered in large regions through the thickness of the sheet. Fig. 2.9 below illustrates the mechanism.

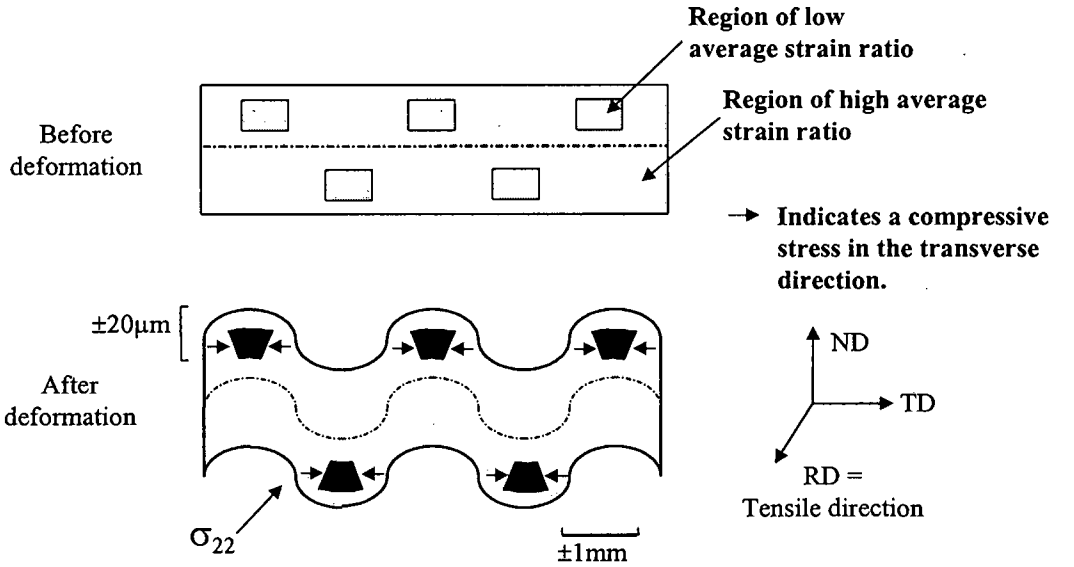

Fig. 2.9: Ridging mechanism due to Wittridge [45].

Remedial measures to counter roping strive at obtaining as much homogeneity of microstructure and texture as possible. This in effect means reducing the contribution of the individual grain, band or colony to shape changes at the surface. The measures are classified into two groups, namely controlled scheduling and selective alloying [41] and almost always, thermomechanical processing involves both. However, in all the research works sampled, [24, 41 47, 50-54], the underlying aim was to encourage recrystallisation which, when it occurred, encouraged the formation of both a favourable texture and a homogeneous microstructure made up of small recrystallised grains.

.....**END**.....

Chapter Three

EXPERIMENTAL PROCEDURES AND MATERIALS

3.1: Introduction:

The experiments had two parts. The first part was designed to study the effect of hot roll finish temperature on the microstructures produced after hot band annealing. The second part was designed to evaluate the effect of the presence and amount of austenite during hot rolling on the evolution of microstructure in the subsequent thermo-mechanical processes and on the ridging characteristics of the final sheet material.

3.2: Effect of Hot Roll Finish Temperature:

The hot roll finish temperature has been reported to have an effect on both the microstructure and texture of a hot band after annealing. Gullen and Jones [2], and D Vanderschueren et al [3], studying low carbon steels have established that a low hot roll finish temperature results in sharper textures. In a study conducted on laboratory rolled ferritic stainless steels by Wittridge and Knutsen [4], it was established that a low hot roll finish temperature led to complete recrystallisation after hot band annealing. Since the industrial problems encountered in the use of ferritic stainless steels have been established to stem from the lack of recrystallisation during hot band annealing, Columbus Stainless Steel (Middleburg, South Africa) was interested in experimenting on the effect of varying the hot-rolling schedules on the microstructure of commercial heats and to this end, they provided the materials for this exercise.

Two melts of ferritic stainless steel AISI 430 were cast to produce 2 heats of near identical composition. The heats were hot rolled after an homogenisation treatment at 1090°C for 6 hours and in each case, the finish temperature was varied to give 2

different hot rolling schedules terminating at 600°C and 800°C. The total hot roll reduction was 95%. The heats were labelled C-600 and C-800 respectively according to the aforementioned finishing temperatures. The C here stands for commercial.

The hot band annealing after hot rolling was a standard plant batch annealing treatment at 840°C for 6 hours. The samples were cropped at the end of each process stage, namely hot roll (1) and hot roll annealed (2). The alloy compositions in weight percentage are as shown in table 3.1 below.

Heat	**C-600**	**C-800**
Carbon	0.035	0.048
Sulphur	0.0047	0.007
Phosphorus	0.020	0.021
Manganese	0.62	0.59
Silicon	0.51	0.45
Copper	0.09	0.06
Cobalt	0.03	0.04
Titanium	0.006	0.006
Molybdenum	0.01	0.02
Chromium	16.53	16.57
Nickel	0.17	0.44
Aluminium	0.003	0.002
Niobium	0.008	0.008
Vanadium	0.11	0.10
Nitrogen	0.0313	0.0258
Boron	0.0003	0.0002
Tin	0.011	0.008
Antimony	0.001	0.001
Lead	0.001	0.001
Zirconium	0.001	0.001

Table 3.1: Composition of commercial heats. All values in weight %.

Microstructural evaluation was done as a metallography exercise using electron microscopy as will be highlighted below.

3.3: Effect of Gamma (Austenite) Potential:

The ferrite phase in a conventional AISI 430 has been known to recover during both hot rolling and the subsequent hot band annealing processes. The lack of recrystallisation in the latter process has been known to be detrimental to the properties of the final sheet and in particular is thought to cause the ridging problem. Suggestions have been made by several researchers e.g. H J McQueen and group (55, 56), to the effect that the presence of austenite during the hot rolling of these steels could influence a deviation in the known response of the ferrite phase to the subsequent hot band annealing. The basis of this proposition comes from the fact that the ferrite phase with its 48 slip systems is softer than the gamma-phase, which has 12 slip systems. During hot rolling, the hard austenite causes a partitioning of strain to the softer ferrite phase. This results in extensive deformation in the ferrite phase that leads to a higher amount of stored deformation energy. Also, as a result of slip incompatibility [55], the ferrite-austenite interfaces become regions of high dislocation density [56] and these regions can enhance the formation of recrystallisation nuclei in the ferrite phase.

There is also a chance that the presence of austenite could result in the development of new textures as a result of the subsequent phase transformation during cooling. The end textures would be the same regardless of the cooling sequence, that is, whether or not martensite is involved [37]. The change of textures could result in a change of the properties of the final sheet.

The materials for this part of the project were also provided by Columbus Stainless Steel. They were hot rolled in the laboratory and attempts were made to provide as similar a hot roll finish temperature as possible. Five melts of ferritic stainless steel AISI 430 were cast into ingots to produce 5 heats of different compositions. The

compositions were intentionally varied according to a computer based Medusa Model (v 3) program [1] by introducing austenite forming elements other than nickel to produce austenite potentials varying between 11 and 61%. The ingots were reheated to and stabilised at 1150°C for 3 hours before hot rolling was begun, at the same temperature. The total hot roll reduction was 88% and the samples were air-cooled after rolling. The heats were labelled A through E following the aforementioned austenite potentials. They were provided as hot bands. The chemical compositions in weight percent are as given in table 3.2.

Heat	A	B	C	D	E
Carbon	0.021	0.04	0.035	0.025	0.055
Sulphur	0.0073	0.0044	0.0067	0.0061	0.0078
Phosphorus	0.02	0.018	0.018	0.02	0.017
Manganese	0.3	0.4	0.48	0.36	0.72
Silicon	0.6	0.69	0.59	0.31	0.32
Vanadium	0.13	0.14	0.13	0.09	0.09
Copper.	0.03	0.03	0.03	0.05	0.04
Nitrogen.	0.019	0.04	0.048	0.084	0.082
Cobalt	0.03	0.02	0.03	0.02	0.03
Titanium	0.005	0.008	0.005	0.009	0.007
Molybdenum	0.01	0.01	0.01	0.01	0.01
Chromium	16.73	16.06	16.69	16.16	16.16
Nickel	0.23	0.21	0.23	0.21	0.21
Aluminium.	0.002	0.003	0.002	0.002	0.002
Niobium.	0.008	0.002	0.008	0.001	0.008
Boron.	0.0008	0.0012	0.0008	0.0018	0.0018
Tin.	0.005	0.004	0.005	0.004	0.004
% Gam. Pot.	11.7	25.5	29.1	40.2	61.2

Table 3.2: Chemical composition of laboratory heats in wt. %.

Although all the compositions are included in Table 3.2 and the relevant transformation temperatures were also determined for all the compositions, only heats A and E were selected for detailed microstructural and ridging analysis. This was primarily due to the amount of time required for the microstructural analysis.

3.3.1: Dilatometry:

Dilatometry experiments were done to determine the Ac_1 transformation temperatures for all the laboratory heats using dilatometric equipment in the department that had been constructed in a previous project. Specimens of square cross-section 2.5 by 2.5-mm and 50 mm long were used. The experiments were carried out under a vacuum and involved an initial heating rate of 20°C/min from room temperature to 600°C. Thereafter, the heating rate was 1°C/min for a temperature increase up to 1000°C. The change of heating rate was meant to enable good accuracy in determining the phase transformation temperatures. The dilatometer consisted of a K-type thermocouple for measuring temperature and a digital displacement transducer to monitor and record extension. Data acquisition was by a Windows based Diladata computer program [57] that also generated extension-temperature graphs that were used to determine Ac_1 temperature according to J Cure [58]. Fig. 3.1 below shows a typical dilation curve obtained in the temperature range near the A_{c1} for heat E.

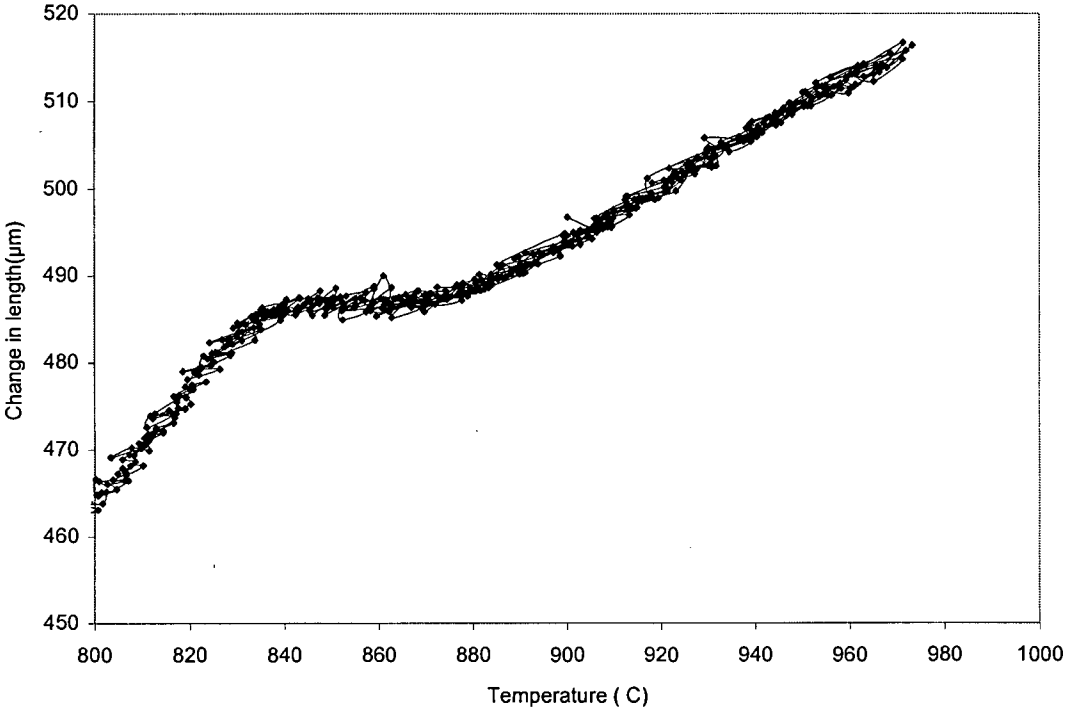

Fig. 3.1: Typical dilation curve for heat E near the A_{c1}.

Table 3.3 below summarises the Ac_1 temperatures.

Heat	Ac_1 temperature (°C)	Hot band annealing temperature (°C)
A	930	880
B	906	850
C	908	850
D	874	820
E	832	780

Table 3.3: Approximate Ac_1 temperatures of the laboratory heats.

3.3.2: Hot band annealing:

The annealing of the hot bands during the processing of ferritic stainless steels has been known to be advantageous for two reasons. Apart from allowing complete softening for the subsequent cold rolling, it also dictates the amount, size and distribution of any precipitates that may form [19]. This latter process could become an important factor in influencing the evolution of microstructure and texture during final recrystallisation, by causing particle stimulated nucleation. However, the concurrent precipitation and softening during hot band annealing could result in a slowing down of the softening processes [25].

Hot band annealing was done only for laboratory rolled heats A and E. It was carried out in a Naber Industrieofenbau D-2804 Lilienthal/Bremen laboratory furnace as an isothermal process. According to conventional practice, the annealing was done below the Ac_1 temperature, with an approximate 50°C margin as shown in table 3.3. The annealing times were chosen to be 10 min, 30 min, 2, 5, 10 and 20 hours. The extreme times could be used to simulate line and batch annealing processes. Prior to loading the samples, the furnace was heated up to the annealing temperature and left for 30 minutes to stabilise. The samples would then be loaded and left to stabilise for five minutes before starting to count the annealing time in order to take into account heat up time as was calculated by Matheson [57]. Samples were cropped after each

annealing time for microstructural evaluation. A sample from heat A was cropped after annealing for 20 hours for orientation measurements. A similar exercise was done for heat E in the as-hot-rolled condition and after hot band annealing for 10 hours.

3.3.3: Cold Rolling and final recrystallisation:

The samples for cold rolling were the laboratory heats that had been given hot band annealing treatments of 10 minutes and 20 hours at their respective annealing temperatures. Laboratory rolling was carried out on a Sundwiger Eisenhutte, W-A5EL laboratory rolling mill at the Columbus Stainless Steel plant in Middleburg. The total cold roll reduction was 80%.

Final recrystallisation was a standard treatment at 820°C for 10 minutes in a Naber Industrieofenbau D-2804 Lilienthal/Bremen laboratory furnace followed by air-cooling. The specimens were loaded only after the furnace was stabilised at the annealing temperature for 30 minutes and counting of time was begun 5 minutes after loading. The samples were then cropped for microstructural evaluation and for ridging tests.

3.3.4: Metallography:

The microstructures of all the specimens were characterised using Electron Channelling Contrast (ECC) obtained in the scanning electron microscope. This method had been shown to be the most economical by Wittridge and Knutsen [4]. They showed that optical microscopy failed miserably to produce any discernible detail while TEM metallography gave the same information but at the cost of longer specimen preparation and samples much less representative of the bulk material.

The interpretation of the ECC images was based on the contrast differences created by the presence of dislocations and misorientation in a microstructure. A uniform

contrast is obtained when a structure is relatively dislocation free. A change in contrast is produced by a misorientation across a boundary. High angle boundaries produce a more abrupt and definite contrast change compared to low angle boundaries. When dislocation arrangements are diffuse either as a result of poorly formed or coalescing subgrain boundaries, then a "mottled effect" is produced.

Conventional metallographic techniques were used to prepare the samples. An automatic polishing machine, a STRUERS A/S, was used to grind the specimens up to a 4000 grit silicon paper and for final polishing. The ECC technique requires that the sample is in the polished condition but without the deformed surface layer. The removal of this layer was achieved by electrolytic polishing after final mechanical polishing. The electrolytic reagent was a solution of 10 ml of perchloric acid in 200-ml acetic acid. The temperature was maintained below 20°C. A stainless steel cathode was used and the specimen was anodically polarised at 26 V d.c. for two minutes. Care was taken to avoid overpolishing which could introduce topographical effects.

Electron channelling contrast images were acquired via a solid state annular backscatter electron (BSE) detector (KE Developments Ltd.) fitted to a Cambridge S200 scanning electron microscope (SEM). Typical images were obtained at a primary accelerating voltage of 25kV with a conventional tungsten filament providing the electron source. Occasionally, a LEICA 440 SEM fitted with a lanthanum hexaboride (LaB_6) filament was used to enhance the resolution of the image at higher magnifications. Again, the images were acquired via a solid state annular BSE detector at an accelerating voltage of 25 kV. The working distance was kept to less than 15 mm to enhance the collection of the back scattered electrons and hence to improve the quality of the images.

Metallographic sections were prepared in the longitudinal (RD-ND) orientations as illustrated below and all micrographs in this thesis represent this orientation (RD = longitudinal, ND = vertical).

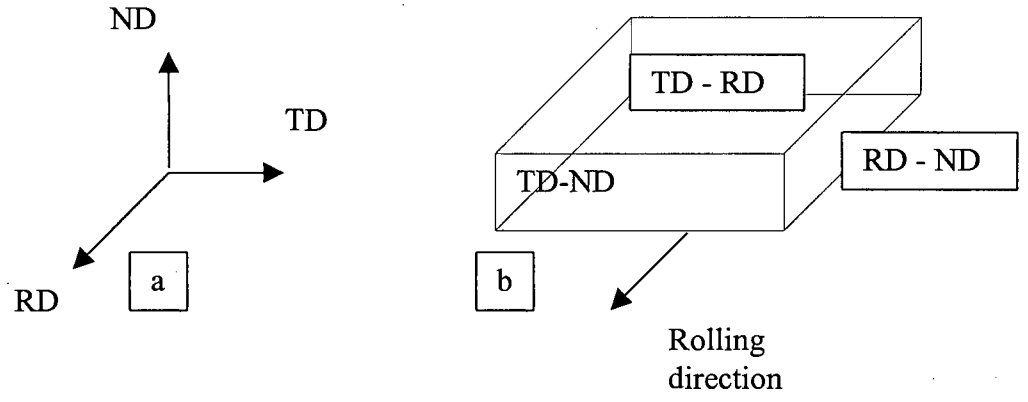

RD: Rolling direction: ND: Normal direction; TD: Transverse direction

Fig. 3.2: Definition of a) axes and b) planar section notation.

Attempts were made to quantify the grain size of the specimens after final recrystallisation. For each sample, SEM micrographs taken at two different magnifications and fields of view were employed. In light of some of the samples having banded microstructures, some measurements were given both as an overall average value and ranges quoting the lowest and highest values. The average value was computed using a circle and the ranges were obtained using directed straight lines as Heyn test lines. The values for the ranges are quoted as averages of readings obtained from four test lines.

3.3.5: Misorientation Measurement:

The measurement of local misorientations was done for heat A after 20 hours hot band annealing and heat E in the as-hot-rolled condition and after 10 hours hot band annealing. The areas of interest were both the prior martensite regions that had acquired a grain-like appearance, the elongated ferrite grains with a mottled contrast and the ferrite grains that contained subgranular structures after the annealing. The objective was to determine whether the regions were recovered or recrystallised by determining the level of misorientation between neighbouring points.

Use was made of a manual microtexture measurement system installed on a LEICA 440 SEM similar to the one used in Ref. 45. Fig. 3.3 below shows a schematic diagram of the set-up of the components.

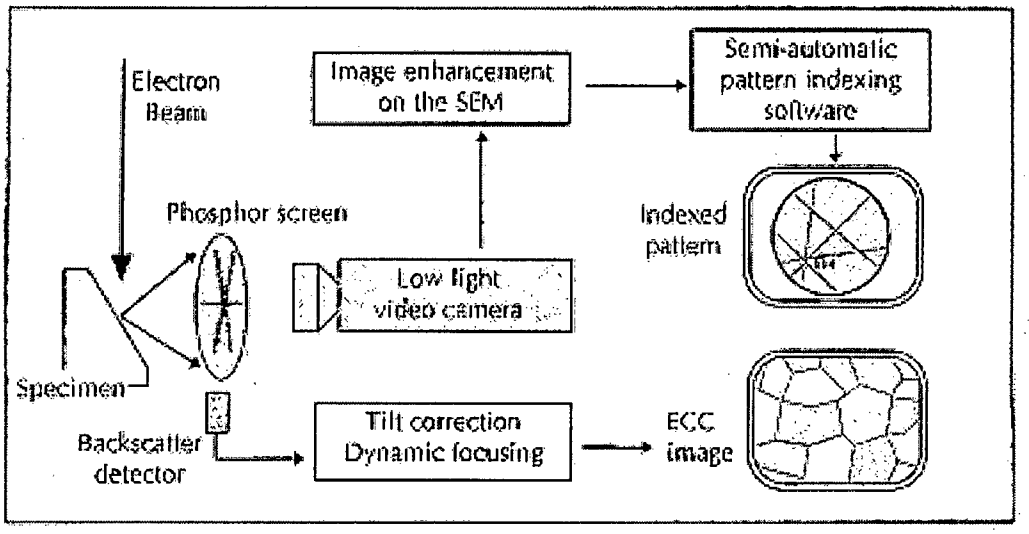

Fig. 3.3: Schematic of manual microtexture measurement [Ref.45].

The sample was loaded and the regions of interest were selected. Orientations were measured by positioning the electron beam within individual regions and the corresponding electron backscattered diffraction (EBSD) pattern was analysed. The beam was then moved to the neighbours of the point in question and the patterns obtained were qualitatively compared. For some regions the orientation data was stored in Miller index (hkl)<uvw> notation and Euler angle representations. They were then fed into another computer program for post processing to provide minimum misorientation curves. The minimum misorientation curves were evaluated as the relative misorientation between neighbouring orientations. Misorientations associated with recovered structures were considered to fall within 15°.

3.3.6: Texture measurements:

Bulk texture measurements were made in order to provide information about the microscopic processes that occurred as a result of the presence of austenite at rolling temperatures. Since the rolling and recrystallisation textures of a conventional ferritic

stainless steel and their development mechanisms are well known, any deviation would be deemed to stem from the austenite. The measurements were carried out on the sheet products after final recrystallisation. The sheets were obtained from samples that had been hot band annealed for 10 minutes and 20 hours. The near mid-section planes were used because they are more representative of the textures in the sheets.

The measurements were performed at MINTEK (Council for Mineral Technology, South Africa), using a Siemens D500TT X-ray diffractometer fitted with a molybdenum anode tube and an Euler cradle. Textures were quantified via incomplete pole figures measured from an area of approximately 14 mm^2 using MoKα_1 radiation in back reflection mode.

Due to the orthorhombic symmetry of the samples, the textures were represented in a reduced Euler space using angles φ_1, φ, and φ_2. Orientation distribution functions (ODFs) were calculated from the three incomplete pole figures (110), (200) and (211) using the series expansion method (l_{max} = 22) [59]. Only φ_1 constant sections at intervals of 5° were plotted. Density contours were plotted at 15% intervals where the contour value represents a percentage of the maximum "times random" value. Fibre diagrams demonstrating the major texture components along the α and γ fibres were also constructed.

3.3.7: Ridging Tests:

Ridging tests were conducted on cold-rolled-annealed laboratory heat specimens that had been hot band annealed for 10 minutes and 20 hours. The specimens were machined to produce 0° tensile axis (parallel the RD) and 90° tensile axis (parallel TD) orientations. A gauge length of 50 mm and a width of 28 mm were used. The thickness was approximately the final gauge thickness, which was about 1.4 mm for heat A and 0.98mm for heat E samples

The surface of each specimen was finally mechanically polished with 1μm diamond paste to produce a surface smooth enough for surface profilometry. Tensile tests were carried out using a ZWICK universal tester equipped with a 200kN-load cell. Care was taken to correctly align the specimen axis with the machine axis. The test strain rate was 10^{-3} per second and the specimens were pulled to 20% strain. After the tests, the surface topography of the deformed samples was qualitatively characterised using an arbitrary visual rating scale. A Surtronic 3P surface analyser was used to obtain a surface roughness value for each specimen and to record corresponding upper and lower surface profiles for further characterisation of the variations in thickness.

.....**END**.....

Chapter Four

RESULTS

4.1: Effect of Hot Roll Finish Temperature:

(Heats C-600 and C-800)

The effect of hot roll finish temperature on the microstructures produced after hot rolling and the subsequent hot band annealing was studied using electron channelling contrast (ECC) in the scanning electron microscope. The interpretation of the microstructures was based on contrast effects as described by Wittridge and Knutsen [4]. Diffuse boundaries are generally associated with subgrains, whereas high angle grain boundaries produce sharp contrast.

4.1.1: Microstructures of the as-hot-rolled samples:

Fig. 4.1 (a) shows the general microstructure of heat C-600 in the hot rolled condition. The grain boundaries in the microstructure could not be discerned, the overall appearance was mottled and material flow lines, characteristic of cold deformation could be seen. A subgranular structure and bands of martensite like stringers emerged at high magnification, as shown in fig. 4.1 (b) below.

(a). General microstructure

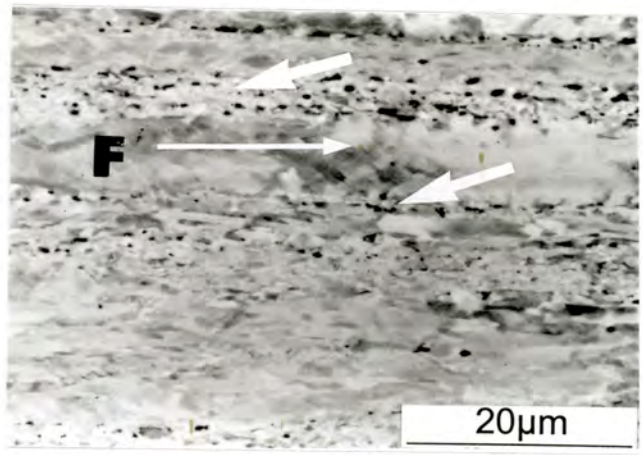

(b). Subgranular structure at high magnification.
Big arrows show bands of martensite stringers; Region **F** is an example of a highly deformed ferrite grain.
Fig. 4.1: Microstructure of commercial heat C-600 in the as-hot-rolled condition.

The microstructure for heat C-800 contained bands of regions with well-formed grain structures bordering thin elongated regions that resembled stringers of martensite. In addition, it was observed that there was a variation in the evolution of microstructure in the regions with well-formed structures as a function of the distance from the surface. Recrystallisation was observed near the surface but its intensity decreased rapidly with distance towards the centre, fig. 4.2 (a) below. Fig. 4.2 (b) shows the microstructure near the centre. The predominance of low angle boundaries in vastly elongated ferrite grains is obvious. It also shows that the martensite-stringers have a lath structure.

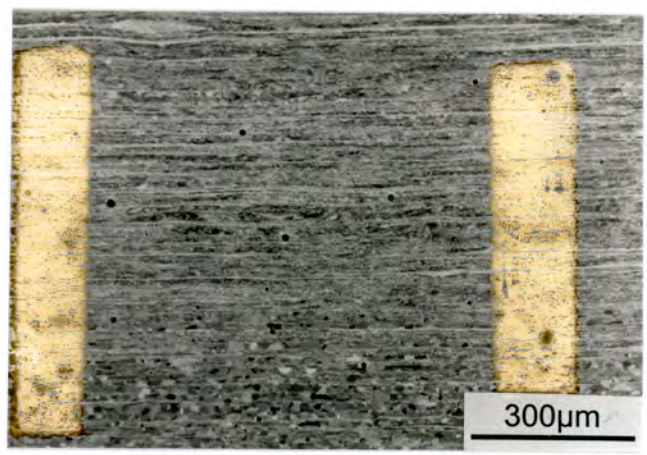

Near surface is low part of micrograph.
a): General microstructure of heat C-800.

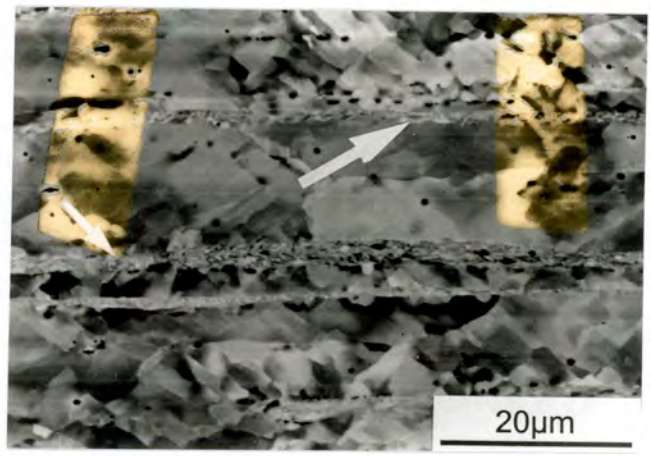

b): Low angle boundaries and lath-like structures
Arrows show thin bands of martensite

Fig. 4.2: Microstructure of commercial heat C-800 in the as-hot-rolled condition.

4.1.2: Microstructures after Hot Band Annealing:

The annealed microstructure of heat C-600 was made up of fully recrystallised, slightly elongated grains. Large and small grains occurred but grain size banding was not obvious. There was a small gradient in grain size moving from the surface to the centre where grains slightly increased in size. Fig. 4.3 below shows the general microstructure.

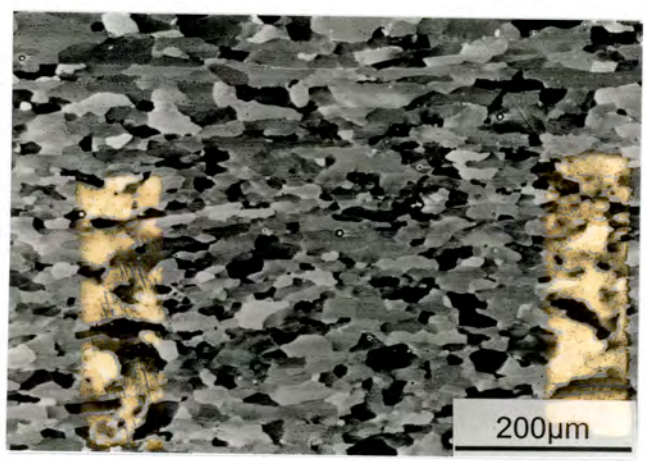

Fig. 4.3: Microstructure of heat C-600 after hot banding annealing.

The annealing produced varying degrees of recrystallisation in the microstructure of heat C-800. Near the surface, the microstructure was fully recrystallised and was made up of small grains, while near the centre, elongated recrystallised grains occurred alongside narrow recovered regions. Grain size banding was prevalent and the grain size gradient from the surface to the centre was very obvious, fig.4.4 below.

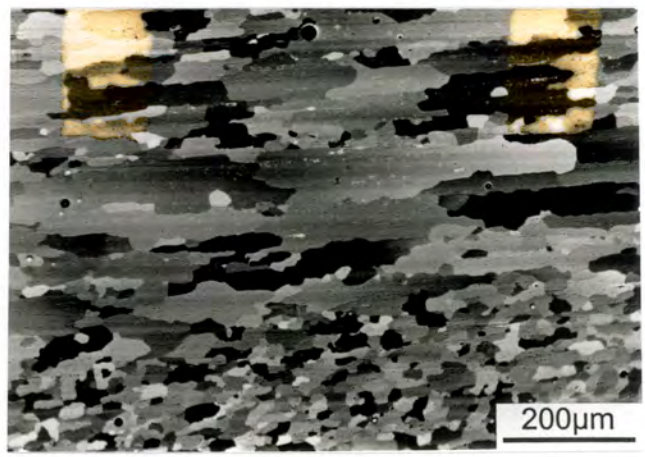

a). Microstructure near surface
Lower part of micrograph shows subsurface region

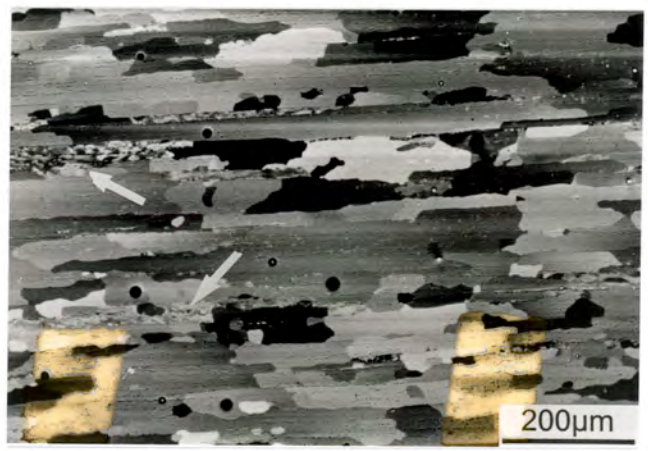

b). Microstructure near centre.
Arrows show recovered regions.

Fig. 4.4: Microstructure of heat C-800 after hot band annealing.

4.2: Effect of Austenite Content:

(Laboratory Heats A and E)

4.2.1: Microstructures After Hot Band Annealing

The effect of austenite content on evolution of microstructure with annealing time was studied for heats A with an austenite potential of 11% and E with an austenite potential of 61% using electron channelling contrast (ECC) in the scanning electron microscope. The interpretation of the microstructures was based on contrast effects as described by Wittridge and Knutsen [4]. Diffuse boundaries are generally associated with subgrains, whereas high angle grain boundaries produce sharp contrast. In view of this, selective orientation measurements have been performed using electron backscattered diffraction (EBSD) pattern analysis. These measurements have assisted in confirming the overall microstructure developments.

4.2.1.1: Heat A:

The hot rolled microstructure consisted predominantly of large ferrite grains and martensite stringers whose structure appeared lath like. This general microstructure is represented in fig. 4.5(a). The ferrite structure far from martensite stringers had elongated low angle grains while in the vicinity of the stringers, the ferrite subgrains were smaller and equi-axed. Fig. 4.5(b) shows the size of primary ferrite subgrains near a martensite stringer while fig. 4.5(c) shows the size of the subgrains between martensite stringers. No incidence of recrystallisation was observed in the microstructure.

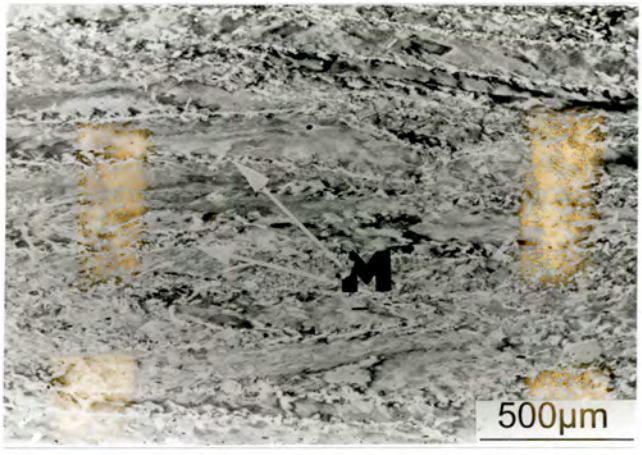

M are martensite stringers in ferrite matrix
a):General microstructure showing ferrite grains and martensite stringers

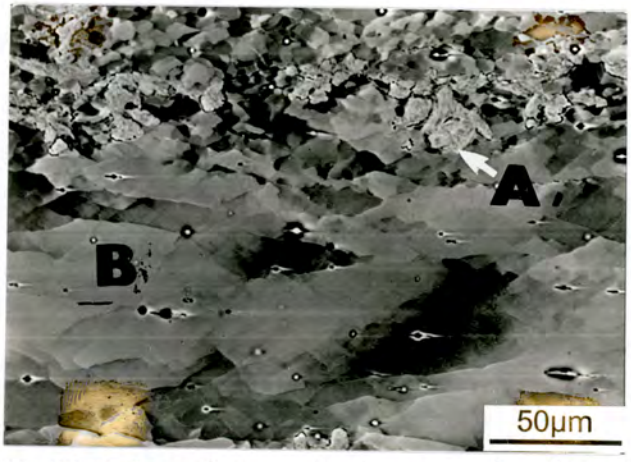

(b): Variation of subgrain size as a function of distance from a martensite stringer
A shows martensite stringer; **B** shows subgrains in primary ferrite grain

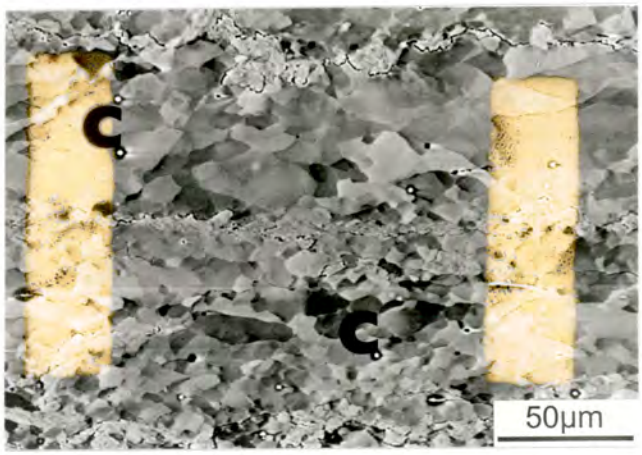

(c): Size of subgrains in primary ferrite that comes between martensite stringers.
C shows subgrains in primary ferrite grains between martensite stringers. Note that they are smaller compared to those in region **B** of (b) above.
Fig. 4.5: Low angle grain boundaries in primary ferrite. (Hot rolled condition)

ANNEALING AT 880°C

After annealing for ten minutes, the subgrains in the prior ferrite, away from the martensite stringers became fuzzy, exhibiting a phenomenon popularly called mottling, [4],(fig. 4.6(a)). Near the martensite stringers, the subgrains had a comparatively better definition. There was an occasional static recrystallisation event in the primary ferrite between prior martensite stringers as shown in Fig 4.6 (b). The martensite was tempered and stringers of fine subgrains could be seen.

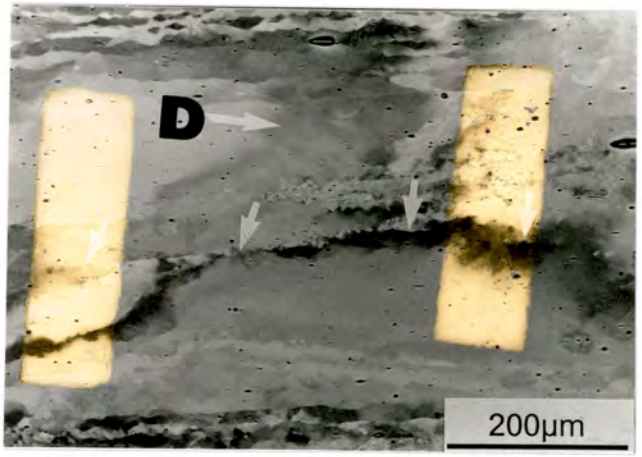

a). Mottled effect in some prior ferrite subgrains. (10 minutes)
Arrows define approximate high angle boundary; Region **D** shows example of mottled effect

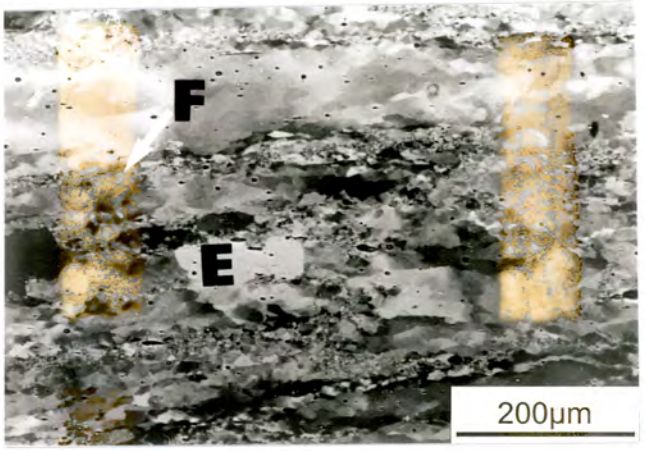

b). Statically recrystallised grains and fine subgrains of tempered prior martensite (10 min)
E shows static recrystallisation in primary ferrite; **F** shows stringer of fine subgrains from prior martensite
Fig. 4.6: Microstructure after annealing for ten minutes.

Annealing for 30 minutes resulted in more recrystallisation events in the prior ferrite regions with the grains appearing elongated in the rolling direction (RD). The

fuzziness in most of the primary ferrite grains was seen to persist even though the structure seemed to be getting more organised. These subgrains were elongated and their boundaries were straight and ran parallel the rolling direction (RD), Fig 4.7(a). Fig. 4.7 (b) shows a large elongated primary ferrite grain with subgrains having boundaries that are getting clearer. The upper part shows some recrystallised grains. Bands of subgrains from prior martensite can also be seen and are bigger compared to those in Fig. 4.6 (b).

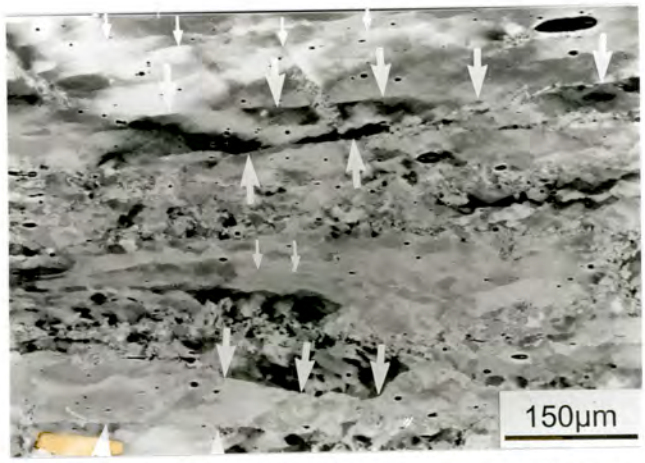

a). Straight boundaries in the subgrains of primary ferrite
Bigger **arrows** show original grain boundaries; **S**maller **arrows** show straight subgrain boundaries

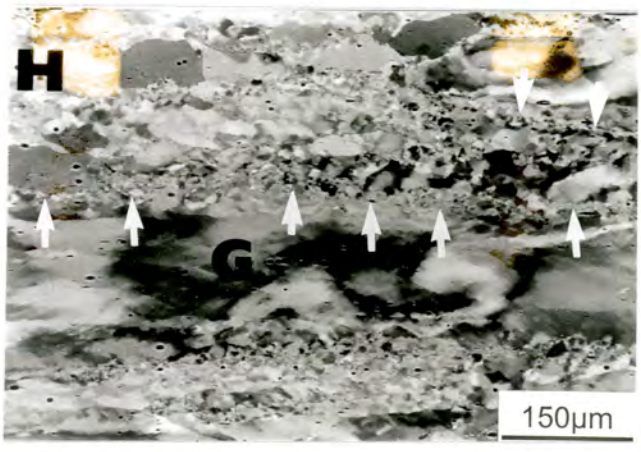

b). Recrystallisation events in primary ferrite grains and stringers of subgrains from prior martensite.
Arrows mark stringers of subgrains from prior martensite; **G** is a large elongated primary ferrite grain exhibiting mottling; **H** shows a string of statically recrystallised primary ferrite grains
Fig. 4.7: General microstructure after 30 minutes.

The level of recrystallisation in the primary ferrite did not seem to change much after annealing for 2 hours. Growth of the recrystallised primary ferrite grains in the normal direction (ND) was minimal and the grains were elongated in the RD. There was an increased perfection of the substructure in the unrecrystallised primary ferrite grains. The subgrains consisted predominantly of boundaries running parallel to RD. The mottling effect was increasingly becoming rare, fig. 4.8 (a). The primary ferrite grains near prior martensite stringers were seen to be bigger. The average size of the subgrains in prior martensite did not change much. There was however the occasional tendency for some subgrain boundaries to become diffuse, fig. 4.8 (b).

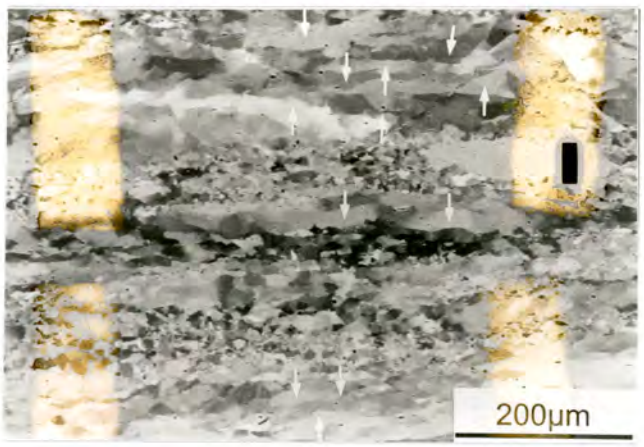

a). More organised subgrains in primary ferrite
Arrows show examples of subgrains in primary ferrite grains having clear boundaries; **I** is an elongated recrystallised primary ferrite grain that is not showing growth in the normal direction (ND).

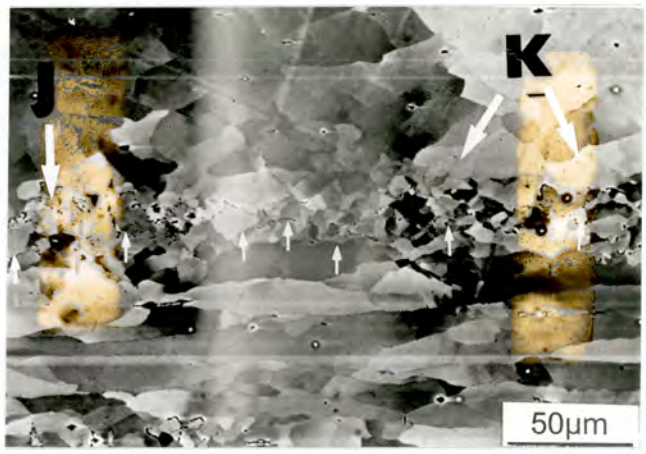

b). Blurring of subboundaries of subgrains in prior martensite.
Small **arrows** show some subgrains in stringer of subgrains from prior martensite; **J** shows an example of a region where subgrain boundaries are fuzzy; **K** shows an example of larger subgrains in primary ferrite next to martensite stringer that have replaced initially smaller subgrains
Fig. 4.8: Microstructure after annealing for 2 hours.

Straight long boundaries became prominent in the primary ferrite after annealing for 5 hours. It is thought that these were the original high angle grains before rolling which have become more pronounced as a result of the decreased mottling effect. The subgrains of primary ferrite near martensite stringers were increasingly being replaced by a continuous subgrain-free region, fig. 4.9 (a). The subgrain boundary fuzziness observed after annealing for 2 hours had cleared. The fuzziness of some of the boundaries of subgrains in prior martensite regions continued, fig. 4.9(b).

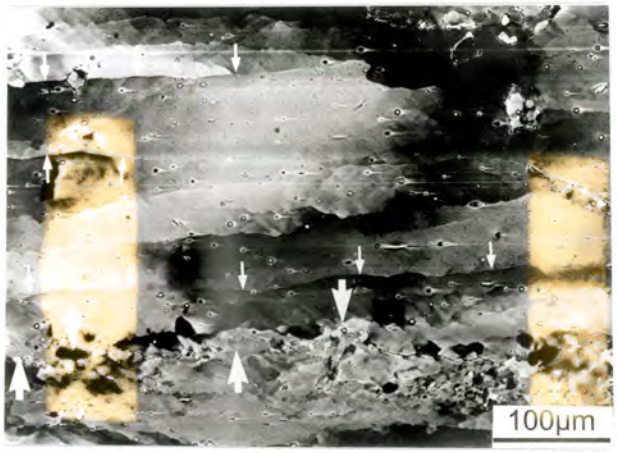

a). Straight boundaries in the grains of prior ferrite.
Small **arrow**s show straight original high angle boundaries in primary ferrite; **B**ig **arrow**s show stringer of subgrains from prior martensite.

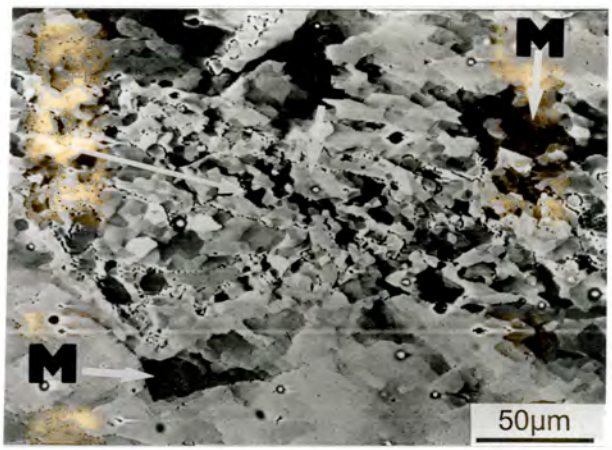

b). Continued fuzziness of boundaries of the subgrains in prior martensite.
Long **arrow** shows direction of prior martensite region; Region **L** is an example showing subgrains in the martensite; **M** shows a few of the remaining subgrains in primary ferrite bordering martensite stringer.
Fig. 4.9: Microstructure after annealing for 5 hours.

The ferrite did not generally change much after annealing for 10 hours and the microstructure here was not appreciably different from that after 5 hours, Fig. 4.10 below. However, the ferrite subgrains between martensite stringers coalesced to produce elongated narrower grains. These grains contained fading subgrain boundaries and appeared mottled. A qualitative analysis of the relative change of

Kikuchi patterns carried out in this regions revealed minimal pattern changes showing that they were at a very advanced stage of recovery.

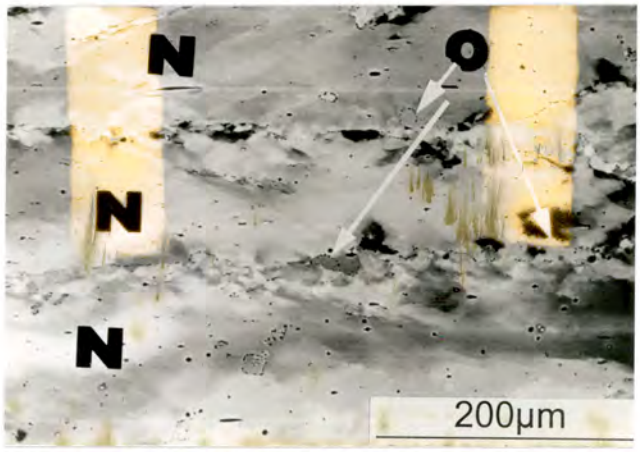

Subgrains in primary ferrite near martensite stringer.
N shows narrower elongated ferrite grains from primary ferrite regions originally between martensite stringers; **O** is tempered martensite stringers.
Fig. 4.10: Subgrains in primary ferrite (10 hours).

Incidences of recrystallised grains in the prior martensite stringers could be seen after annealing for 10 hours and were seen as grains having a sharp contrast. These grains formed with patterns of black dots, thought to have been carbides, in their interiors, fig. 4.11(a). Fig 4.11(b) shows the resulting overall microstructure in which bands of small grains occur alongside big elongated primary ferrite grains.

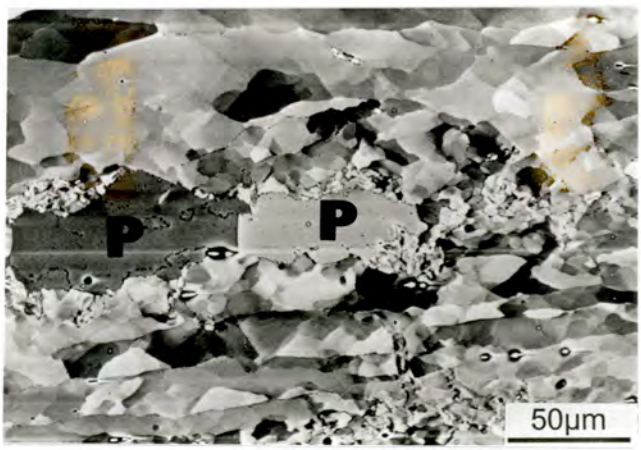

a). Recrystallisation in prior martensite
P are recrystallised grains in prior martensite. Note that they contain patterns of dots that correspond to shape of subgrains that were replaced.

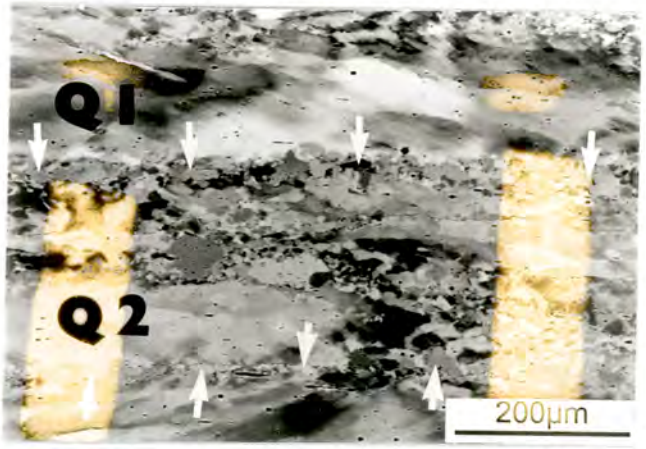

b). Bands of small grains from prior martensite
Arrows show some of the grains in stringer of grains from prior martensite stringers; **Q1** shows a large mottled primary ferrite grain while **Q2** shows a primary ferrite grain that still contains subgrains.
Fig. 4.11: Grains from prior martensite (10 hours).

Annealing for 20 hours did not seem to produce any change in the primary ferrite grains. Elongated subgrains with straight boundaries could still be seen as were grains with a mottled contrast. These were grains in which subgrain coalescence was very advanced to the point where subgrain boundaries were indiscernible. A few subgrain free grains were also seen, Fig. 4.12(a). Fig. 4.12(b) shows the general microstructure. This microstructure consists of primary ferrite grains that have undergone continuous recrystallisation, mottled primary ferrite grains, and prior martensite stringers that have both recovered and recrystallised. The determination of misorientation in the primary ferrite regions revealed that the grains with a mottled contrast had a near constant Kikuchi pattern. Fig. 4.12(c) shows a sample region that was evaluated. A linescan carried out in a region with subgranular structures produced the relative misorientation curve in Fig.4.12(d). The relative misorientation was observed to be low, in the range of low angle grain boundaries.

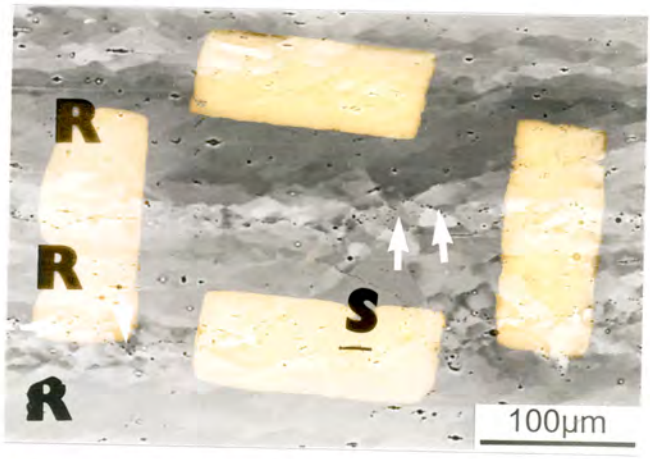

a). Network of subgrains in prior martensite stringers (20 hours). **Arrows** show grains from prior martensite stringer; **R** shows elongated primary ferrite grains; **S** shows a clean subgrain free.

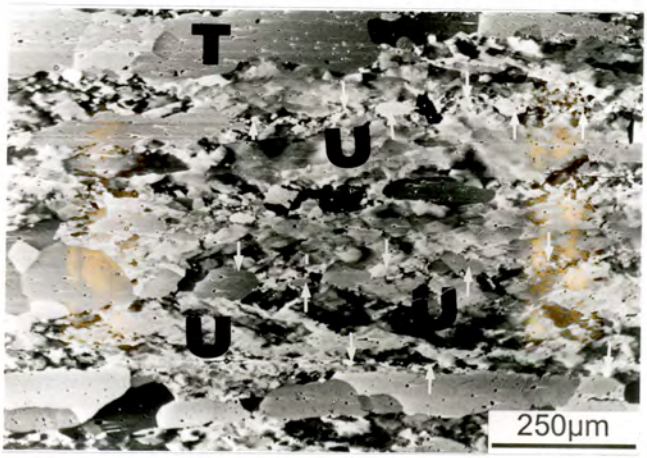

b). General microstructure (20 hours)
Arrows show prior martensite stringer now made up of recrystallised and recovered regions; **T** is a continuously recrystallised primary ferrite grain; **U** are mottled primary ferrite grain

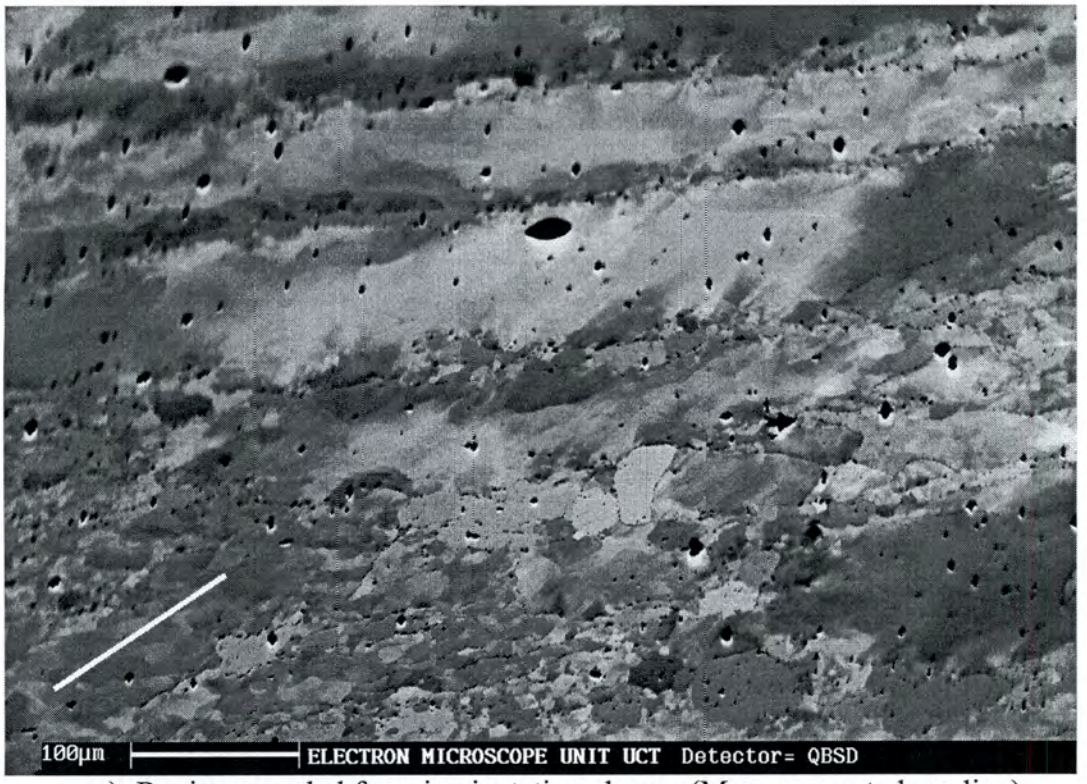

c): Region sampled for misorientation change (Measurement along line).

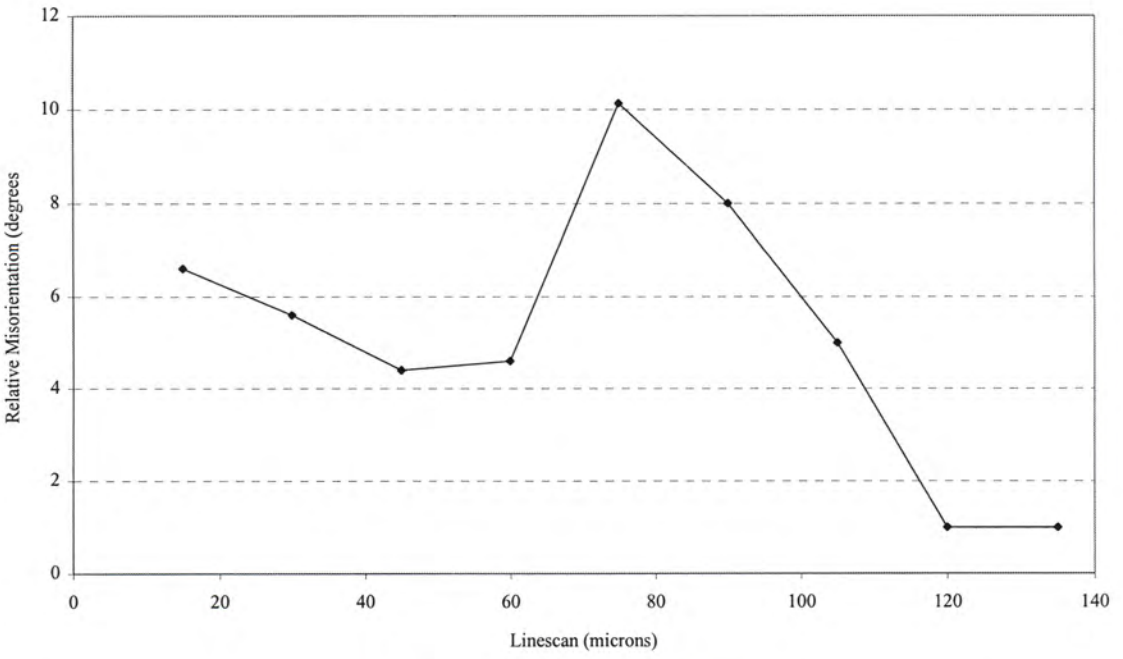

d): Relative misorientation curve of sampled region in c) above.
Fig. 4.12: Microstructure after annealing for 20 hours.

In summary, after annealing for 20 hours, the primary ferrite exhibited limited continuous recrystallisation and extensive extended recovery. The prior martensite

stringers underwent both recovery and recrystallisation. The microstructure produced consisted predominantly of elongated grains.

4.2.1.2: Heat E:

The hot rolled microstructure consisted of layers of lath martensite and elongated ferrite grains that had clearly delineated equi-axed subgranular structures as shown in Fig. 4.13 (a). Fig. 4.13 (b) shows a region where Kikuchi pattern evaluations were carried out in order to determine the state of the subgranular structures in the ferrite grains. This was carried out as a linescan, with points spaced 5 microns apart. Three rows, also 5 microns apart, were evaluated. Fig. 4.13 (c) shows the relative misorientation curves for each row. The trend in the relative change of the minimum orientation from one data point to the next along each row is for it (change) to be relatively low, certainly less than 15°. This observation shows that the subgranular structures were subgrains. The high change in the vicinity of 45μm in each row is thought to represent an original high angle grain boundary.

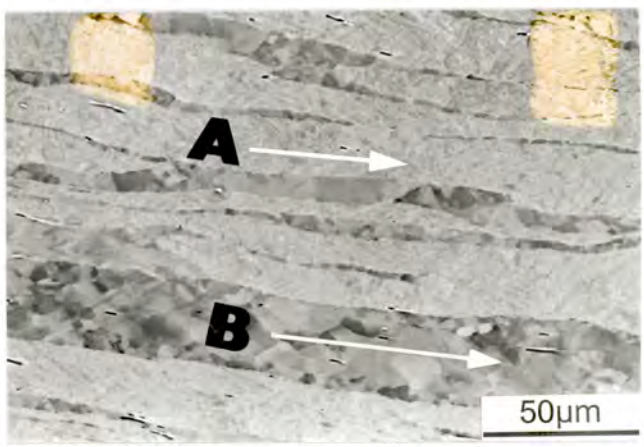

a): SEM micrograph of hot rolled "E"
A shows a martensite region; **B** shows fine subgrains in ferrite band.

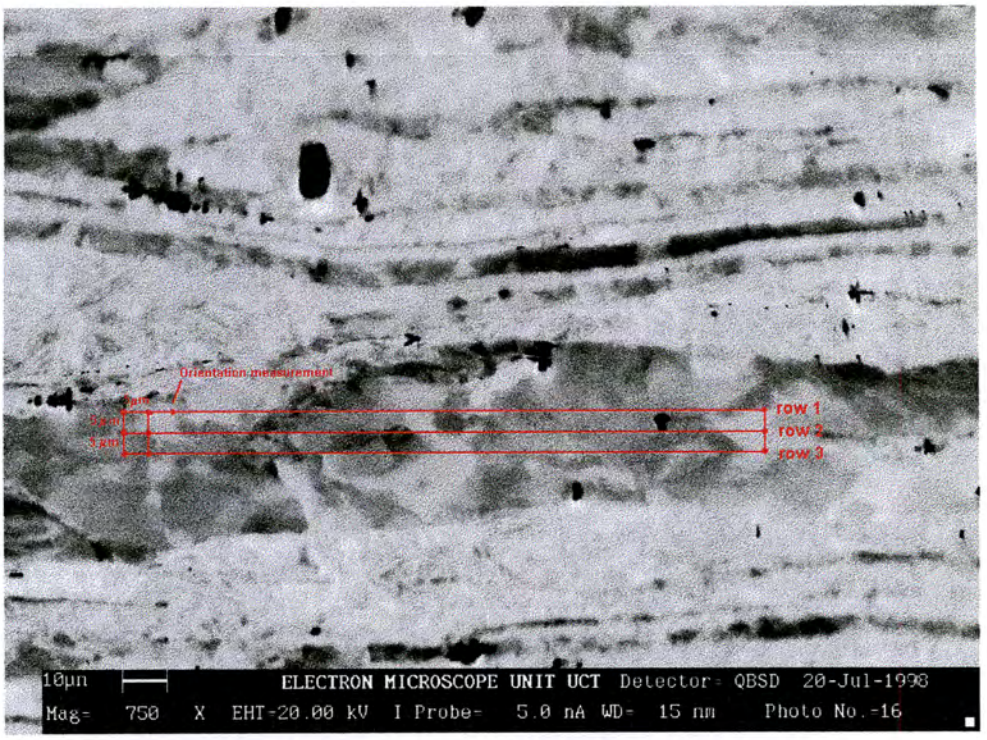

Data File Names: Hote-r1 (row 1), Hote-r2 (row 2), Hote-r3 (row3).

Sample E Hot Rolled Condition

b): Ferrite region sampled for misorientations.

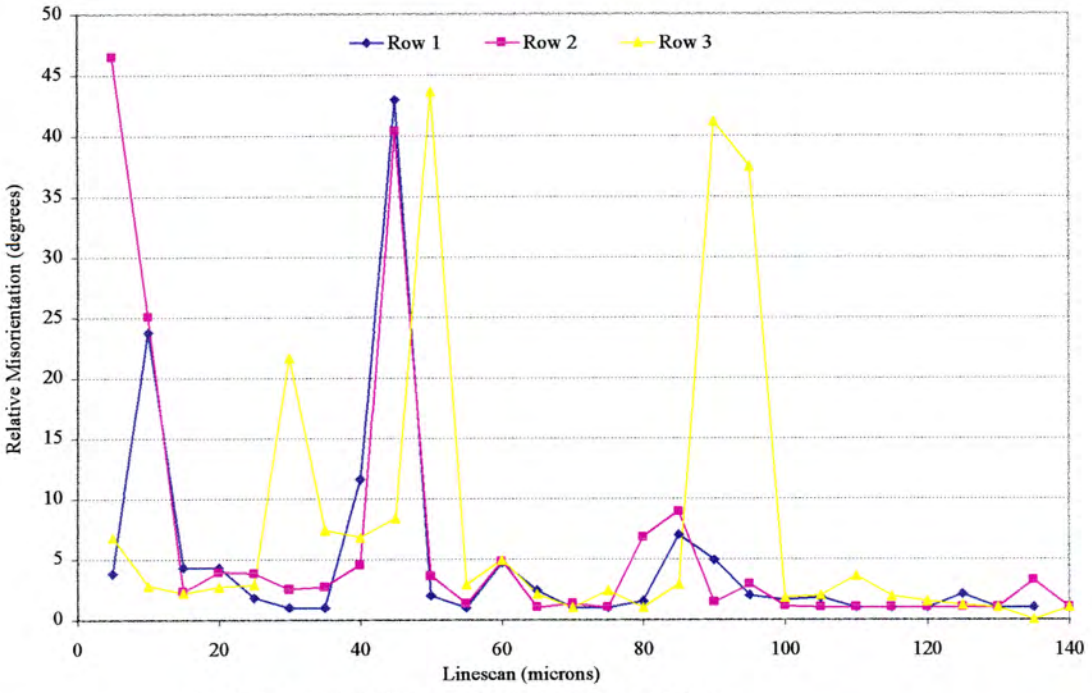

c): Relative misorientation curve for ferrite region in b) above

Fig. 4.13: Microstructure and misorientation in the ferrite phase of hot rolled `E`.

ANNEALING AT 780°C:

Annealing for 10 minutes produced well-formed subgrains in the microstructure of the martensite. Sections of a few of the elongated primary ferrite grains seemed to clear up, losing subgrains in the process to acquire the appearance of recrystallised grains. However, this was a rare occurrence and except for the appearance at the subgrain boundaries of dark spots, which were thought to be carbo-nitride precipitates, the bulk of the subgrains resembled those in the hot rolled condition. Precipitation was however most pronounced along the major grain boundaries. These processes were better picked up after annealing for 30 minutes as shown in Fig. 4.14 below. Here, a few of the primary ferrite regions appear mottled after their subgrains coalesced to the extent of disappearing. This was accompanied by an increased occurrence of precipitation along some subgrain boundaries and a copious precipitation along all the high angle grain boundaries. The martensite became tempered and acquired a subgranular structure with the subgrains forming in the direction of the lath units. In some regions however, the delineation of the subgrains was fuzzy. A few cases of precipitation along lath boundaries could be seen, as were regions that did not contain any subgrains. The latter regions were thought to have been recrystallised. They seemed to bulge into tempered martensite regions. The curved boundaries between these recrystallised and tempered martensite will hereafter be referred to as recrystallisation fronts.

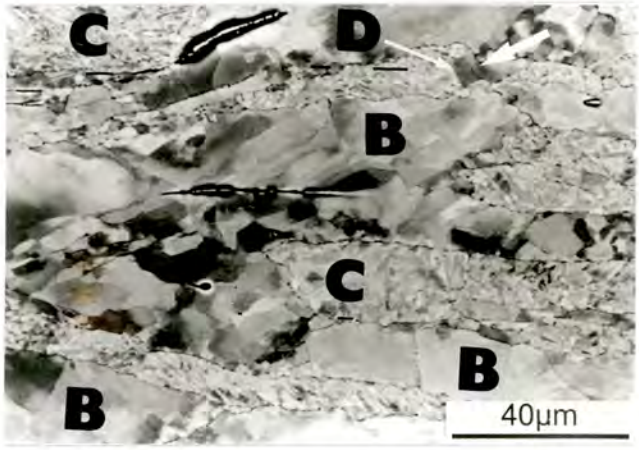

Fig. 4.14: Subgrains in prior ferrite becoming less dense; emerging subgrains in prior martensite. (30 min.)
Big **arrow** shows what appears to be martensite recrystallisation; Region **B** shows partial coalescence of subgrains in primary ferrite; **C** shows martensite recovery to produce fine subgrain structure; **D** shows recrystallisation front in martensite region.

Fig. 4.15 below represents the general microstructure after annealing for 2 hours. The disappearance of subgrains in the primary ferrite had become increasingly common. The continuously recrystallised grains contained patterns of precipitates in their interiors that corresponded to the shape of the disappeared subgrains. The grains also had several precipitates at their boundaries. These are the grains marked **E** at the top and near the bottom of the figure. There are also primary ferrite grains with subgrains for example **F**. The precipitation of carbides was very advanced, as can be seen by the intragranular precipitates in the elongated primary ferrite grains, which now appear fragmented. The subgrains in the prior martensite had increased in size as can be seen in the near centre of figure (region **H**). Recrystallisation events in these regions had also increased and their action produced recrystallised grains (e.g. **G**) whose interiors contained more precipitate patterns but less precipitates at the grain boundaries than the grains from primary ferrite.

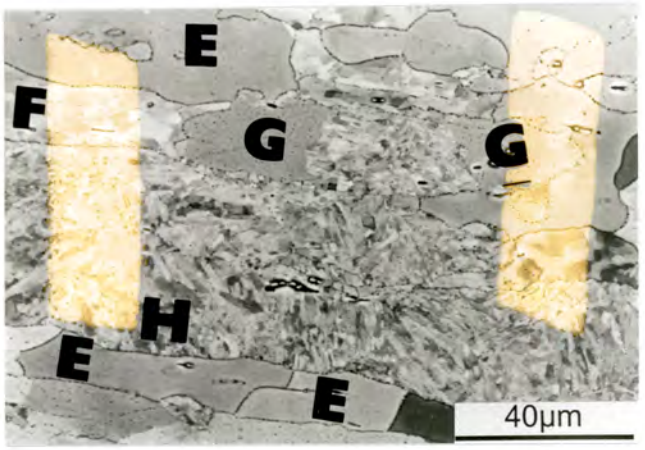

Fig. 4.15: Recrystallisation in both primary ferrite and prior martensite regions. (2 hours.)
E shows continuously recrystallised primary ferrite grains; **F** shows primary ferrite containing subgrains; **G** shows recrystallising prior martensite; **H** shows tempered prior martensite.

The subgrain network in the primary ferrite did not change appreciably after annealing for 5 hours. The subgrains in the prior martensite also did not show any discernible size change but recrystallisation continued as shown in fig. 4.16(a). Higher magnification revealed coalescing subgrains and the formation of precipitates within others, fig. 4.16(b).

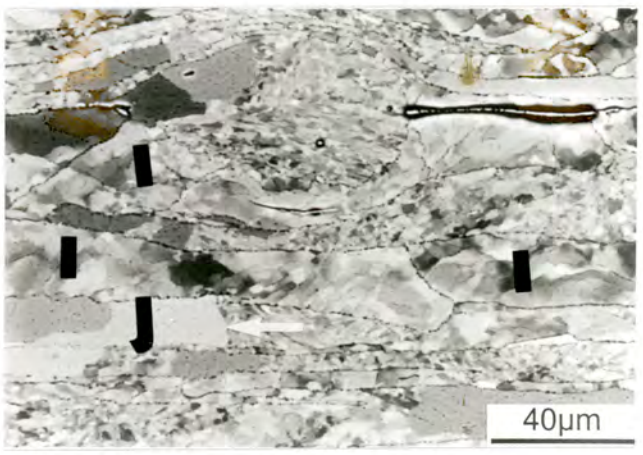

a). General microstructure (5 hours)
Arrow shows boundary (recrystallisation front) between recrystallised and tempered martensite; **I** shows primary ferrite grains containing subgrains; **J** shows recrystallisation in prior martensite

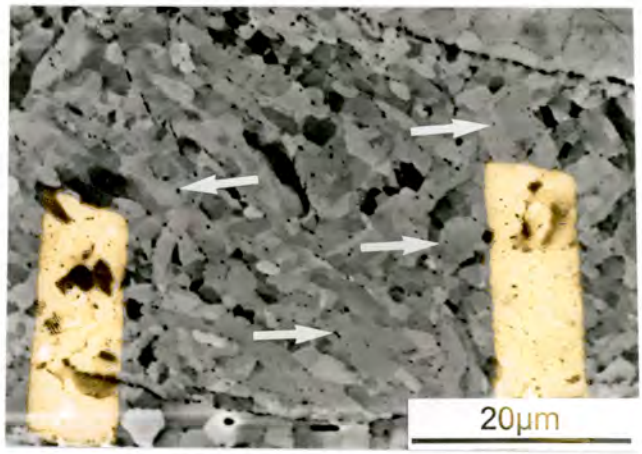

b). Coalescing subgrains in prior martensite (5 hours)
Arrows show dots in subgrains of prior martensite that indicate subgrain coalescence
Fig. 4.16: SEM micrographs after annealing for 5 hours.

After annealing for 10 hours, most of the boundaries of the subgrains of the primary ferrite grains were observed to have become diffuse. These grains acquired a mottled contrast. Microtexture measurements revealed that these grains had Kikuchi patterns that changed little within them, pointing to the fact that they were highly recovered and about to acquire a state of continuous recrystallisation. The previously formed static recrystallisation (SRX) grains from the prior martensite regions did not seem to change shape on continued annealing. Fig. 4.17(a) shows the general microstructure. No substantial change in size occurred for the subgrains in other prior martensite regions. Instead, recrystallisation continued as shown in Fig.4.17(b).

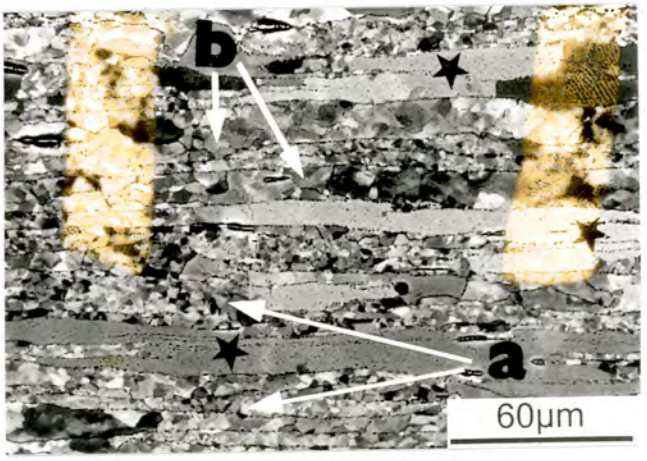

a). General microstructure (10 hours)
a shows prior martensite regions; **b** shows some primary ferrite grains. The very elongated subgrain free grains, marked with **asterisk** are continuously recrystallised primary ferrite grains.

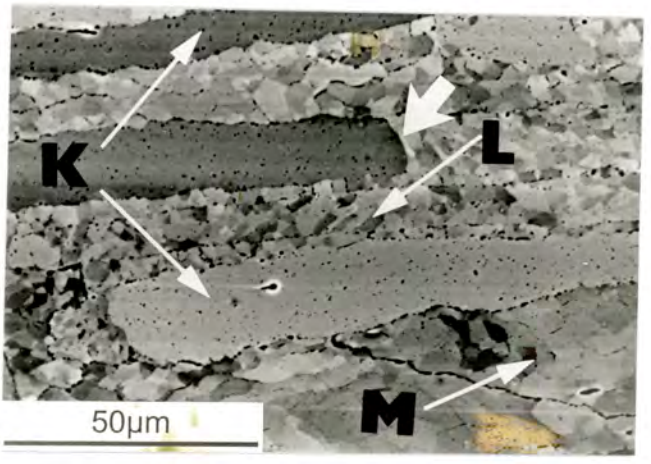

b). Recrystallisation front in some prior martensite regions. (10 hours).
Big **arrow** shows boundary (recrystallisation front) between recrystallised and tempered martensite; **K** shows recrystallised prior martensite; **L** shows tempered prior martensite; **M** shows state of subgrains in primary ferrite.
Fig. 4.17: SEM micrographs after annealing for 10 hours.

The variation of misorientation in the unrecrystallised prior martensite regions was found to be a mixed event. While it was high in some regions, in other regions, it was characterised by a near identical Kikuchi pattern. This variation that reveals both high and low angle grain boundaries is deemed to point to the concurrent occurrence of

recovery and recrystallisation. Fig. 4.18 below shows one of the regions that was evaluated (a) and the corresponding curve of the variation of relative misorientation, (b).

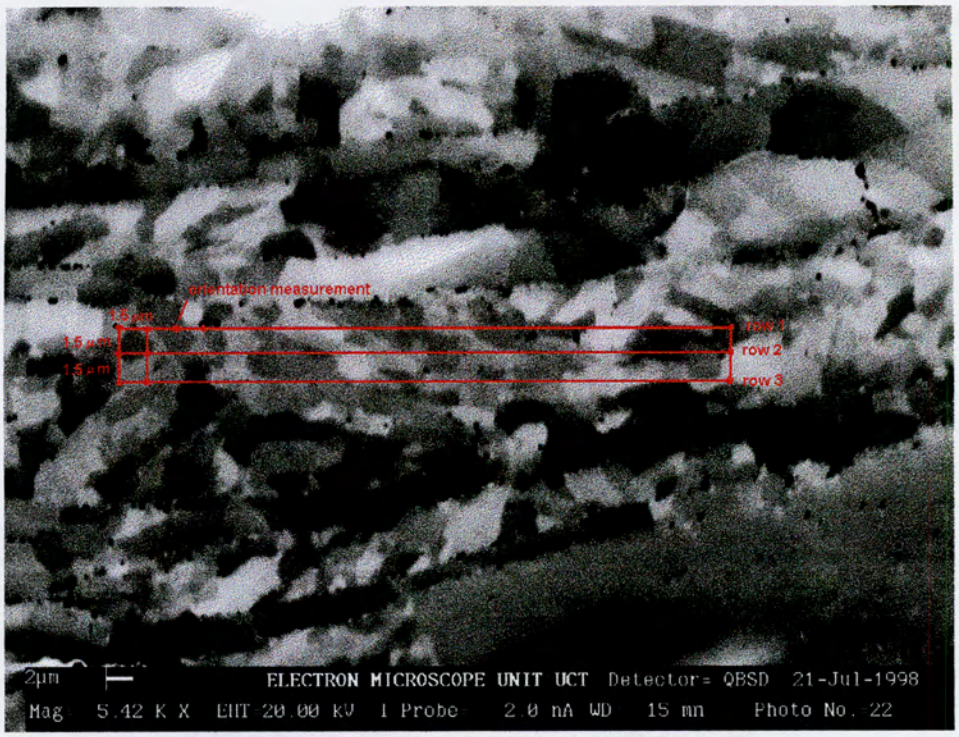

Data File Names: ane10-r1 (row 1), ane10-r2 (row 2), ane10-r3 (row 3).

Sample E Annealed for 10 hours

a):Prior martensite region evaluated for misorientation. (After 10 hours annealing).

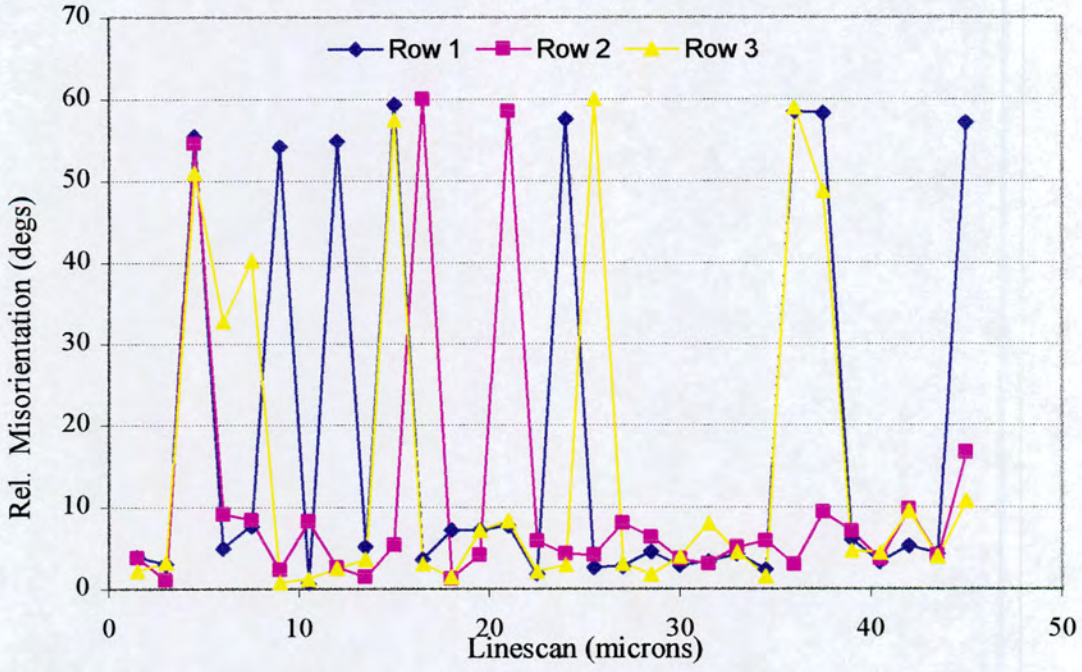

b): Misorientation curves for region in (a).

Fig. 4.18:Microstructure and misorientation in prior martensite region.

A few primary ferrite grains remained mottled after annealing for 20 hours and subdivision of elongated ones by precipitates was prevalent. However, most of these grains had undergone continuous recrystallisation. Recrystallisation in the prior martensite was very advanced and only few regions were observed to have subgrains. These subgrains in some regions had coalesced producing mottled grains. The few remaining subgrains were relatively unchanged in size and seemed to have precipitates on their boundaries. Fig. 4.19(a) shows the general microstructure. Fig. 4.19(b) shows the mottling effect in both the primary ferrite grains and prior martensite regions.

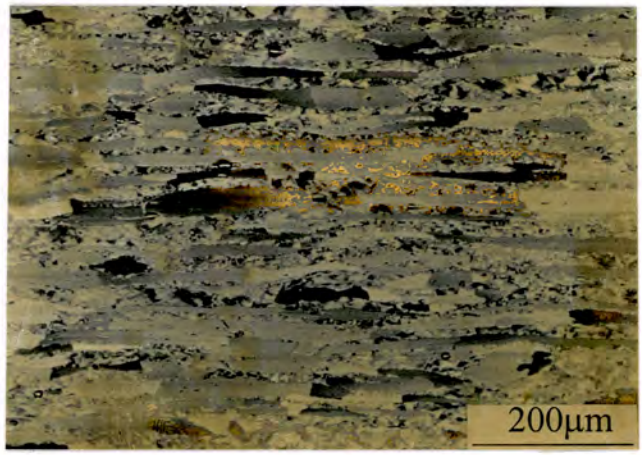

a): General microstructure

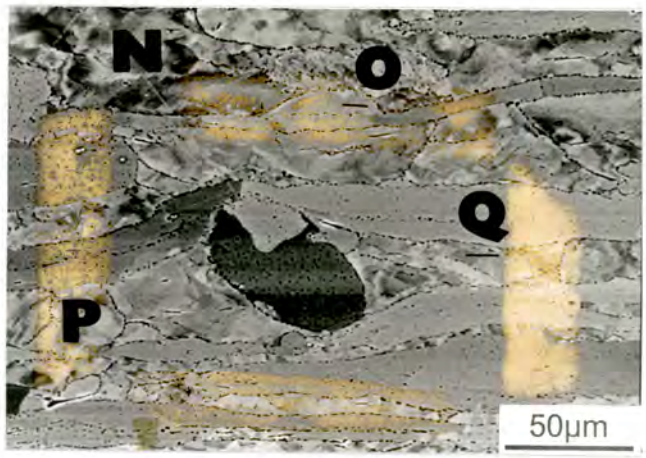

N shows coalescence of subgrains in prior martensite region producing mottled effect; **O** shows prior martensite region having subgrains; **P** shows mottling in primary ferrite, **Q** shows continuously recrystallised primary ferrite grains (grains very elongated).
b): Mottling effect in both primary ferrite and prior martensite
Fig. 4.19: General microstructure after annealing for 20 hours.

In summary, the primary ferrite underwent accelerated continuous recrystallisation that saturated after annealing for 5 hours. The precipitation of carbides was observed first at the subboundaries and then in the grains. This resulted in the elongated grains becoming fragmented. On continued annealing to 10 hours, grains that contained subgrains became mottled. The softening mode here was continuous recrystallisation. On the other hand, the martensite underwent accelerated tempering to form first well-defined subgrains after 30 minutes before the onset of recrystallisation. The growth of the recrystallised grains was confined to the rolling direction by the precipitates at the grain boundaries and this resulted in the formation of elongated grains. The subgrains grew on continued annealing but this seemed to saturate after 10 hours. No change occurred thereafter and some subgrains remained in the microstructure after annealing for 20 hours. The martensite exhibited both recovery and recrystallisation.

4.2.2: Cold Roll Annealed Microstructures:

The annealing after cold rolling was a standard treatment at 820°C for all the samples and was carried out for 10 minutes.

Effect of Hot Band Annealing Time:

a) 10 minutes:

The microstructure of the sample of heat A had obvious grain size banding, with rows of small grains alternating with rows of big grains, fig. 4.20(a). Except for a few small grains that appeared equi-axed, the grains in the microstructure were slightly elongated, fig. 4.20(b). The grain ranged from the very small to the very big with sizes varying between 8 μm and 100 μm.

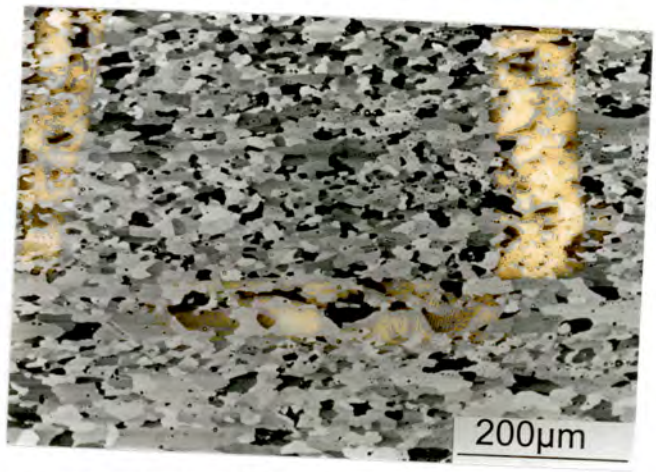

a): General microstructure

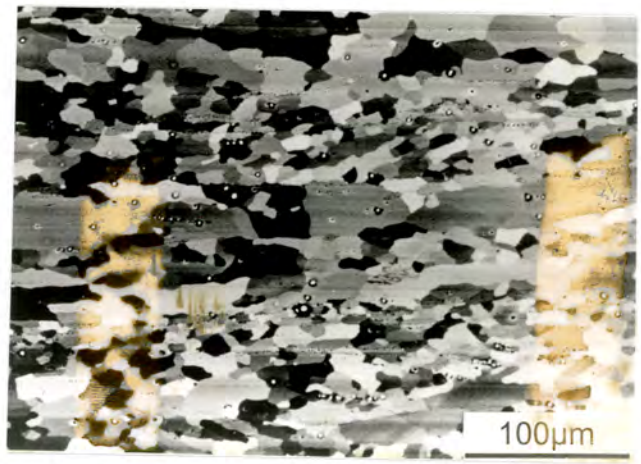

b): Bands of small and large grains

Fig. 4.20: General microstructure of heat A hot band annealed (HBA) for 10 min. after final recrystallisation.

On the other hand, the microstructure of the sample of heat E consisted of bands of fully recrystallised very elongated grains and recovered regions interspersed with recrystallised regions. Grain size distribution was characterised as a clustering of coarse and fine grains, figs. 4.21(a) and (b). The average grain size was found to be about 8μm but grains far much bigger (100 μm) could be seen in the microstructure.

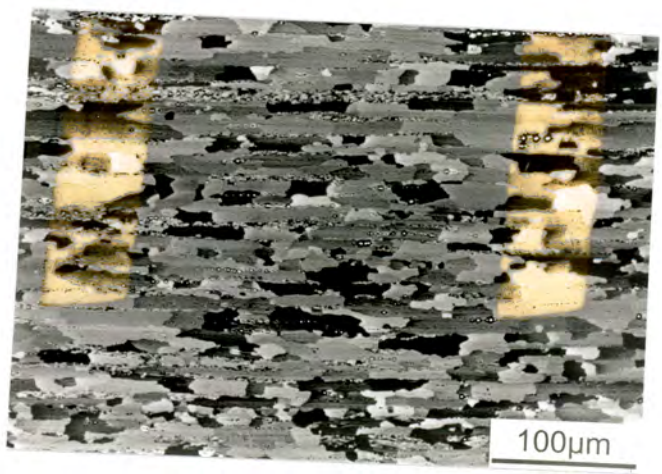

a): General microstructure

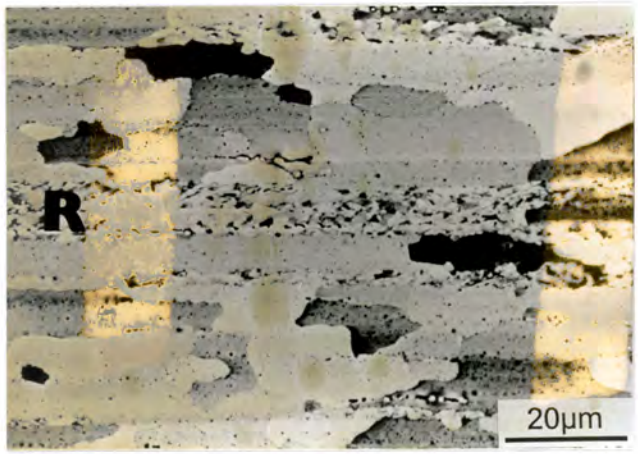

b): Recovered region marked **R**
Fig. 4.21: Microstructure for heat E, HBA for 10 min. after final recrystallisation

b): 20 hours:

The microstructure of the sample of heat A had several characteristics. The general microstructure appeared banded with small and large grains occurring alongside each other. The bands of small grains were not continuous and contained the occasional very big grain. The grain size in the banded matrix ranged between 6 μm and 15 μm. The very big grains averaged 50 μm in size. Fig. 4.22(a) shows the general microstructure. The very big grains were observed to have boundaries that seemed to bulge into the surrounding grains, showing that grain growth was taking place, fig. 4.22(b).

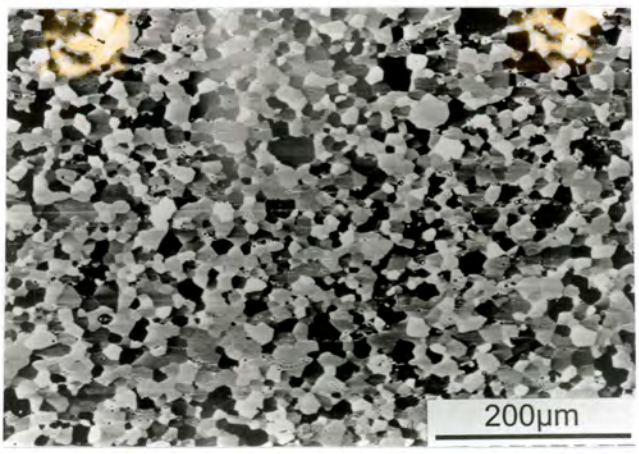

a): General microstructure

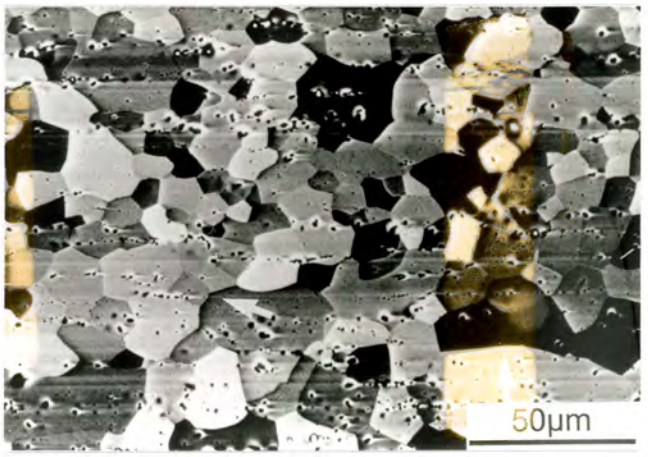

b): Big grains (with **arrow** near micron marker) that appear to be growing

Fig. 4.22: Microstructure of heat A HBA 20hrs, after final recrystallisation.

The microstructure of heat E was made up of fully recrystallised grains that seemed straddled by parallel strings of carbides that were arranged parallel to the rolling direction. The grain size distribution appeared banded, fig. 4.23(a). Fig. 4.23(b), shows that some grains, especially the very black contrasted ones, seemed to be disappearing. The average grain size was found to be 6µm.

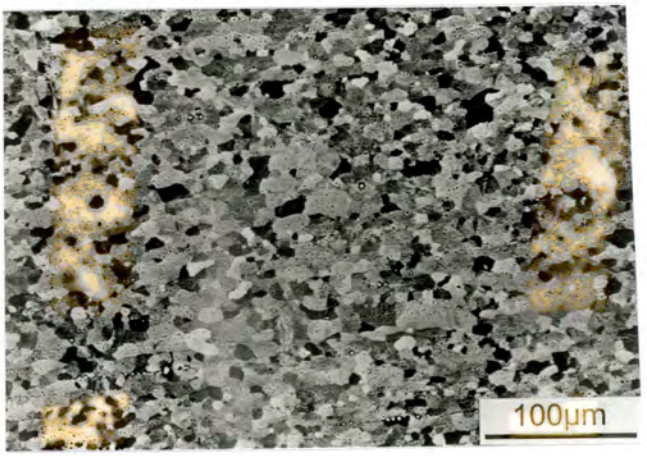

a): General microstructure.

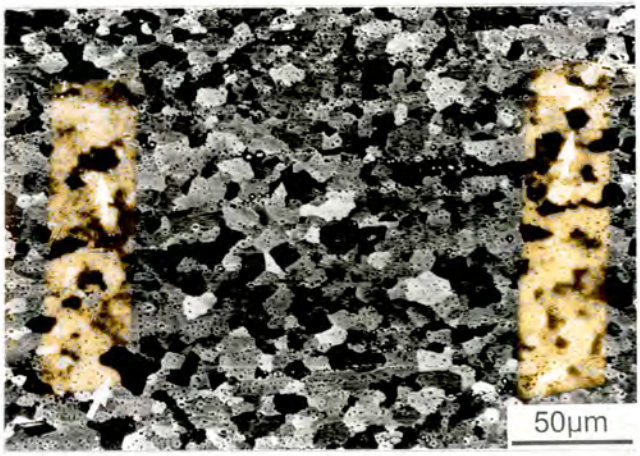

b): Disappearing grains (Pointed with **arrow).**
Fig. 4.23: Microstructure of heat E HBA 20 hrs, after final recrystallisation.

4.2.3: Textures:

Bulk texture measurements were carried out for samples of heats A and E after recrystallisation following cold rolling. The samples are those that had been hot band annealed for 10 minutes and 20 hours. The nomenclature used below is such that the first letter stands for the heat and the number stands for the duration of hot band annealing. 1 stands for 10 minutes and 2 is for 20 hours.

The evolution of texture is marked by a number of differences. Sample A 1 reveals a major gamma fibre with a maximum at (111)[112], an equally strong Goss at (011)[001] and a minor alpha, fig.4.24 (a). Sample A 2 shows a near random texture with traces of both alpha and gamma fibres and some cube, fig. 4.24 (c).

Sample E 1 shows typical deformation textures, with sharp alpha fibres having a maximum at both (001)[011] and (112)[011] accompanied by a minor gamma fibre, fig.4.24 (b). Sample E 2 on the other hand had gamma fibre as the major texture. The recrystallisation components (111)[110] and (111)[112] are both prominent. The alpha fibre is minor with (001)[110] only appearing as a trace, fig. 4.24 (d).

Figs. 4.24 (e) and (f) show the intensities of the major components on both the alpha and gamma fibres. The intensity decreases in the order E 1, E 2, A 1 and A 2.

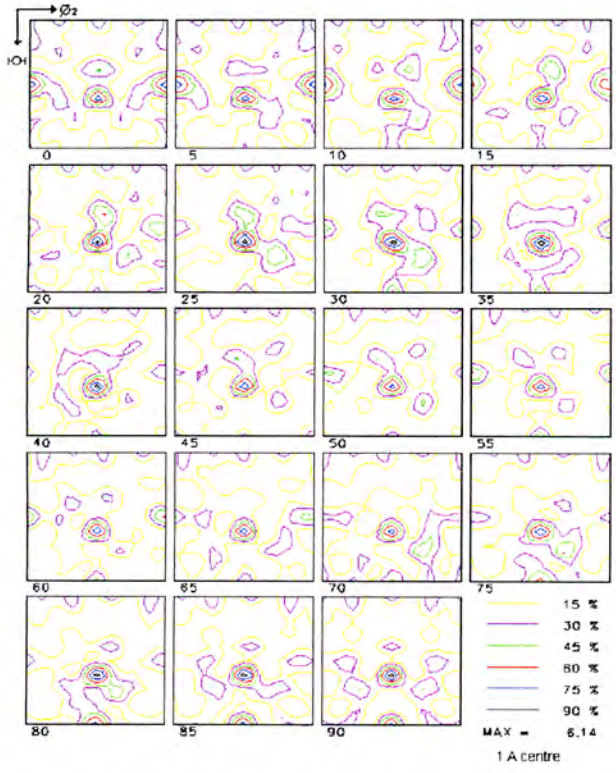

a) ODF for heat A HBA for 10 min.

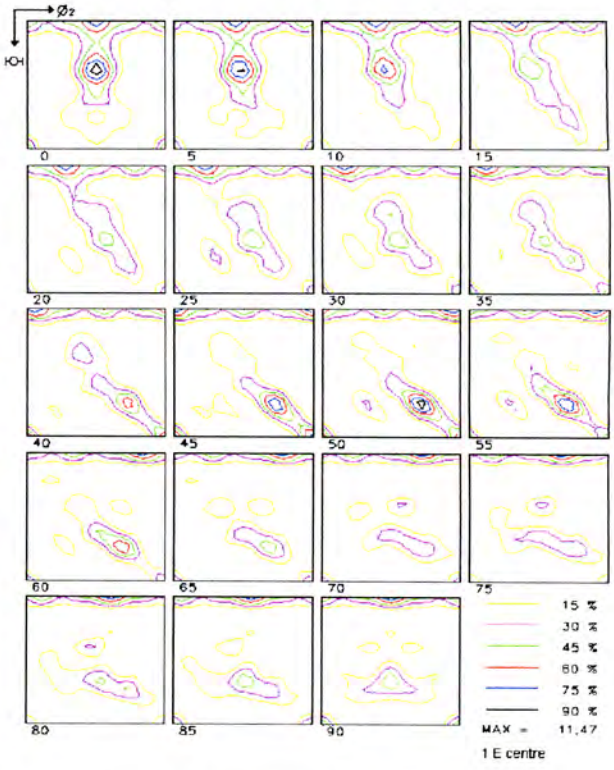

b) ODF for heat E HBA for 10 min.

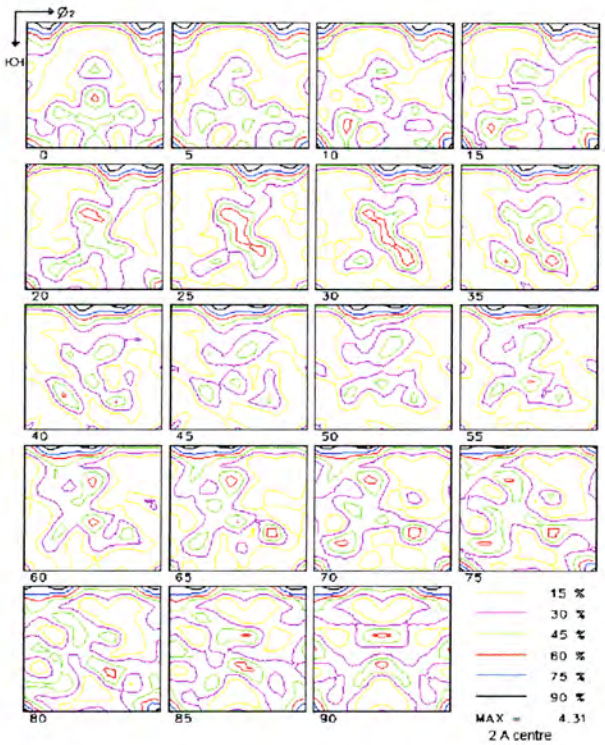

c): ODF for heat A HBA for 20 hours.

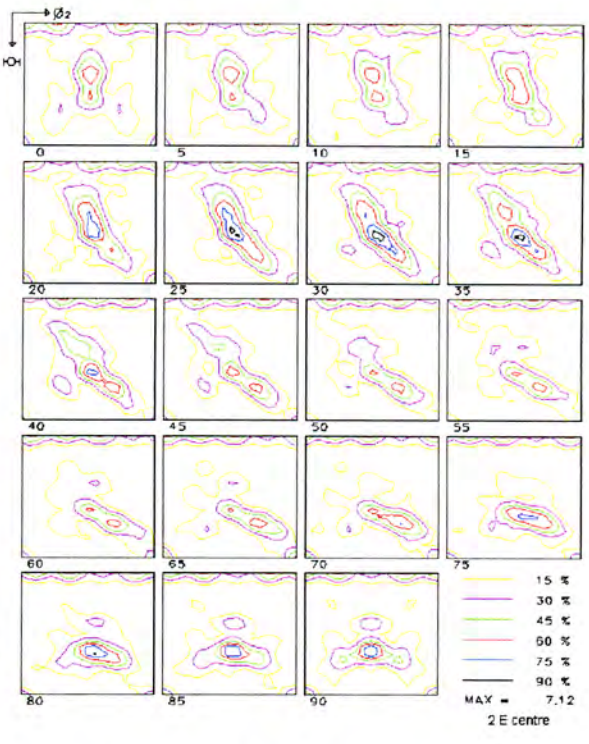

d):ODF for heat E HBA for 20 hours.

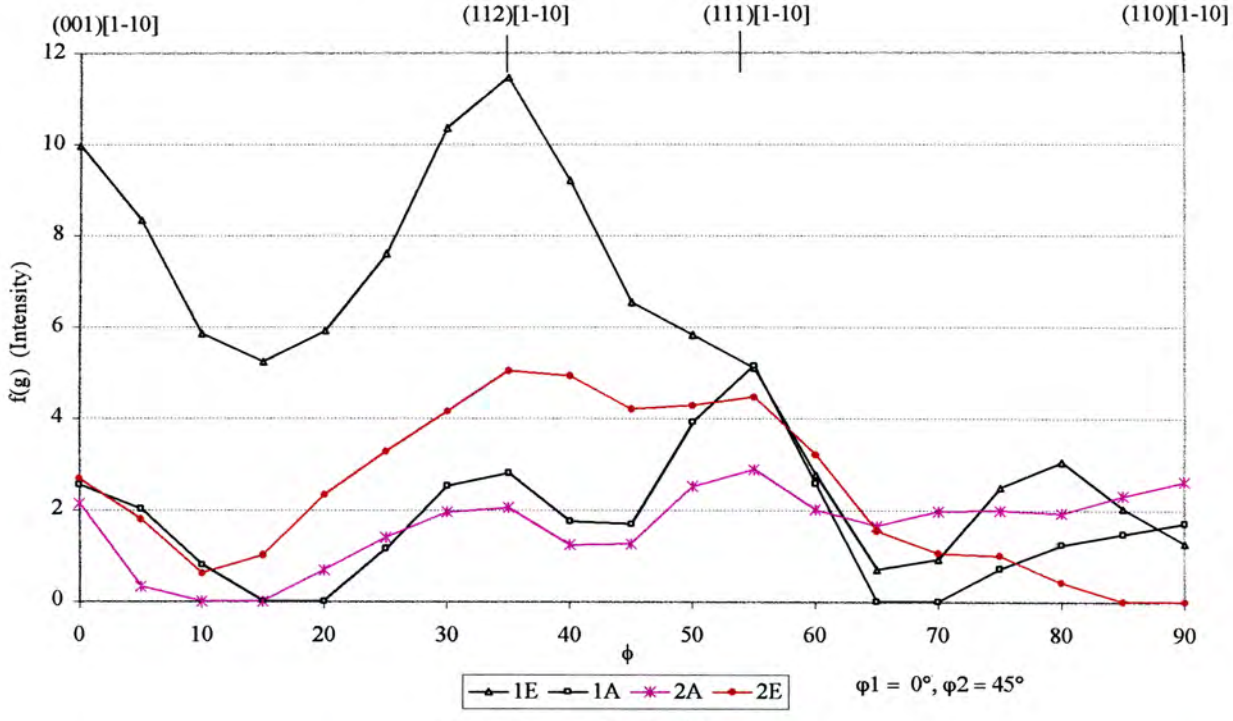

e) Alpha Fibres of Ferritic SS's

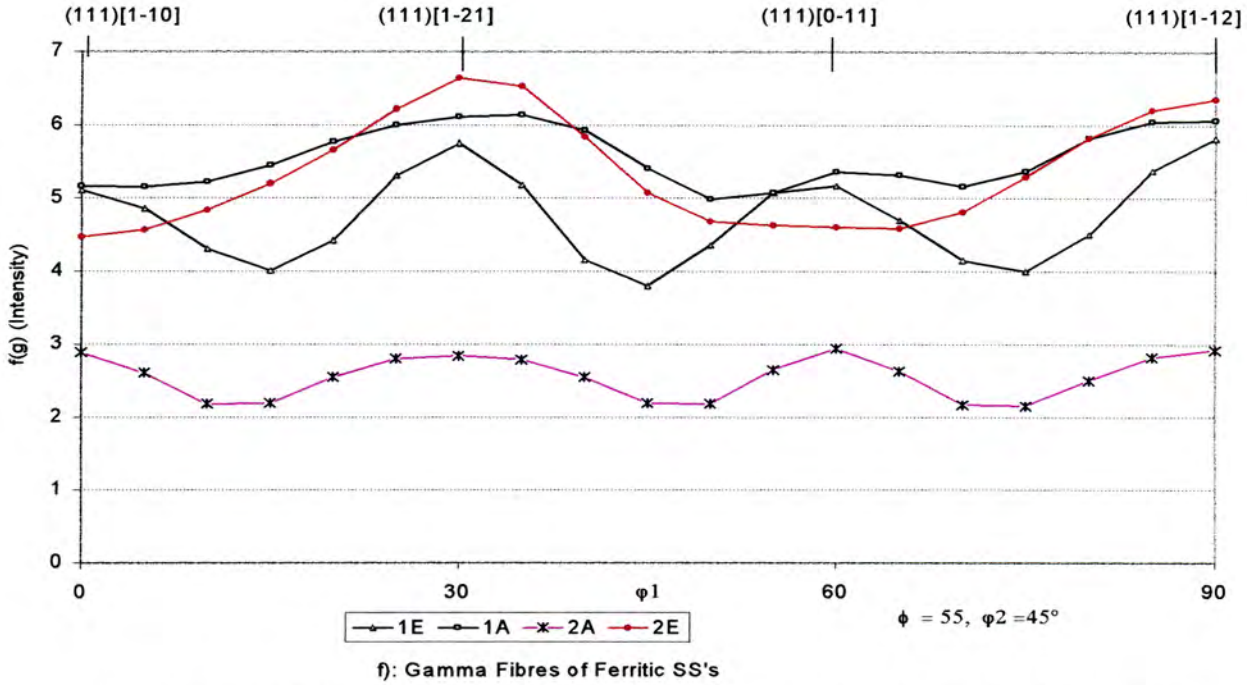

f): Gamma Fibres of Ferritic SS's

KEY: 1 = Stands for hot band annealing of 10 minutes, 2 = Stands for hot band annealing of 20 hours, HBA-Hot band annealed.

Fig 4.24: Orientation Distribution Functions (ODFs) and fibre representations.

4.2.4: Ridging Properties

The photographs in Fig. 4.25 below show the appearance of the surfaces of the specimens after testing. For comparison purposes, the photograph of an aluminium alloy, A3002, which does not ridge is also shown.

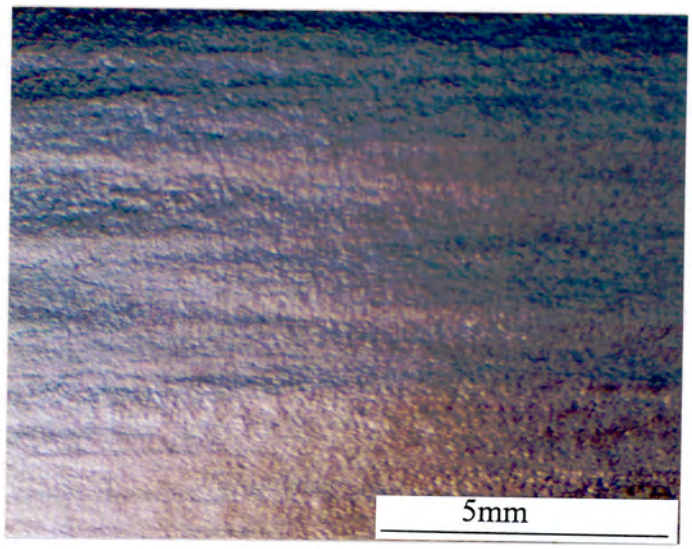

a). Heat A, HBA 10 min. (A 1).

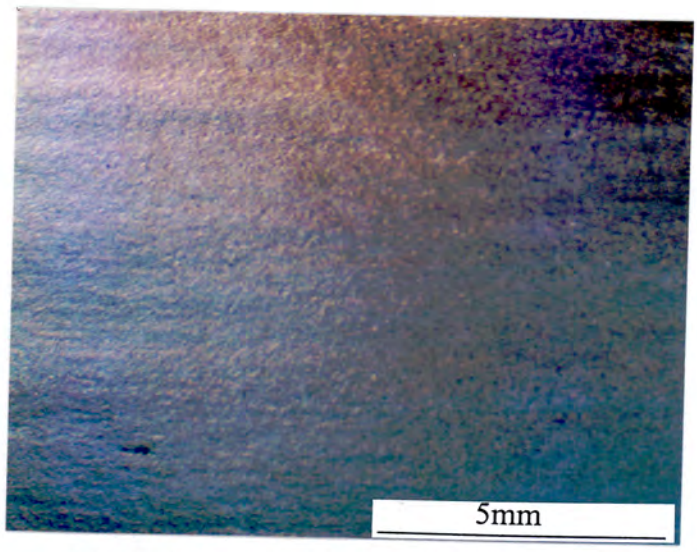

b). Heat A, HBA 20 hours, (A 2).

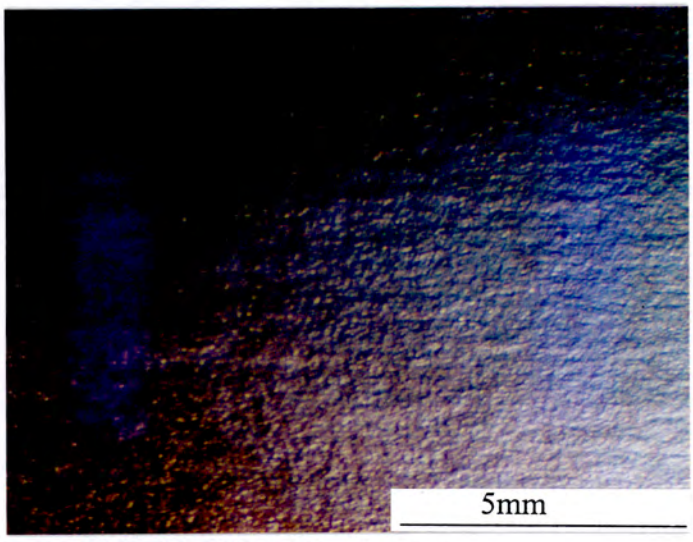

c). Heat E, HBA 10 min.(E 1).

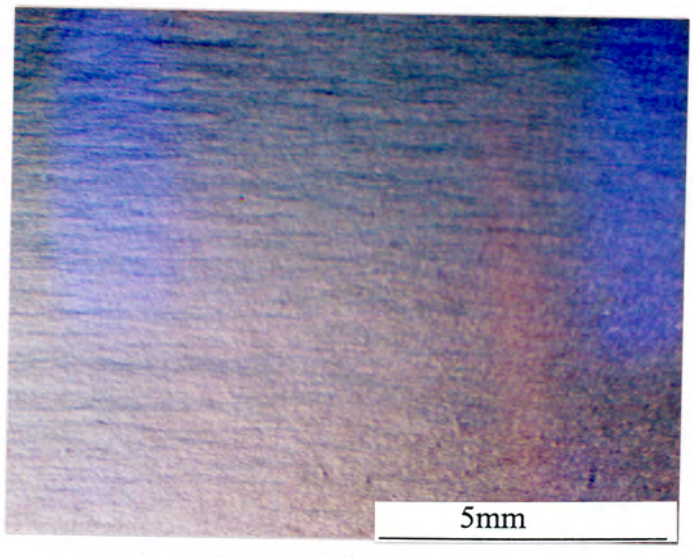

d). Heat E, HBA 20 hours, (E 2).

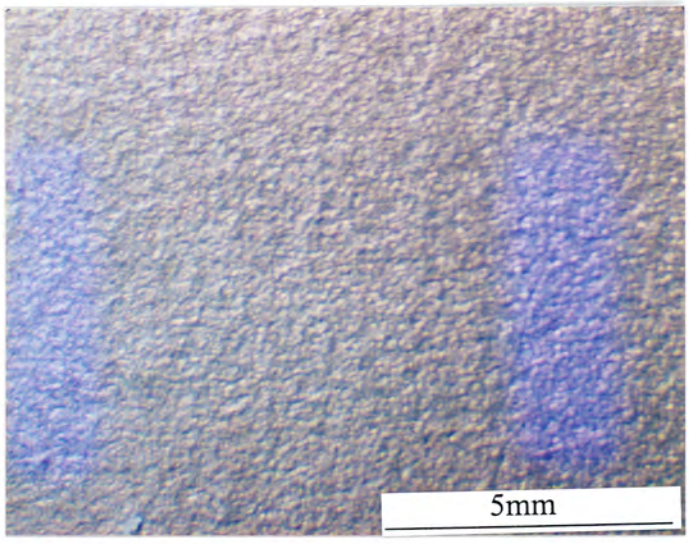

e). Al, A3002, standard non-ridging sample

Fig. 4.25: Surface appearance of samples after tensile test.

The surface profiles obtained for the specimens whose tensile axis is parallel to the rolling direction (RD) are as shown in fig. 4.26 below. For ease of interpretation, the profiles for upper and lower corresponding surfaces have been aligned and placed one below the other. *It is noted that classical ridging does actually occur for all the cases.*

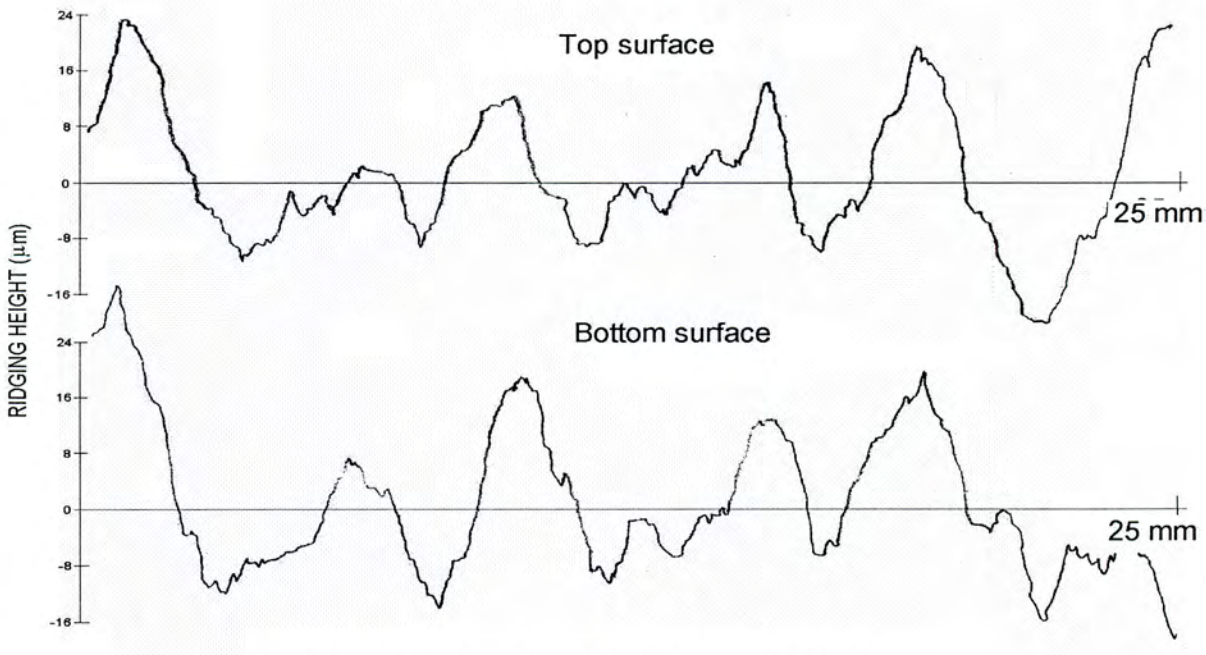

a). Heat A, hot band annealed for 10 min. (A 1).

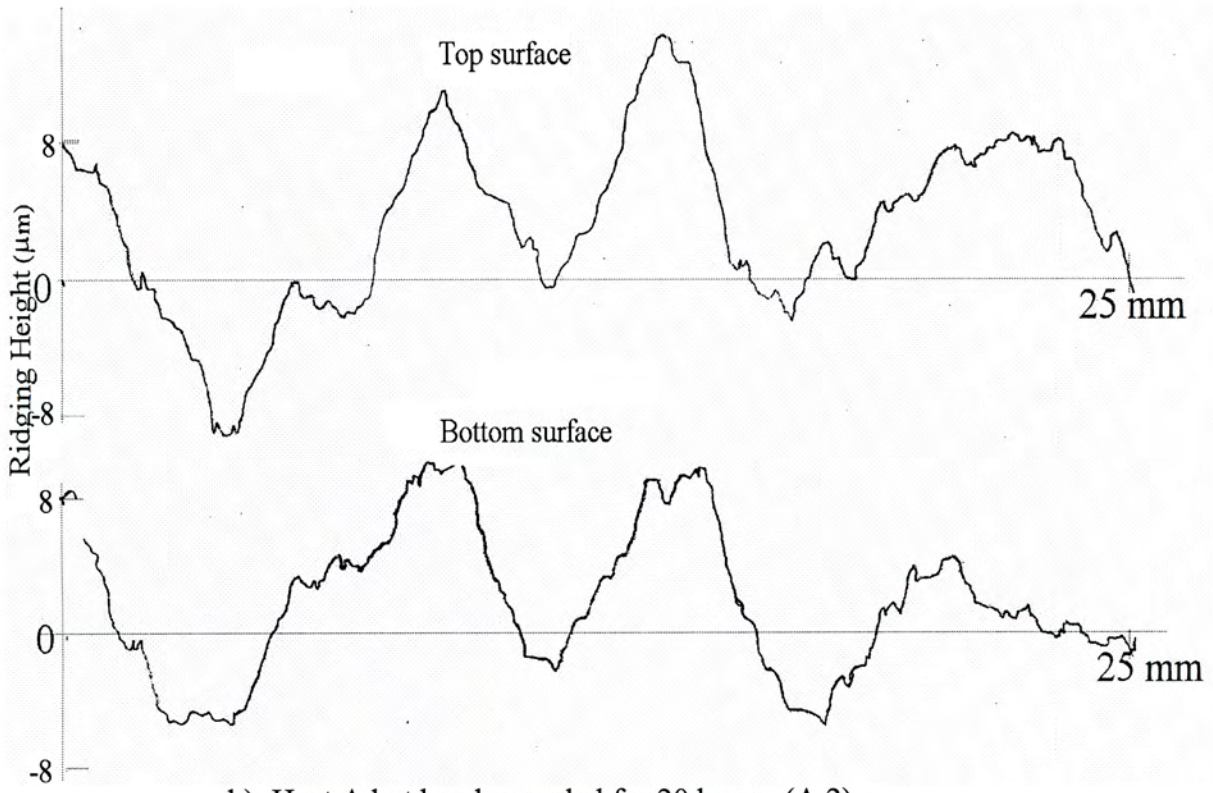

b): Heat A hot band annealed for 20 hours. (A 2)

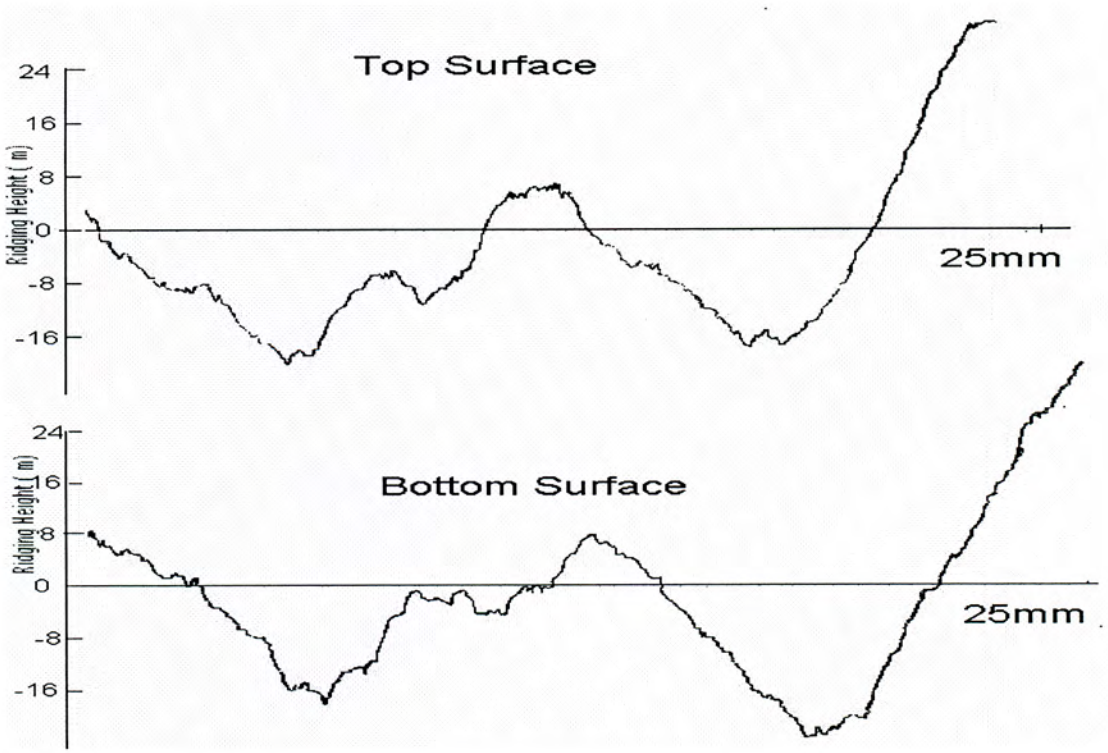

c): Heat E hot band annealed for 10 min. (E 1).

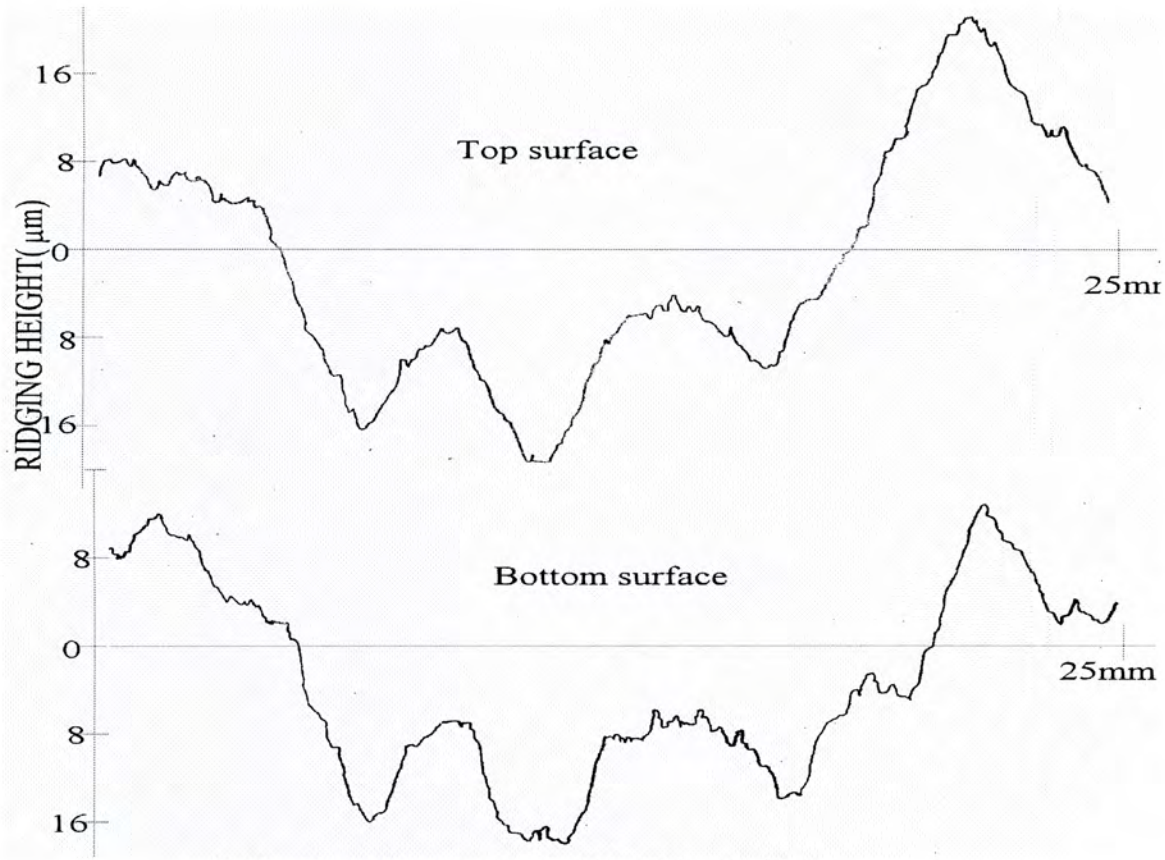

d). Heat E, hot band annealed for 20 hours (E 2).

Fig. 4.26: Scans from corresponding top and bottom surfaces

The roping degrees, rated by an arbitrary visual scale, are given in table 4.1.

Table 4.1.

Specimen	Rating	Degree
A 1	5	Very Severe
A 2	3	Moderate
E 2	3	Moderate
E 1	2	Slight

The scale ratings were as follows: 0 nil, 1 nil to slight, 2 slight, 3 moderate, 4 severe, and 5 very severe. Table 4.2 below gives the values of surface roughness for the RD and TD specimens.

Table 4.2

Specimen	Ra (μm)
A 1	1.01
A 1,T	1.25
A 2	0.63
A 2, T	1.14
E 1	0.58
E 1, T	0.60
E 2	0.60
E 2, T	0.43

(T Transverse, 1 Hot Band Annealing for 10 min., 2 Hot Band Annealing for 20 hours.)

.....**END**.....

Chapter Five

Discussion

5.1: Effect of Hot Roll Finish Temperature (Commercial Heats):

The hot roll microstructures show marked differences. The microstructure of heat C-600 (fig. 4.1) is defined by metal flow lines and lack of grain structure at low magnifications. These features show that the microstructure was highly deformed and indicates that little softening occurred during the rolling and the subsequent cooling before annealing. Since softening processes are thermally activated, the limited occurrence of any is accounted for by the low hot roll finish temperature that acted to retard kinetics. The martensite stringers observed in the microstructure were formed during the rapid cooling of austenite after the last hot roll pass.

The overall microstructure of heat C-800 in the as-hot-rolled condition was found to be banded. The whitish regions, which were shown at high magnifications to contain lath-like structures indicate the presence of martensite which formed during cooling after the last hot roll pass. The major part of the microstructure however exhibited the occurrence of some kind of softening, figs. 4.2 (a) and (b). The high hot-roll-finish temperature in this case facilitated the occurrence of softening. The softening was however not homogeneous. It comprised of limited recrystallisation that was confined to the subsurface regions and predominant recovery in the major part of the sample. A similar evolution of microstructure has been reported before by Raabe and Lucke [31]. The recrystallisation at the subsurface is a result of the apparently higher Zener-Hollomon parameter there. This parameter is higher because deformation occurred at a slightly lower temperature, the sheet having been cooled during contact with the rolls. The result is a higher residual strain energy there that provides a higher driving force for recrystallisation.

After annealing, heat C-600 undergoes complete recrystallisation (fig. 4.3) to produce a microstructure in which grain size banding and the gradient in grain size from the surface to the centre are not obvious. The homogeneity of this microstructure is a result of the occurrence of homogeneous recrystallisation that was occasioned by the vast amount of stored deformation energy. Also, the hot roll finish temperature was low enough for the microstructure to be insensitive to any slight cooling effects at the surface. A similar evolution of microstructure was observed by Y D Lee et al [27]. This, they noted was because the low finishing temperature provided higher strain and deformation bands, both of which acted to favour the formation of uniformly recrystallised grains after annealing.

The grain size banding observed in the microstructure of annealed heat C-800, (fig. 4.4), was caused by a number of factors. First, the prior martensite regions could recrystallise to produce smaller grains. It is worthwhile to note the correspondence of the bands of small grains to the previous martensite bands. Also, the stored deformation energy would be expected to be low and its distribution inhomogeneous as a result of the advanced softening during the rolling process and the inhomogeneous nature in which it occurred. This would result in varying degrees of driving pressures within the microstructure that would result in varying degrees of recrystallisation.

The small grains near the surface in the annealed microstructure of heat C-800 result from the cooling that occurs during contact between the rolls and the sheet. The sheet surface is deformed at a lower temperature and hence stores more deformation energy. Also, the friction during contact results in shear deformation, and possibly, the formation of shear bands, which during annealing provide sites for the formation of more recrystallisation nuclei.

The incomplete recrystallisation at the centre of this heat (Fig. 4.4(b)) goes to show that the amount of stored deformation energy here is less, deformation having taken place at a slightly higher temperature that allowed substantial recovery to take place. Also, the concurrent occurrence of recrystallisation and martensite→ferrite phase

transformation can retard recrystallisation. The accompanying precipitation of carbides would pin any new grain boundaries that might have a tendency to want to migrate.

The effect of hot roll finish temperature can thus be thought of as dictating the amount of deformation energy stored in the hot rolled metal. A high hot roll finish temperature reduces the work-hardening in the metal and reduces its stored deformation energy. The recrystallisation that occurs in the subsequent batch annealing is affected, either slowed or stopped from going to completion. A similar reasoning has been put forward before by Pouillard and Osdoit [60].

5.2: Effect of Austenite Content (Laboratory Heats):

Microstructure has been known to dictate both the mechanical properties and the formability of ferritic stainless steels. For this reason, manufacturers of these steels have sought to manipulate it in order to optimise properties. This has met with difficulty because of the unimpeded grain growth of the ferrite phase that occurs at high temperatures due to the lack of phase transformations [26]. Also, these steels have been known to undergo recovery, both dynamic and static [21-23], that helps perpetuate the existence of elongated grains.

It has been suggested that the existence of 2 phases (ferrite and austenite) during hot rolling could affect both dynamic and static softening processes, (55). The harder austenite phase would cause partitioning of strain to the softer ferrite phase. As a result, the ferrite phase would undergo extensive deformation that would result in a higher amount of stored deformation energy than would have the case otherwise. Also, the ferrite/austenite interfaces would become local regions of high dislocation density as a result of slip incompatibility (55). These inhomogeneous regions would enhance the formation of recrystallisation nuclei in the ferrite.

5.2.1: Effect of Austenite Content on Hot Band Annealing Behaviour:

5.2.1.1: Laboratory Heat A:

The microstructure in the hot rolled state in which elongated primary ferrite grains are seen to contain low angle boundaries [Fig. 4.5] is typical of recovery and in accordance with previous research work on the softening mode of the ferrite phase during both hot rolling and the subsequent annealing [21, 22, 25, 26]. The islands of martensite seen in the ferrite matrix formed during the cooling of the prior austenite. The lath-like structure is in accordance with the classification in Ref. 15 since the carbon content here was approximately 0.02%.

The distribution of the size of subgranular structures in the primary ferrite in the microstructure is found to be inhomogeneous, being smaller in the cases where the ferrite bordered martensite stringers and comparatively larger elsewhere. This was the most obvious effect of the austenite. The smaller subgrains can be accounted for by the fact that partitioning of strain occurred during deformation. In this scenario, the ferrite near the martensite underwent preferential deformation because it is softer than the austenite from which the martensite formed. However, there were no recrystallised grains in the as-hot-rolled microstructure, and therefore, the increased apparent deformation in the ferrite regions was not sufficient to precipitate recrystallisation during and immediately after hot rolling.

The annealing behaviour of the primary ferrite was inhomogeneous and depended on the location of the region relative to the martensite stringers. This inhomogeneity is a direct consequence of the distribution of subgrain size. The inhomogeneous distribution of subgrains implied that the distribution of stored deformation energy was also inhomogeneous, being higher where the subgrains were smaller, a consequence of equation 1. A few cases of static recrystallisation of the ferrite that came between prior martensite stringers were observed. The process took on the

appearance of discontinuous recrystallisation that involved first nucleation followed by growth. This seemed to saturate after annealing for 2 hours.

The ferrite subgrains near martensite stringers softened faster than other subgrains in the primary ferrite grains. They were bigger after 2 hours, fig. 4.8(b), and had fully coalesced after 10 hours, fig. 4.10(b), to produce elongated mottled grains. This is due to their small size that implied a higher amount of stored deformation energy and therefore a higher driving pressure for softening. The mottling effect is associated with recovery [4] and its occurrence here means the subgrains coalesced to produce recovered grains. This recovery was confirmed by microtexture measurements when it was found that the relative Kikuchi patterns within this grains was very small. On continued annealing to 20 hours, most of these grains underwent continuous recrystallisation.

For the ferrite subgrains far from martensite stringers, subgrain boundary fuzziness cleared only after annealing for 5 hours to leave original straight boundaries (Fig. 4.9(a)). The softening kinetics here are slower because the stored deformation energy was low. Continued annealing to 20 hours caused only minimal boundary merging (Figs. 4.10(a), 4.11(b) and 4.12(b)) and this left mottled grains in the microstructure.

The annealing behaviour of the martensite stringers was characterised by first tempering to produce fine subgrains that got bigger with annealing time (Figs. 4.6(b), 4.7(b) and 4.8(b)). Subgrain boundary fuzziness was then observed after annealing for 2 hours. It is thought that the fuzziness was caused by subgrain coalescence. Some recrystallisation was observed after annealing for 10 hours. This could have been a consequence of subgrain coalescence that produced recrystallisation nuclei. However, whole scale recrystallisation could not occur because of the pinning of any mobile grain boundaries by precipitates. There is a chance that some nuclei overcame this pinning effect and grew into the primary ferrite grains that had undergone extended recovery. This occurrence could have contributed to the recrystallisation of primary ferrite observed in Fig. 4.12(b).

The pinning effect of these particles also explains why some of the martensite stringers remain recovered even after annealing for 20 hours. This annealing behaviour of martensite where it both recovers and recrystallises has also been found to occur in the martensite of low carbon steels, [15, 16, and 17].

In summarising, the general annealing behaviour of the ferrite regions can be termed extended recovery in which subgrains form and grow through rotation and coalescence that produces grains that appear mottled even after annealing for 20 hours. However, many grains show clear contrast which indicates that in many situations the extended recovery process has progressed to continuous recrystallisation. This is shown by the large elongated ferrite in Fig. 4.12(b). The martensite regions showed both recovery first and then some recrystallisation. However, the recrystallisation did not go to completion as a result of the pinning effect of carbides.

A diagrammatic representation of the evolution of microstructure after annealing for 20 hours is as shown in Fig. 5.1 below.

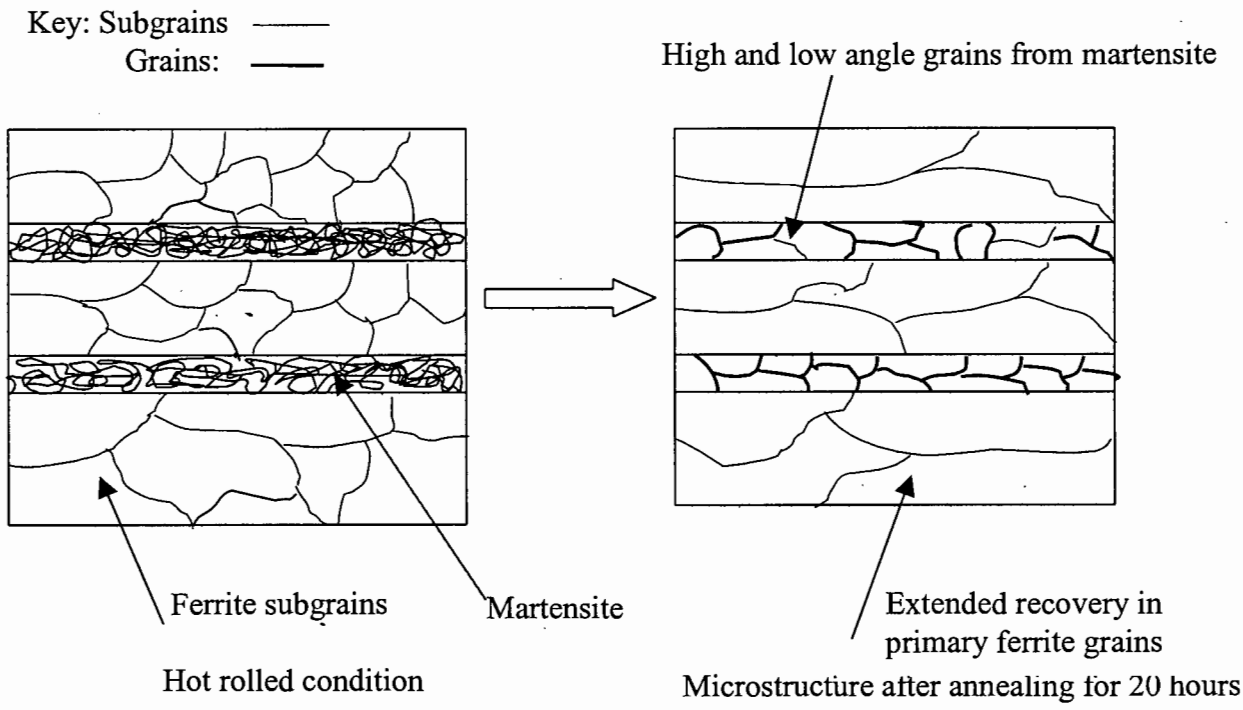

Fig. 5.1: Schematic showing the general evolution of microstructure in heat A.

5.2.1.2: Laboratory Heat E

No recrystallised ferrite grains were observed in the as-hot-rolled microstructure. The small, clearly delineated subgranular structures in the ferrite phase of the hot-rolled microstructure were found after microtexture measurements to be subgrains. Recovery of the ferrite phase after hot rolling in the two phase ($\alpha + \gamma$) region has been observed before, [25, 26, 61]. Raabe and Ylitalo [26] explained the recovery using the low hot roll start temperature and the lack of hold time between roll passes during the hot rolling. The two factors acted concurrently to cause the deterioration of nucleation conditions. The context of this reasoning was based on comparison to another sample that had undergone recrystallisation. The rolling of this sample had been started in the high temperature α-single region and rolling schedule had allowed hold time between roll passes. However, Yoshimura and Ishii [61] observed recovery in a sample that had undergone a one-pass hot rolling sequence in the high temperature α-phase. The lack of recrystallisation here was thought to have been caused by the low rolling reductions and the depletion of nucleation sites since the high temperature precluded the existence of the γ-phase that provided them [25]. The occurrence of recovery in the present case tends to amplify the reasoning in Ref. [25], that despite the high austenite content, its strain partitioning was insufficient to cause a large enough apparent deformation in the ferrite to precipitate recrystallisation.

The subgrains in the hot rolled microstructure here are smaller compared to those in hot rolled sample A, (cf. Figs. 4.5 and 4.13). This is thought to imply that the ferrite in sample E underwent a higher apparent deformation than that in sample A despite similar total reductions in both cases. This deduction is based on the observation by Y D Lee, et al [27] and Masao Koike et al [62] where increased hot rolling reduction was observed to result in smaller subgrain sizes. Consequently, the ferrite in E will have a higher amount of stored deformation energy.

The contrast of the ferrite subgrains decreased after annealing for 10 and 30 minutes, fig. 4.14 and there was a marked fading away of others. This is accounted for by

dislocations annihilating each other after they become mobile at the annealing temperature.

The fading away of subgrain boundaries was advanced after annealing for 2 hours. Here, fig. 4.15, subgrain-free grains with heavy grain boundary precipitates had formed from deformed elongated primary ferrite grains. Their formation is deemed a classic case of continuous recrystallisation where subgrain boundaries evaporate on annealing. This behaviour of the ferrite was not observed during the annealing of sample A. The difference in behaviour results from the fact that the ferrite in sample A has a lower amount of stored deformation energy because the partitioning of deformation was minimal. The continuous recrystallisation however seemed to saturate after annealing for 5 hours and the interplay of a reduced driving force and the action of particles is thought to have been the cause.

The occurrence of continuous recrystallisation aside, ferrite grains with subgrains still existed in the microstructure even after annealing for 10 hours, fig. 4.17 (b). Their size however seemed little changed, and this was a result of the action of the precipitates at their boundaries that pinned them to the extent of stabilising the subgranular structure. This structure disintegrated in some ferrite grains after annealing for 10 hours, in which case the subgrain boundaries became fuzzy. The fuzziness is a result of particle coarsening that led to a reduced pinning effect that allowed subgrain rotation and coalescence.

Compared to the ferrite phase, the prior martensite regions appeared to follow a different softening mechanism. Subgrains had already formed after annealing for 10 minutes and became well defined after annealing for 30 minutes to acquire the direction of the lath units, fig. 4.14. This fast recovery is due to the high driving force emanating from the elastic energy of the dislocations inherent in the martensitic structure. Similar kinetics were also observed by Caron and Krauss [18] working on a Fe-0.2%C lath martensite as an abrupt change in hardness after a very short annealing time.

The recovery, in some regions, of the lath units to form subgrains in was accompanied by the occurrence of poorly defined subgrain boundaries in some other regions producing a fuzzy contrast and the appearance of recrystallisation. Fuzziness was associated with growth in the annealing of heat A and its occurrence here would imply that the subgrains were already growing. That recrystallisation is occurring would also imply that a few subgrains had grown to acquire a critical radius that enabled them to change into recrystallisation nuclei.

The subgrains within the martensite even though bigger, were still elongated after annealing for 2 hours, fig. 4.15, and for the first time, precipitates were seen on the lath boundaries. That the subgrains are unchanged in shape points to a pinning action as a result of the precipitates. The precipitates were observed [18] to form very early during annealing when transmission electron microscopy was used. The scanning electron microscopy and the magnifications used in this study failed to reveal them earlier.

The subgrains within the martensite became equi-axed after annealing for 5 hours, fig. 4.16. This seems to have been accomplished by subgrain boundary migration and evidence for this could appear to come from the observation of precipitates in some subgrains. The particles coarsened (underwent Ostwald ripening) and reduced the pinning force. This allowed the subgrain boundaries to break loose and migrate to leave the particles behind.

Further annealing for 10 and 20 hours did not change the size of the subgrains, figs. 4.17 and 4.19. Fig. 4.18(b) however shows that the boundaries were a mixture of high and low angle boundaries. This behaviour of the martensite is similar to that of the samples of heat A. The recovery here is a result of the pinning effect of the particles as some were observed on the subgrain boundaries. There are indications that many of the subgrains started to coalesce after annealing 20 hours as shown in Fig. 4.19.

A diagrammatic representation of the evolution of microstructure after annealing for 20 hours is as shown in Fig. 5.2 below.

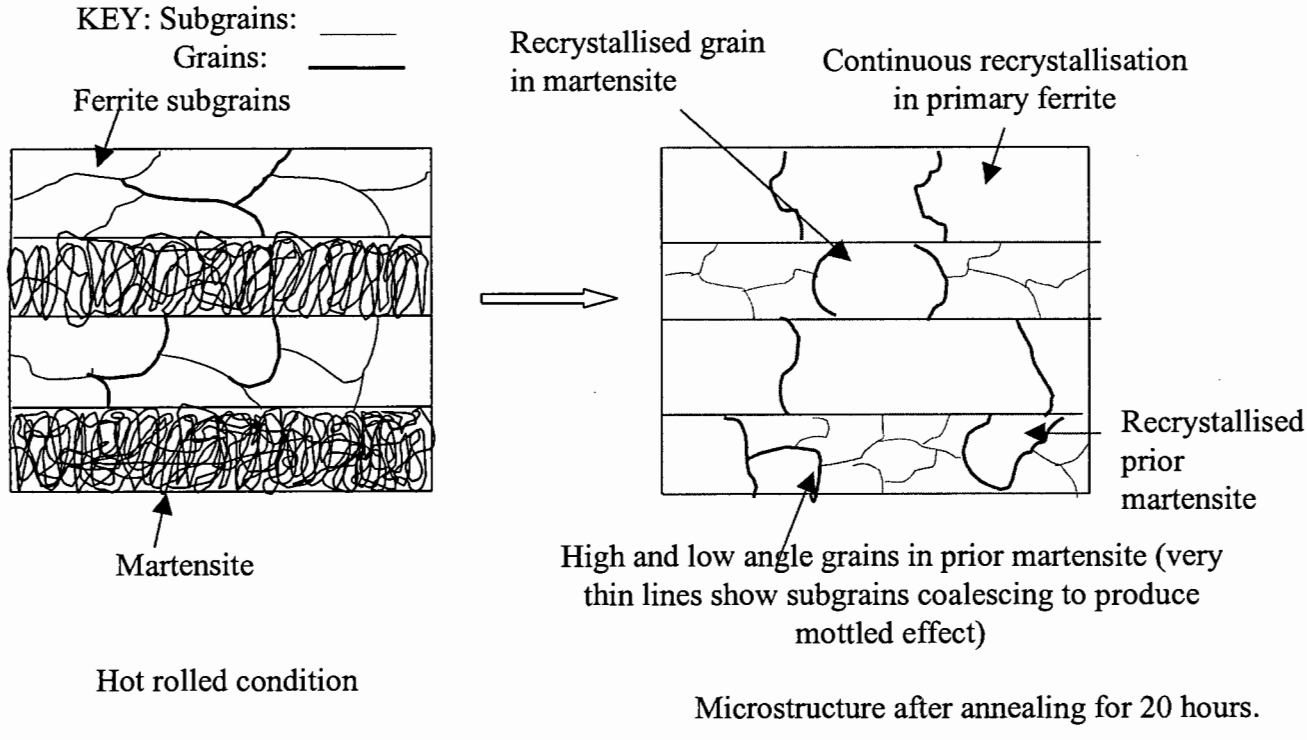

Fig. 5.2: Schematic diagram showing evolution of microstructure in heat "E".

Comparisons Between Heats A and E during hot band annealing

The following comparisons can be made:

- The ferrite subgrains in E are smaller compared to those in A. This is because the partitioning of deformation to the ferrite phase is greater in E.
- The kinetics of the softening of the ferrite phase in A are limited by the driving force. Particle pinning of subgrain boundaries might have played a bigger role in heat E.
- The primary ferrite in heat A shows signs of having undergone only extended recovery in some cases, whereas there is also evidence to suggest that some primary ferrite grains have continuously recrystallised. For heat E, the higher stored energy has led to continuous recrystallisation in most cases.
- The end microstructures after annealing for 20 hours have elongated grains.

5.2.3: Microstructures after final recrystallisation:

(Following Cold Rolling)

The obvious grain size banding observed in the sample of heat A hot band annealed for 10 minutes is characteristic of the microstructures in these steels, (cf. Wittridge and Knutsen [4], and Raabe and Lucke [31]). This banding has been attributed to a textural effect whereby some of the texture components formed during hot rolling are difficult to recrystallise. This reasoning seems to have relevance in this situation considering the microstructure after hot band annealing was only recovered.

The clustering grains in the sample annealed for 20 hours is thought to have been caused by grain growth, typified by the occurrence of curved boundaries and a few very black contrasted grains that appeared to be vanishing, Fig. 4.22.

The importance of the duration of the hot band annealing process is clearly demonstrated by heat E. The recovery at the grain boundary regions of the sample hot band annealed for 10 minutes [fig. 4.21(a)] was reminiscent of the behaviour of the high temperature prior martensite regions. That these regions could be actually tempered prior martensite regions implies that the recrystallisation kinetics were very retarded. The possible reason for this could be the concurrent occurrence of recrystallisation and precipitation of carbides which after they form, pin migrating subgrain boundaries to stop them from growing to form recrystallisation nuclei.

The formation of both small and big aspect ratio grains in this sample is thought to have resulted from growth of new grains in primary ferrite and prior martensite regions respectively. A similar evolution of microstructure was obtained by Masao Koike, et al [62].

In contrast to this sample, the sample annealed for 20 hours had a fully recrystallised microstructure. The slight grain size banding observed is a direct consequence of the

distribution of carbides in bands after cold rolling. Grains coming between closely spaced carbide bands would be smaller that those coming between bands far apart. The action of the carbides on pinning migrating boundaries can also account for the fact that some of the bigger grains were slightly elongated. Grain growth, too, seemed retarded and only a few grains appeared to be vanishing, Fig. 4.23 (b).

Comparison Between A and E During Final Recrystallisation Following Cold Rolling:

The comparison here could be better done as a function of the hot band annealing time.

After 10 minutes hot band annealing:

- Sample A underwent complete recrystallisation to produce a banded microstructure. Sample E on the other hand contains retained tempered martensite and has a microstructure that is partially recrystallised.
- The recrystallisation kinetics in heat A are faster than in heat E. The reason for this could be the concurrent occurrence of recrystallisation and precipitation of carbides in sample E. The precipitation process retards recrystallisation because the precipitates that form produce a Zener drag on migrating boundaries. The fact that precipitation has a greater influence in heat E is due to the much higher interstitial content in this alloy, and hence the greater affinity for carbo-nitride precipitates to occur. It is expected that the precipitation process could not have been completed during the initial 10 minute hot band anneal, and in addition, those precipitates already formed would not have coarsened.

After 20 hours hot band annealing:

- The long anneal has coarsened the particles to such an extend that they have less influence on controlling recrystallisation and complete recrystallisation has occurred for both heats A and E. However, the grain size distribution is still

influenced by the inhomogeneous structures which occur in Figs. 4.12(b) and 4.19 respectively.

5.2.4: Evolution of Texture:

The cold rolling of ferritic stainless steels produces a strong partial alpha fibre with maximum intensities at {001}<110> and {112}<110> and a weak complete gamma fibre with maximum intensities at {111}<110> and {111}<112>. During the subsequent final recrystallisation, the components on the alpha fibre, especially {112}<110>, tend to disappear while those on the gamma fibre, especially {111}<112>, grow. These two components have a rotation relationship of 27°<110> [30] that allows the recrystallisation component to grow into the deformation component by growth selection.

The above described texture evolution is well exhibited by sample A 1, (heat A hot band annealed for 10 minutes). Here, it is observed that the maximum in the alpha fibre is at (111)[110]. This texture doubles both for deformation and recrystallisation but its high intensity in this case is being attributed to the latter process. The gamma fibre plot also shows the expected maximum at the (111)[112] recrystallisation component. This component is in line with the microstructure in Fig. 4.20 which shows that recrystallisation had occurred. The strong (011)[100] Goss seen in the orientation distribution function (ODF) of this sample is attributed to the initial large grain size before cold rolling (Fig. 4.5). The large initial grains favour the formation of shear bands [9] in which the texture nucleates [33].

The textures of sample A 2, hot band annealed for 20 hours, are weaker than all the samples studied. The effects of deformation and primary recrystallisation, which dictate the strength of either alpha or gamma fibres, are diminished. This very random texture could be a consequence of bigger particles formed during the long hot band anneal that influence recrystallisation by causing particle stimulated nucleation. Holscher and Staubwasser [19] also noted a similar effect in which longer annealing randomised texture.

The evolution of texture in the samples of heat E has been strongly influenced by the initial high austenite level. Sample E 1, hot band annealed for 10 minutes, shows typical deformation textures, with peaks at (001)[1-10] and (112)[1-10] on the alpha fibre. These textures are consistent with the initial microstructure before cold rolling that was largely deformed and by the microstructure after final recrystallisation following cold rolling (Fig. 4.21) which shows incomplete recrystallisation. Raabe and Ylitalo [26] have shown that the presence of a {112}<110> martensite component after hot rolling can be attributed to the formation of a {112}<111> austenite texture during rolling. Although the hot rolled texture was not measured in the present study, it could be postulated that the {112}<110> component was strong after hot rolling in view of the high initial austenite content. In view of the limited microstructural changes which occur in the martensite after annealing for 10 minutes, it can be further postulated that a strong {112}<110> component existed at the start of cold rolling. Further enhancement of this component, as well as the {001}<110> component, during cold rolling would produce a particularly strong α-fibre after cold rolling. Thus it is understandable that the incomplete recrystallisation observed in this case after the final anneal would promote the appearance of strong α-fibre components. In addition, since it seems that the areas which have not recrystallised most likely correspond to the prior martensite (very fine structures), it is not surprising that the {112}<110> component is particularly strong.

The very low (001)[1-10] in sample E 2 typifies the evolution of texture after final recrystallisation in these steels. The prominence of (112)[1-10] on the alpha-fibre is attributed to the martensite-ferrite phase transformation and the prominence of the (111)[112] recrystallisation component on the gamma fibre is due to the complete recrystallisation after final recrystallisation following cold rolling, Fig. 4.22.

The role of the second phase austenite in the evolution of texture is better analysed with the duration of hot band annealing in mind. For longer annealing times, the austenite is very beneficial in promoting the formation of sharp recrystallisation textures, especially (111)[112]. For shorter hot band annealing times, the gamma is

found to sharpen the deformation textures and to produce a slightly less intense (111)[112]. For the conventional ferritic stainless steel i.e. low austenite content as in heat A, increasing the duration of hot band annealing randomises the texture.

5.2.5: Ridging Properties:

The aluminium sample was included to clearly show the phenomenon of surface roughening. In this case, it shows that in all cases during tensile deformation, a surface roughness accompanies any other defect that may form.

The use of grain size for analysing the ridging results requires caution. This is because the grain sizes were determined using the Heyn intercept method and a circle as the test line. The exercise did not put in consideration the grain size distribution, the level of recrystallisation and any effects of anisotropy in the grain shape. The grain sizes are the same for samples A 1 and A 2 but the grain size distribution in A 1 was banded and the grains were slightly elongated. The same goes for samples E 1 and E 2 where the former is partially recrystallised and has elongated grains while the latter is fully recrystallised and the grains are more equi-axed.

The surface profiles for samples A 1 and A 2 are very different, with A 2 having fewer ridges than A 1, figs. 4.26 (a) and (b). The difference has been caused by the long hot band anneal given to A 2. The annealing encouraged the development of a very random texture in this sample. This random texture decreased the effect of textural inhomogeneity during deformation hence decreasing the severity of ridging.

Samples A 2 and E 2 have been given the same ridging rate. This is because they contain the same number of ridges and their R_a values for the RD specimens also vary only very slightly, with that of A 2 being higher. The importance of this rating is that the conventional AISI 430 ferritic stainless steel can have its ridging properties improved by increasing the hot band annealing time. Also, the random texture produced as a result of the long annealing is as important a factor as an increase in the

austenite potential in reducing ridging. Sample A 2 however exhibited a more advanced surface roughening. This was a result of its larger average grain size, this being in accordance with Fukuda, M et al (as quoted in Becker (39)).

The effect of the duration of hot band annealing is found to have an opposite effect on ridging for heat E to that observed for heat A. The longer hot band annealing induced a poorer ridge rating for heat E. This observation has been shown before by Holscher and Staubwasser [19], Sheppard and Richard [41] and Masao Koike et al [62]. The effect seems to be linked to the precipitation of carbides, where the longer hot band annealing leads to bigger particles. The difference in the rating might have been caused by the homogeneity of the distribution of these particles. In E 1, the particles could have been randomly distributed while in E 2, they (particles) occurred in rows running parallel the RD. This would result in a highly pronounced anisotropy in E 2.

Overall, the effect of austenite and long hot band annealing in reducing ridging has been clearly demonstrated. A higher austenite potential encourages the formation of strong gamma fibres while a long hot annealing treatment, in the case where the austenite potential is low, encourages the formation of random textures, during the final recrystallisation treatment.

.....**END**.....

Chapter Six

CONCLUSIONS

6.1: Effect of hot roll finish temperature:

The following observations can be made regarding the hot roll finish temperature:

- Lower hot roll finish temperatures result in a greater retention of a deformed microstructure after hot rolling.
- The microstructure obtained after annealing is more homogeneous for a low hot-roll-finish-temperature. This is because the distribution of deformation energy is homogeneous and recrystallisation is encouraged throughout.

6.2: Effect of Austenite Content:

a): On Hot Band Annealing behaviour:

From the simulation of hot band annealing, the following observations can be made:

- The presence of austenite increases the deformation in the neighbouring ferrite regions, and the higher the content the higher the deformation;
- Extended recovery is the predominant mode of softening of the ferrite phase in heat A;
- The ferrite phase in heat E undergoes restoration by continuous recrystallisation;
- The annealing behaviour of the martensite regions in both A and E is the same. In both cases, subgrains are formed and especially for heat E, some subgrain coalescence occurs that sometimes resulted in the formation of recrystallised grains.
- Elongated ferrite grain structures persist in both heat A and E after annealing.

b): On Microstructures after final recrystallisation:

- A high austenite content coupled with a short hot band anneal time results in a partially recrystallised microstructure after final recrystallisation;
- A high austenite content lessens the effect of grain size banding.
- An increased austenite content decreases the average grain size.

c): On textures:

- For a short hot band annealing time, a high austenite content encourages the formation of strong alpha texture components while long hot band annealing encourages formation of strong gamma fibres, after final recrystallisation following cold rolling;
- In the case where the austenite content is low, long hot band annealing randomises texture (as shown by sample A2).

d): On Ridging Properties:

Even though ridging was observed for all the compositions studied, in general:

- A longer hot band annealing time decreases the tendency for ridging;
- Increased austenite content is beneficial for reducing the severity of ridging.

.....**END**.....

REFERENCES

1. Columbus Stainless Steel, Middleburg, South Africa.
2. Butron-Guillen M P and Jonas J J*: Effect of Finishing Temperature on Hot band Textures in an IF Steel*: ISIJ International, vol. 36b (1996), No. 1, pp. 68-73.
3. Vanderschueren D, Van Houtte P, Aernoudt E, Dilewijns J, and Standaert, C: *Hot Rolling Textures of Low Carbon Steels and their influence on the Texture after Continuous Annealing,* ;In Advances in Hot Deformation and Microstructures: JJ Jonas, T R Bieler and K J Bowman, (editors), MMM, 1994, pp. 95-106.
4. Wittridge N J, Knutsen R D: *Recovery and Recrystallisation Characterisation in Ferritic Stainless Steel by Using Electron Channelling Contrast*: Materials Characterisation, Vol. 37, 1996, pp.31-37.
5. R A E Hooper, T Llewellyn and V T McNeely: *Ferritic Stainless Steels*; Sheet Metal Industries, 1972, pp. 26.
6. B Barouz: The 17%Cr Ferritic Stainless Steels; Symposium, Stainless Steel '77, Climax Molybdenum Company, pp. 507.
7. R W K Honeycombe: Steels, Microstructure and Properties: Metallurgy and materials, 1981, Edward Arnold (publisher), pg. 212-13.
8. F J Humphreys and M Hatherly: Recrystallisation and Related Phenomenon: 1ed. 1995, Pergamon.
9. D Raabe and K Lucke: *Textures in ferritic stainless steels*: Materials Science and Technology; vol. 9, 1993, pp. 302-312.
10. K Tsuzaki, H Matsuyama, M Nagao and T Maki: Mater. Trans. JIM, **31**, 1990, 983

11. A Belyakov, R Kaibyshen and R Zaripova: *High Temperature Mechanism of Dynamic Recrystallisation of Ferritic Stainless Steels:* Mater. Sc. Forum, Vols. 113 - 115, 1993, pg. 385-390.

12. Huang Xiaoxu, K Tsuzaki and T Maki: *Subgrain Growth and Misorientation of the Ferrite Matrix in an (α and γ) Microduplex Stainless Steel*: Acta Metall. Mater. Vol. 43, No. 9, 1995, pg. 3375-3384.

13. Humphreys, F J: Scripta Metall. Vol. 27, 1992b, pg. 1557.

14. K. Bungardt, E Kunze and E Horn: Arch. Eisenhiittenw, **29**, 1958, pg. 193.

15. G R Speich and W C Leslie: *Tempering of Steels*: Metall Trans. Vol. 3, 1972, pg. 1043-1054.

16. Galibois A and Dube A: *Recrystallisation Kinetics of Martensitic Extra-Low Carbon Steels*: Canadian Metallurgical Quarterly, vol. 3, no. 4, Oct.-Dec. 1964, pg. 321-343.

17. G R Speich: *Tempering of Low-Carbon Martensite*: Trans. Metallurgical Society of AIME, vol. 245, 1969, pp. 2553-2564.

18. R N Caron and G Krauss: *The Tempering of Fe-C Lath Martensite*: Metallurgical Transactions, Vol. 3, 1972, pp. 2381-2389.

19. M Holscher and L Staubwasser: *Influence of Hot Band Annealing on Texture and Formability of Cold Rolled X6CR17 Ferritic Stainless Steel*: Innovation of Stainless Steel, Florence, Italy, Oct. 1993, pg. 2339-2344.

20. F Robbe-Valloire, B Osdoit and R Penelle: *Influence of Recrystallisation on the Ridging and Formability of Ferritic Stainless Steels*: 7 ICOTOM, Holland, 1984, pp.681-685.

21. R Wusatowski: *Influence of hot working conditions on recrystallisation of Stainless Steel*; J, Iron Steel Inst., Vol. 204, 1966, pp.727-736.

22. G Glover and C M Sellars: *Static Recrystallisation after Hot Deformation of α-Iron*; Metallurgical Transactions, Vol. 3, 1972, pp. 2271-2280.

23. B A Hugaas, D C Collinson and P D Hodgson: *The Static and Dynamic Recrystallisation of Hot Worked Ferritic Fe-Si. Alloy*: In, Recrystallisation'90, The Minerals, Metals and Materials Society, 1990, ed. T Chandra, pp. 573-578

24. Takuji Shindo and Takashi Furukawa: *Colony Structure and Its Texture in a Ferritic Stainless Steel*: 6 ICOTOM, ISIJ, 1981, pg. 846-851.

25. Tetsurou TAKESHITA, Jirou HARASE and Hiroshi YADA: *Effects of $\alpha \leftrightarrow \gamma$ partial transformation on recrystallisation after Hot Deformation in 17%Cr. Stainless Steel*; ISIJ (Iron and Steel Inst. of Japan), Vol. 27, 1987, pp. 432-438.

26. D Raabe and M Ylitalo: *Experimental Investigation of the Transformation Texture in Hot Rolled Ferritic Stainless Steel Using Single Orientation Determination*: Metall. and Mater. Trans. vol. 27A, 1996, pg. 49-57.

27. Y D Lee, D Y Ryoo, Y Y Lee and S H Park: in Int'l Conf. on Recrystallisation in Metallic Materials; Recry.' 90, T Chandra, (ed.), pg. 435-440.

28. Martin Holscher, D Raabe and Kurt Lucke: *Rolling and Recrystallisation textures of BCC steels*: Steel Research, 62, 1991, No. 12, pg. 567-75.

29. D Raabe, K Lucke: *Texture and Microstructure of Hot Rolled steel*: Scripta Metall. et Mater. Vol. 26, 1992, pg. 1221-1226.

30. D Raabe and K Lucke: *Annealing Textures of BCC Metals*: Scripta Metall. Mater., vol. 27, 1992, pg. 1533-1538.

31. D Raabe, K Lucke: *The Role of textures in FSS: In Proc. Int. Conf. On Strip Casting, Hot and Cold Working of Stainless Steels*, City of Quebec, PQ, Canada, 1993, N D Ryan, A J Brown and H J McQueen, eds. TMS-CIM, 1993, pg. 221-35.

32. D Raabe and K Lucke: *Rolling and Annealing Textures of Bcc Metals*: Materials Science Forum, vol. 157-162, '94, pp. 597-610.

33. W B Hutchinson: *Recrystallisation Textures in Iron Resulting from Nucleation at Grain Boundaries*: Acta Metall., vol. 37, no. 4, pp. 1047-1056, 1989.

34. M Hatherly, W B Hutchinson: *An introduction to textures in metals*: The Institute of Metallurgists, Monograph no.5, Chameleon Press Ltd., London (pub.).

35. D Raabe, K Lucke: *Selective Particle Drag During Primary Recrystallisation of Fe-Cr Alloys*: Scripta Metall. et mater. vol. 26, 1992, pg. 19-24.

36. D Raabe: *On the influence of Cr content on the Evolution of Rolling Textures in Ferritic Stainless Steels*: Journal of Material Science, vol. 31, 1996, pg. 3839-45.

37. R K Ray and J J Jonas: *Transformation Textures in Steels*: International Materials Review, vol. 35, No. 1, 1990, pp.2.

38. Chen Guangnam, Shen Huan, Hu Shiguang and Bernard Bauledet: *Roughening of the Free Surfaces of Metallic Sheets During Stretch Forming*; Mater Sci. and Eng., A 128 1990, pp. 33-38.

39. R Becker: *Effects of strain Localisation on Surface Roughening During Sheet Forming*; Acta mater., vol. 46, No. 4, 1998, pp. 1385-1401.

40. D V Wilson, A R Mirshams and W T Roberts: *An experimental Study of the Effect of Sheet Thickness and Grain Size on the Limit Strains in Biaxial Stretching*; Int. J. Mech. Sci., vol. 25, No. 12, 1983, pp. 859-870.

41. T. Sheppard and P Richards: *Roping Phenomenon in Ferritic Stainless Steels*; Materials Science and Technology, vol. 2, 1986, pp. 693-699.

42. Hung-Chi Chao: *Recent Studies into the Mechanism of Ridging in Ferritic Stainless Steels;* Metall. Trans. vol. 4. 1973, pp. 1183-1186.

43. K. Sztwiertnia, J Pospiech, and K Bethke: *Ridging Phenomenon in Ferritic Stainless Steels*; Private Communication to N Wittridge [43].

44. Roger N Wright: *The Direction of Tensile Strain and The Roping Phenomenon in Ferritic Stainless Steels;* Metall. Trans., vol. 7A, 1976, pp. 1385-1388.

45. Nicola Wittridge, PhD. Thesis, University of Cape Town, 1998.

46. Hiroshi Takechi, Hiroshi Kato, Tatsuya Sunami and Tadashi Nakayama: *The Mechanism of Ridging Formation in 17%Cr Stainless Steel*; Trans. JIM, vol. 8, 1967, pp. 233-239.

47. J Harase, K Ohta, T Takeshita, R Shimizu: *Grain Orientation Distribution in a Hot Rolled 17%Cr Ferritic Stainless steel*: Material Forum, 14, 1990, pp296-303.

48. Roger N Wright: *Anisotropic Plastic Flow in Ferritic Stainless Steels and The Roping Phenomenon*; Metall. Trans., vol. 3, 1972, pp. 83-91.

49. Hung-Chi Chao: *The Mechanism of Ridging in Ferritic Stainless Steels*; ASM., vol. 60, 1967, pp. 37-50.

50. G. Abbruzzese, S Fortunati, A Campopiano, L Micucci: *Relationship between microstructure, texture inhomogeneities and drawing properties of 17%Cr Steels: Effect of infracritical Annealing*: In Conf. Proc. Innovation Stainless Steel, Florence, Italy, 1983, pp. 2345-2351.

51. Tadashi Sawatani, Mitsuo Ishii, Hirohumi Yoshimura, Takeo Ashiura, Akio Yamamoto and Michio Wakamatsu: *Development of Continuous Annealing Process for 17%Cr Stainless Steel Strip*: Trans. ASM, 1980, pp. 1-14.

52. Tadashi SAWATANI, Kunihiko SHIMIZU, Tadashi NAKAYAMA, and Masanori MIYOSHI: *The r-values and Recrystallised Textures of Ti-Stabilised Low C, N 17%Cr Stainless Steel Sheets*: 6th. ICOTOM, ISIJ, Tokyo, Japan, 1981, pp. 862-871.

53. Masao Koike, Yutaka Hayashi and Masayoshi Ogaya: *Development of Nb-Stabilised Ferritic Stainless Steel Sheets with extra clean Surface and good formability*: Trans. ASM, 1980, pp263-268.

54. Takashi Zaizen, Taketomo Yamazaki, Tetsu Sakamoto, Yasuhiro Nakagawa, Isamu Yamauchi, and Tomoo Sekine: *Effects of Ti and Zr on the formability of High Purity Ferritic Stainless Steels:* Trans. ISIJ, vol. 3, part 20, 1980, pp. 94.

55. H J McQueen, E Evangelista, P Mengucci, N D Ryan and J Bowles: in Application of Stainless Steels, 1992: Nordberg, M, Bjorkund J, (eds.), pg. 924-933.

56. H J McQueen, N D Ryan, E Evangelista and X Xia: *Flow Stresses, Grain and Subgrain Structures Developed by Hot Working in As-Cast 409 Stainless Steel*: 34th MWSP Conf. Proc., ISS-AIME, Vol. XXX, 1993, pp. 101-107.

57. Ian M Matheson: MSc Thesis, Department of Materials Engineering, University of Cape Town, February, 1998, pp. 39-43.

58. J Cure: Traitement Thermique, 1968, Vols. 36-68, pp. 71-80.

59. H J Bunge: Texture Analysis in Materials Science, Butterworth and Co., London, 1982.

60. E Pouillard and B Osdoit: *Mecanisme de formation du cordage dans les aciers Ferritiques a 17%Cr.; Revue de Metallurgie*, Nov. 1969, pp. 763-769.

61. H Yoshimura and M Ishii: *Recrystallisation behaviour of 17%Cr. Ferritic stainless steel during hot rolling*; Tetsu-to-Hagane, 1983, 69 (11), pp. 1440-1447.

62. Masao Koike, Yasuhiro Maehara, Keibun Kaneko and Hisao Fujikawa: *Development of In-Line γ Treatment Process for Elimination of Ridging in AISI 430 Ferritic Stainless Steels*; In Proc. of Int'l Conf. On Stainless Steels, 1991, Chiba, ISIJ, pp. 864-871.